UNIVERSITY OF OKLAHOMA

GRADUATE COLLEGE

EXPERIMENTAL PRODUCTION OF DUST BY REPLICATING AEOLIAN AND GLACIAL ABRASION

A DISSERTATION

SUBMITTED TO THE GRADUATE FACULTY

in partial fulfillment of the requirements for the

Degree of

DOCTOR OF PHILOSOPHY

By

STEVEN MICHAEL ADAMS
Norman, Oklahoma
2023

EXPERIMENTAL PRODUCTION OF DUST BY REPLICATING AEOLIAN AND GLACIAL ABRASION

A DISSERTATION APPROVED FOR THE
SCHOOL OF GEOSCIENCES

BY THE COMMITTEE CONSISTING OF

Dr. Gerilyn S. Soreghan, Chair

Dr. Michael J. Soreghan

Dr. Megan E. Elwood Madden

Dr. Brett Carpenter

Dr. Elinor Martin

TABLE OF CONTENTS

Supplemental Materials

ACKNOWLEDGEMENTS

I would like to express my sincere gratitude to everyone who has contributed to the completion of this dissertation. First and foremost, I would like to thank my committee chair, Dr. Lynn Soreghan, for her invaluable guidance, support, and encouragement throughout this academic and research journey. Her insights, feedback, and expertise have been instrumental in shaping my ideas and research questions.

I am also deeply grateful to Dr. Megan Ellwood-Madden, Dr. Kato Dee, Dr. Lily Pfeifer, and everyone involved in sample collection, for their tireless efforts in gathering samples and making this research possible. Their willingness to collect rocks from around the world made these studies infinitely richer. Furthermore, I would like to acknowledge the contributions of all those who helped provide a wider selection of sediments and lithologies to experiment with and made this research more robust and complete. Your generosity and kindness have been invaluable.

I offer thanks to the many professors, colleagues, and advisors I have had over the years. I am deeply indebted to all of them for their endless support and mentorship; their patience, wisdom, and encouragement have been essential to my achievements so far.

Thank you to the members of my committee for their insightful feedback, valuable suggestions, and constructive criticism. Each of them has helped strengthen this work and pushed me to consider new possibilities.

I would like to acknowledge and appreciate the School of Geosciences staff. Thank you to Robert for letting me borrow his tools and lending a hand when building machines, and the office staff, for their assistance in a wide range of administrative matters. Each of them has helped me resolve countless small issues and contributed to this achievement.

Last but not least, I would like to express my heartfelt gratitude to my family for their unwavering love, encouragement, and support. I would like to especially thank my dad for his help with experimental design and building devices. Without his expertise and problem-solving skills, this research would not have been possible.

Funding for this research was provided by the Eberly Family Chair in Geosciences.

ABSTRACT

Dust is a highly mobile and influential class of sediment. Dust influences the climate, biosphere, and soils, and holds information about Earth's paleoclimate when preserved in the rock record. In this work we define dust as rock and mineral fragments, generally less than 100 µm, which are transported in suspension by the wind (Tsoar & Pye, 1987). We adopt size categories of dust proposed by Adebiyi et al. (2023, preprint) with fine dust 0-2.5 µm, coarse dust 2.5-10 µm, super coarse 10-62.5 µm, and giant dust >62.5 µm. When transported through the atmosphere, dust interacts with incoming solar radiation, outgoing infrared radiation, and clouds, altering the climate of the planet (Conen et al., 2011; Dufresne et al., 2002; 2023; Rosenfeld et al., 2001; Tang et al., 2016). The exact radiative effects are poorly understood and difficult to quantify and are the subject of ongoing research. One of the limitations in studying the radiative effects of dust is accurate particle size distributions (PSDs) for dust in the atmosphere (Kok et al., 2017). The effects of dust on the atmosphere depend on the composition, shape, and size of the dust particles. Fine dust (<2.5 µm) is assumed to scatter and reflect incoming shortwave solar radiation causing a cooling effect, while coarse dust (>2.5 µm) tends to have a warming effect by absorbing and reemitting longwave radiation (Adebiyi & Kok, 2020; Kok et al., 2023). Dust can influence cloud formation, precipitation, and nucleation of ice crystals, although the relationships are poorly understood (Kok et al., 2023).

When deposited in oceans or into soils, dust brings nutrients that promote biological productivity, which generally draws CO_2 out of the atmosphere, causing cooling (Bristow et al., 2010; Mahowald et al., 2011; Okin et al., 2011; Skiles et al., 2018). When deposited on snow and ice it reduces albedo and the amount of solar radiation reflected from the surface. Dusty snow with its lower albedo is also easier to melt as it absorbs incoming solar radiation (Bristow et al., 2010; Mahowald et al., 2011; Okin et al., 2011; Skiles et al., 2018). Dust as a sediment in soils and the rock record preserves information about the climate and environment at the time of deposition (Jordanova et al., 2022; Daniel R. Muhs, 2013). For example, loess and paleosol sequences preserve intervals of aridity and rapid dust accumulation followed by stability and a low sedimentation rate where a soil horizon develops. If the source of dust is identified, then paleowind patterns can be determined, yielding information about the climate of the past.

Several processes have been proposed as mechanisms capable of producing dust including glacial grinding, aeolian saltation, explosive volcanism, high-altitude alpine weathering, chemical weathering, and biogenic siliceous diatoms (Aleinikoff et al., 1999, 2008; McTainsh, 1989; Nahon & Trompette, 1982; Smalley, 1995; Smalley, 1966; Smalley & Vita-Finzi, 1968). Not all of these processes have been thoroughly investigated, however. Many loess accumulations—structureless deposits of eolian silt—have been linked to glacial erosion by spatial proximity to the margins of former ice sheets. However not all loess deposits are geographically proximal to loess. For example, the Chinese Loess Plateau (CLP) is an immense loess deposit composed of silt-sized dust, but it is not proximal to any recently glaciated area (Muhs, 2013). This has led to speculation of other processes capable of producing dust. The CLP is downwind of a large desert and this has spurred debate about whether aeolian abrasion of sand grains in desert environments could produce abundant silt-sized dust. A series of experiments followed, attempting to replicate the process of aeolian saltation in the lab to determine if the

mechanism was viable (Whalley et al. 1987; Wright et al. 1998; Bullard et al. 2004, 2007). Experiments have also been performed in the lab replicating glacial grinding. Initially, glacial grinding experiments did not produce abundant silt; however subsequent experiments determined that this was because crushed Brazilian vein quartz, which contained few crystal defects compared to plutonic quartz, was used in the experiments (Wright, 1995; Jefferson et al. 1997; Kumar et al., 2006). Experiments using sand from Cretaceous sandstones readily produced silt when ground in a ring-shear device, considered an analog for glacial grinding (Jefferson et al. 1997; Kumar et al., 2006).

While there have been several experiments exploring the physical abrasion processes capable of producing silt and dust, several knowledge gaps remain. Few studies have adequately investigated abrasion of basalt sands via aeolian abrasion and these previous results are not scalable to determine the geological significance. Most experiments have focused on the abrasion of quartz or granitic rocks, with few studies investigating the production of dust by abrading basalts, sedimentary rocks, or metamorphic rocks. Previous glacial grinding experiments that did not use ring shear devices used wheels of rock and sediment, ground against each other, rather than focusing on subglacial clasts and their shapes (Matthews, 1979; Lee and Rutter, 2004).

In this study two new experimental devices are used, which have been designed to better replicate aeolian abrasion and glacial grinding. The aeolian abrasion chamber is designed to simulate grain-on-grain collisions of sand saltating in a windstorm at high velocities (~40 m/s). The glacial grinding device abrades small rock fragments cut with flat and pyramidal (pointed) surfaces against a flat rock slab to emulate the grinding of clasts beneath a glacier. The aeolian abrasion experiment focuses on the abrasion of basalt sands from Hawaii and Iceland as analogs for Mars and compares them to results from quartzose sand from the Imperial Sand Dunes of southern California. The glacial grinding device abrades five basalts as analogs for Mars and eleven different rocks (granitoids, quartzites, a schist, sandstones, and limestones) as analogs for Earth-based glaciation.

We compare our results with previous dust production experiments and studies of dust to test two questions: (1) Do different abrasion mechanisms produce representative particle size distributions (PSDs) tied to the mechanism of production? (2) When abraded, do different lithological compositions produce dust at different rates and PSDs with defining traits based on composition? Results show that basaltic sand from Iceland produced 4 times more dust and 2.5 times more fine sand than Hawaiian samples. These experiments demonstrate the significance of dust production by aeolian saltation of basalt sand at the planetary scale and infer the possible influence of produced dust on the climate of early Mars. Results are scaled to determine dust production at the planetary level and suggest Mars would produce a geologically significant amount of dust capable of influencing the climate.

Results from experimental glacial grinding of small (~3 cm) clasts of varying lithologies (representing Earth and Mars) show that rock-on-rock abrasion produces sediment with PSDs containing silt modes (~30 μm). Pointed styluses generally produce more sediment than flat styluses. Pointed and flat styluses of the same lithologies generally produce similar PSDs. PSDs across all lithology and stylus types produce similar modes at 0.5 μm, 4-8 μm, 30 μm, and 100-

300 µm. When our PSD results are compared to natural dust sources and previous experiments replicating a range of abrasion processes (e.g., volcanic dust, lunar dust, glacial grinding, aeolian abrasion, fluvial abrasion, mechanical crushing) the same modal ranges occur. Our study suggests an underlying physical process operating across abrasion mechanisms, varying mineralogical compositions, and clast shapes that limits PSD modes to specific ranges.

CHAPTER I

ANALOG STUDY OF MARTIAN DUST THROUGH EXPERIMENTAL AEOLIAN ABRASION OF BASALT SANDS

ANALOG STUDY OF MARTIAN DUST THROUGH EXPERIMENTAL AEOLIAN ABRASION OF BASALT SANDS

ABSTRACT

Dust covers a significant portion of Mars' surface, with dust storms periodically engulfing the planet. Despite this, the origins of Martian dust are poorly understood. To address this deficit, we conducted experiments to replicate the mechanical abrasion of saltating sand grains in a Martian desert dune field under storm wind conditions, measure rates of dust production, measure the particle size distributions of dust produced, and scale results to determine planetary-wide significance. Two basalt sand samples were collected to act as Martian dune sand analogs (one from Hawaii and one from Iceland). Samples were processed to remove any pre-existing dust-sized sediment and then abraded inside a novel device designed to replicate the grain-on-grain collisions experienced by saltating sand in a desert dune field. These experiments demonstrate the significance of dust production by aeolian saltation of sand at the planetary scale. Results show basaltic sand from Iceland produced 4 times more dust and 2.5 times more fine sand than Hawaiian samples, suggesting that differences in sand composition, grain shape, and sand PSDs influence the amount of dust produced. If our experiments are valid replications of natural dust production, then aeolian saltation on Mars would produce a geologically significant amount of dust capable of influencing the climate.

INTRODUCTION

Dust is an important component of surface processes on terrestrial planets, particularly Earth and Mars. As it undergoes atmospheric transport, dust can influence the climate through radiative effects—both positive (warming) and negative (cooling). In addition, it can alter precipitation, act as ice- and cloud-nucleation points, and alter albedo (Conen et al., 2011; Dufresne et al., 2002; Kok et al., 2017, 2023; Rosenfeld et al., 2001; Tang et al., 2016). Once deposited, it influences soil composition, provides nutrients to soil and water for organisms residing in both, and alters albedo of the surface it mantles, particularly ice and snow (Bristow et al., 2010; Mahowald, Ward, et al., 2011; Okin et al., 2011; Skiles et al., 2018). After deposition dust becomes incorporated into the rock record and provides geologists with important clues about planetary climate (McGee et al., 2010), potential processes that created the dust (Muhs, D. R., 2013), and the environment(s) of deposition (Jordanova et al., 2022).

Aeolian processes currently predominate on the surface of Mars and have likely remained important for much of its history (Ehlmann et al., 2017; Greeley et al., 2001). Aeolian bedforms occur widely in both modern surficial sediment and ancient strata exposed on the surface (Banham et al., 2018; Bristow & Moller, 2018; Chojnacki et al., 2020). A mantle of dust covers a significant portion of Mars' surface and dust storms can grow to engulf the entire planet (Christensen, 1986; Gillespie et al., 2020; Tanaka, 2000). The vast quantity of dust on Mars has formed extensive duststones (Bridges & Muhs, 2012). The Medusae Fossae Formation has been interpreted as a large dust deposit and the presumed source for much of the present surficial dust on Mars. Dust eroded from this unit is estimated to be of sufficient volume to cover the planet in a layer 2-12 m thick (Ojha et al., 2018); the origin(s) of Martian dust, however, remain poorly understood. Proposed methods for dust production—by which we mean the generation of the particles, rather than their emission—include volcanic eruptions, bolide impacts, aeolian abrasion, glacial grinding, and chemical weathering. Arid, physical abrasion processes are the preferred methods for primary dust production because of the presence of olivine, which would have weathered away in the presence of abundant liquid water (Bridges & Muhs, 2012; Goetz et al., 2005). The characteristics of dust produced by each of these methods, such as typical particle size distributions (PSDs), are unknown. Each process might produce dust with different distinguishing characteristics. Depending on the characteristics of the dust produced, specifically the PSD, composition, and albedo, the dust could affect the climate in different ways (Kok et al., 2023).

Particle size distributions of modern airborne dust on Mars are measured using remote sensing techniques from rover, lander, and orbital platforms (Chen-Chen et al., 2019; Kahre et al., 2008). PSDs measured by these techniques generally indicate atmospheric dust is <2.5 μm, but this may not be representative of the large volume of dust that exists on Mars. Coarser dust in surface regolith or ancient duststone deposits is difficult to image and measure owing to the limitations of image resolution (Rivera-Hernández et al., 2019; Vaughan et al., 2023; Weitz et al., 2022). A coarser dust component might be abundant on Mars but escapes direct measure because it is rarely entrained in the modern atmosphere or is too small to measure with rover-based cameras. While this coarse dust component may be inactive today, it may have been transported more actively in the past. To better understand the coarse component of ancient Martian dust PSDs we need analog experiments that produce dust. Results of these experiments will aid collective understanding of how dust affected Martian climate because identifying dust PSDs and compositions improves climate models (Kok, 2011; Mahowald, Albani, et al., 2011; Miller et al., 2006; Skiles et al., 2018; Tegen & Lacis, 1996).

The purpose of this work is to conduct experiments designed to replicate the mechanical abrasion of saltating sand grains in a desert dune field under storm wind conditions, measure rates of dust production and PSDs of produced dust, and scale results to determine planetary-wide significance. The importance of these experiments is their ability to show the significance of dust production by aeolian saltation of sand at the planetary scale and thus enable assessment of the possible influence of produced dust on the climate of early Mars.

EXPERIMENTAL BACKGROUND

Aeolian abrasion of sand has likely been an important process on Mars since planetary formation and increased in significance as the effects of water and ice on weathering, erosion, and transport of sediments diminished (Ojha et al., 2018). For this reason, several studies have focused on aeolian abrasion experiments to produce Mars-dust analogs using basaltic sands from Earth (refs below).

Krinsley et al. (1979) studied the abrasion of basalt and quartz at Martian and Earth atmospheric pressures using an apparatus that used a motorized paddle wheel to propel sand at a target wall studded with sand grains. The apparatus mimicked wind speeds of 10 to 75 m/s. While the results showed textures on abraded grains similar to those found in arid dune fields on Earth, the abrasion mechanism of grains colliding with grains mounted to a solid surface differs from intergranular impacts that would likely prevail under realistic conditions. The authors did not measure PSDs of the material produced from the collisions.

Cornwall et al. (2015) studied the abrasion of sand grains in a modified air mill. Their experiments used batches of 100 grains of mafic minerals and basalt. Angular grains abraded and rounded rapidly at first, followed by a decrease in abrasion rate. PSDs of produced material were not reported, but results suggested that basalt grains and volcanic glass are more resistant to breakage than mafic minerals.

Bristow and Moller (2018) were the first to focus on dust produced from abrasion experiments of Mars-analog sediments. They used an abrasion chamber similar to Bullard et al. (2004, 2007), Whalley et al. (1987), and Wright et al. (1998) to study dust production in eolian environments of Earth. Their apparatus used compressed air blown toward the bottom of a large glass test tube to abrade sand grains, and electrostatic traps to catch the produced dust as it exited the chamber. They abraded a wide selection of basalt and mafic samples from Hawaii, Arizona, and Iceland, as well as a Martian soil simulant (JSC Mars 1-A) and gypsum sediments from New Mexico. While their results suggested aeolian abrasion of basalt sands produces dust, the experimental design precluded accurate measurement of the volume of produced dust because they used sand that contained resident fines. Through comparative analysis of the percentage of resident fines and dust produced, only a few samples produced dust masses that exceeded the dust fraction already in the samples. When considering new dust produced via aeolian abrasion, these results cannot be used for scaling.

In this work we use physical experiments to study both the volume and character of basalt dust produced via aeolian saltation. Our experiments differ from previous studies by using a new experimental apparatus that better replicates the saltation and grain collisions experienced during windstorms, starting with the intent to determine the mass and particle size distributions of new dust produced via aeolian abrasion, removing resident fines prior experimental abrasion, using control samples to ensure resident fine removal, and scaling results to determine geological significance at the planetary scale.

MATERIALS AND METHODS

Sample Collection

Two basalt sand samples were collected to act as Martian dune sand analogs. One sample was collected from an aeolian dune of the Ka’u Desert in Hawaii (HI) and one from a beach in southwest Iceland (ICE). Additionally, a sample of quartz-rich dune sand was collected from Imperial Sand Dunes (ISD) in southern California to compare dust production rates. Table 1 lists location and sample details.

Sample Preparation

To ensure that dust collected and analyzed post experiment was indeed produced in the experiment, samples were processed to remove pre-existing fines. To accomplish this, a sieve size was selected that would retain the majority of sand but allow fines to pass through (250 µms for HI and ISD, 125 µms for ICE, owing to the difference in starting modes). About 50 g was placed on the sieve and submerged in a water bath. The sieve and sand were agitated in an oscillating and undulating motion to drive the fines through the sieve. Each sample was agitated for approximately five minutes then transferred to a large beaker to dry. Once ~800 g of clean sand was wet sieved, it was dried in an oven at 90^{o} C. After drying, samples were split into 100 g aliquots using a sample splitter. Half the aliquots were for abrasion and half were reserved as controls to ensure significant removal of pre-existing fines.

Experimental Design

We designed a novel device to replicate the grain-on-grain collisions experienced by saltating sand in a desert dune field. Figure 1 illustrates a cylindrical acrylic chamber of 12.5 cm diameter. A vacuum motor pulls air through a central cylindrical filter (5 cm diameter) of 5 µm steel mesh. Air enters the chamber through four 0.635 cm tubes that direct the air to circulate in a clockwise or counterclockwise manner depending on the direction of the nozzles. The device operates at ambient atmospheric pressure. At the start of the experiment, in the clean chamber wind velocity measures ~50 m/s at the nozzle and ~45 m/s at 1 cm from the nozzle. After 24 hours, dust accumulation on the filter causes velocities to slow to ~20 m/s at the nozzle and ~12 m/s 1 cm from the nozzle. As air circulates around the chamber it mobilizes sand and typically forms three to four small "dunes" or "ripples." The flowing air entrains grains from the lee side of the bedforms and impacts them on the stoss side. Sand is removed from and returned to dunes so quickly that the dunes generally remain stationary. Accordingly, most sand grains remain stable in the core of the dune and do not participate in abrasion. To ensure full participation of all grains in abrasion the sand is mixed every five minutes by rotating the air nozzles with servo motors so they sweep back and forth across the dunes. The tubes reverse direction after each mixing and dunes quickly restabilize.

Abrasion is halted every 24 hours to remove and clean the filter because it slowly clogs with accumulated dust. This reduces the air velocity in the chamber and thus buffers the collisional energy, reducing the potential to create dust. The dust accumulated on the filter is rinsed into a beaker and the filter is scrubbed with a nylon brush. After all the dust is collected and the filter cleaned, the filter is returned and abrasion resumes. Total abrasion time for each sample is 96 hours.

Post-Abrasion Processing

After 96 hours the device is disassembled and the sand and dust removed by rinsing the chamber contents into beakers using distilled water. The process of rinsing the filter and removing sediment from the chamber requires several liters of water and the resultant mixture settles in large beakers for two days, after which the water is decanted. Samples are then wet sieved at either 250 µm (HI) or 125 µm (ICE) and at 63 µm to separate coarse sand, fine sand, and dust fractions. Water and sediment passing through the sieves are collected, along with the sediment remaining on sieves. The dust (<63 µm) fraction is set aside to settle. The coarser fractions 63-125 µm (ICE), 63-250 µm (HI and ISD), >125 µm (ICE), and >250 µm (HI and ISD) are rinsed into beakers, the water decanted, and placed to dry in an oven at 90^{o} C.

The dust fractions (<63 µm) settle in a large beaker for two days. The water is then decanted and the sample rinsed into centrifuge tubes, centrifuged, transferred to pre-weighed vials, frozen, freeze dried, then weighed to acquire a dry mass; sand fractions are also weighed.

Control samples are post-processed identically to samples removed from the abrasion chamber but are never abraded. They are used to verify that little to no residual dust-sized sediment is present in sand entering the abrasion chamber. This gives us confidence that any dust measured resulted from experimental abrasion.

Sample Analysis

Samples are first weighed to compare the mass of dust produced between sample types and between experiment and control samples, then particle size distribution (PSD) of the dust (<63 µm) fraction is analyzed using a Malvern Mastersizer 3000 Laser Particle Size Analyzer (LPSA) after one minute of sonication with ~3 ml of water and 5% sodium hexametaphosphate (Calgon). Wet samples are mixed to a slurry within a pipette and drops are added to the LPSA small-volume module for analysis.

Scaling Method

We define dust here as mineral grains or rock fragments transported in suspension by the wind. We adopt the classification scheme of dust sub-categories proposed by Adebiyi et al. (2023, preprint) with fine dust 0-2.5 µm, coarse dust 2.5-10 µm, super coarse 10-62.5 µm, and giant dust >62.5 µm. For this study, the limitations of distribution bin sizes resulting from laser particle-size analysis software dictate that the actual measured intervals are 0-2.4 µm, 2.4-9.9 µm, and 9.9-66.9 µm. See Appendix 1 for raw data and distribution bin ranges. Dust measured by the LPSA in our study passed through a sieve at 63 µm, therefore giant dust is likely underrepresented.

To scale results, we use the mass of dust (<63 µm) produced and the surface area of the abrasion chamber. We use surface area because estimates for dune surface area on Mars exist in the literature and this metric is readily measurable in our experimental device. As sand abrades and fines become entrained, dunes have sufficient sand supply to replenish fractured grains. Mass and sand supply are thus not considered limiting factors. We use the total area of dune fields on Mars (980,000 km^2) estimated by Chao and Zhibao (2022).

We also must consider a target mass of dust for scaling. We selected the estimated mass of dust eroded from the Medusae Fossae Formation (MFF) as our target. Ojha et al. (2018) estimated 3×10^5 –1.8×10^6 km^3 has been eroded from MFF. This is a significant mass, which they suggest has contributed greatly to the dust deposits of Mars. We calculate how many days of abrasion at storm wind velocities are required to produce this quantity of dust assuming equal sustained wind velocity over all dune fields. We then calculate how many days and hours annually would be required over geologically significant intervals to match this quantity of dust (over 1 billion, 100 million, 10 million, and 1 million Earth years). See Appendix 1 for step-by-step methods for scaling results.

Sample Description: Mineralogy and Texture

Point counts (n = 400) were conducted for all three starting materials and two dust samples (ICE-4 and HI-4) using standard thin sections stained for plagioclase feldspar. Table 2 lists grain categories and count results and Figure 2 shows minerals and clasts representative of point count categories. We used photomicrographs of starting sand samples to qualitatively describe grain shape and angularity (Table 1 and Figure 3). Roundness and sphericity were determined qualitatively using images of sand grains according to the criteria outlined by Powers (1953). X-Ray Diffraction (XRD) analysis was performed on the ICE starting sand, HI starting sand, ICE-3 dust, and HI-2 dust to determine if dust was preferentially created by specific compositional components (see Appendix 2).

RESULTS

PSDs of Starting Sands

Starting sands used in the experiments have inherent PSDs that could influence the types of fines produced during abrasion (Figure 4). ICE sand has a mode of 262 µm and a wide unimodal distribution. HI and ISD sands have narrow unimodal distributions with coarser modes of 392 µm and 310 µm, respectively. All three distributions are generally symmetrical with no skewing. While the ISD sample exhibits a finer mode than HI, its broad distribution includes the full range of particle sizes contained in the HI sand. However, the finer sands of ICE do not occur in the PSD of HI sand.

Point Counts, Grain Shape of Starting Sands, and Composition

HI starting sands have abundant (~85%) glass with the majority being vesicular (~56%). Volcanic lithics and minerals (e.g., albite, olivine, pyroxene) are a minor (~15%) fraction combined. ICE samples have abundant lithics (~55%), less glass (~24%) than HI sand, and more mineral grains (~14%) than HI sand. ISD sand is ~75% quartz with minor lithics (~14%) and feldspar (~9%). See Table 3 for details. ICE sands are angular to subangular with a general mix of sphericity between low and high. HI sands are angular to subrounded with high sphericity. ISD sands are well rounded to subrounded with high sphericity (Table 1).

XRD analysis of starting sands confirms the presence of olivine, pyroxene, and plagioclase (albite and bytownite) as the primary phases (other than glass) in the samples. ICE samples have forsterite, augite, bytownite and hematite. HI samples contain forsterite, augite, and albite. HI sand also has a broad peak suggesting an abundant amorphous phase which we interpret as glass. XRD analysis of the dust fraction of ICE-3 shows the presence of forsterite, augite, and bytownite; however, the curve also shows a broad rising peak that indicates the presence of amorphous material which we interpret as glass clasts. HI-2 dust results indicate the presence of plagioclase (bytownite, albite), augite, and indialite. Like HI sands, HI-2 dust has a broad peak suggesting an amorphous component which we identify as glass (Appendix 2).

Point counts of the dust fractions of samples HI-4 and ICE-4 shown in Table 2 show HI dust contains 76% glass along with feldspars, olivine, and other minerals (generally pyroxene). ICE-4 differs from ICE sands with an increase in glass (~41%) and a larger amount of feldspars (~38%). We interpret these results to show the abundance of lithics in ICE sands being made of feldspars with glass. These sand-sized lithic fragments when broken became glass and feldspar clasts in the dust fraction.

Mass of Dust Fraction

Basalt sands produced 0.42 – 2.22 g of dust (<63 µm), whereas quartzose sands produced only trace amounts (0.026 – 0.041 g; n=2). Sands from Hawaii produced an order of magnitude more dust than the quartzose sands (0.42 g – 0.53 g; n=4), and basaltic sand from Iceland produced the most dust (1.69 – 2.22 g; n=4)—approximately four times the dust of the HI samples (Figure 5).

Control samples produced trace amounts of dust that were below detection limits of the LPSA. This dust was present in the original sediment collected in the field and escaped removal during the intensive pre-experiment wet sieving. The dust masses present in the basaltic controls are lower than those from the abrasion experiments, confirming measurable dust production during abrasion. The uniformly low masses observed in the controls are considered negligible, requiring no modification to the scaling calculations.

Mass of Fine Sand Fractions

In addition to producing dust-sized particles, the experiments also produced fine sand. For this work, fine sand is defined as sand that passed through the sieve size used to remove resident fines, which differed owing to the natural conditions of the starting material. For ICE samples we used a 125 µm sieve; for HI samples we used a 250 µm sieve. ICE samples produced 1.5 – 1.9 g of fine sand with an average of 1.7 g. HI samples produced 0.57 – 0.82 g with an average of 0.69 g. ICE samples produced ~2.5 times more fine sand than HI samples. ICE control samples had more fine sand than HI control samples as well. See Figure 5 for comparison of samples.

PSD of Dust Fractions

Following experimental abrasion, ICE dust samples exhibited a unimodal, fine-skewed distribution with modes of ~42 µm, all in the super coarse dust range. HI dust samples produced bimodal distributions with modes ~7-10 µm and ~20-30 µm (coarse and super coarse dust ranges, respectively). ISD dust samples exhibit bimodal distributions with modes at ~6-8 µm and ~20-64 µm similar to the HI samples. See Figure 6 for details.

Fractional Mass of Dust Produced

Using PSD results reported from the LPSA, dust mass fractions are summed at intervals 0-2.5 µm, 2.5-10 µm, and 10-67 µm. The LPSA reports in volume percent, and we assume that volume percent roughly approximates mass percent, albeit with small error associated with density differences between particles of different compositions. For all samples, the super coarse dust (10-67 µm) mass is the largest fraction and the fine dust (0-2.5 µm) fraction is the smallest. The coarse dust (2.5-10 µm) fractions are smaller in the ICE samples than the HI and ISD samples. The ICE samples overall had larger super coarse (10-67 µm) fractions than HI and ISD samples. See Figure 7 for sample comparison.

Scaling Results

Scaling assesses the amount of time required to produce the target mass of dust using the existing total surface area of dune fields on Mars. Using the average rate of dust produced by ICE samples, ~41ky Earth years of constant abrasion is needed to produce the lower value of the target mass range of dust thought to have eroded from the MFF, and ~245 ky Earth years of constant abrasion to reach the upper mass target eroded from the MFF. For HI dust production rates, the equivalents are ~166 ky and ~997 ky Earth years for the lower and upper mass target (Table 3).

To judge the feasibility of maintaining these rates over geological spans of time, the years required to reach mass targets are divided into long time intervals. This reveals how often storm winds need to blow through dune fields annually to produce target masses over geological time spans. It takes 0.36 to 8.73 Earth hours (0.015-0.36 days) of annual abrasion for the dune fields of Mars to produce target dust masses over a billion years. The required abrasion time increases to a range of 357 to 8734 hours (15-364 days) annually over just 1 million years.

DISCUSSION

Starting Sand PSD

Particle-size distribution curves in Figure 4 show that the HI sand is much more homogenous than the ICE sands. The diversity of grain sizes in ICE sands could play a part in its ability to produce more dust and fine sand. The presence of both large and small grains presents the potential for large grains to collide with small grains, given that the larger mass carries more momentum and thus potential to shatter finer grains rather than simply chipping and spalling grain edges.

Mass of Dust Produced

The Iceland sands produced the greatest volume of dust, more than four times the amount from Hawaiian sands, and approximately 50 times the amount of dust produced from Imperial Sand Dunes. We infer that these differences in dust production relate primarily to differences in composition, PSD of the starting sands, and texture of the starting sands.

The starting sands from Iceland are >50% lithics and ~21% glass while the sand from Hawaii comprises ~11% lithics and ~85% glass (Table 2). The abundance of glass fragments in Hawaiian sands makes these sands more resistant to physical weathering by intergranular collisions. Previous abrasion studies also found glass to be more resistant to abrasion if unaltered by chemical weathering (Bristow & Moller, 2018; Cornwall et al., 2015). Collisional energy likely exploits intergrain boundaries and mineral cleavage planes present in lithic grains, resulting in more dust in ICE samples related to the abundance of glass and feldspars.

The differences in dust produced between basaltic and quartzose sands reflect primarily composition and grain shape. Quartz makes up ~75% of the composition for sands from Imperial Sand Dunes with ~14% lithics and ~9% feldspar, whereas the basaltic sands contain glass (~85-24%), minerals (~24-3%), and lithic fragments (~55-11%) (Table 2). Quartz is more durable than glass, minerals in the basalt sands, and lithics. The quartz grains have likely experienced more physical weathering in transport than the basalt sands. Rounded quartz has a lower potential for chipping and spalling relative to the more angular basalt lithics, glass, and minerals. The quartz in ISD sands has likely experienced significant fluvial transport along the Colorado River, prior to aeolian saltation in sandsheets and dunes (Muhs et al., 1995). Our experiments reinforce results from earlier work (Adams and Soreghan, 2020) that quartz-rich aeolian dune sand produces minimal dust.

The differences in dust produced between the ICE and HI samples may also reflect aspects of the experimental design. As experimental abrasion proceeds between cleanings and dust is produced, it accumulates on the filter through which air is pulled, blocking the filter and reducing the internal air velocity, thus lowering the potential for emission, acceleration, and abrasion of sand grains. The larger the sand grain, the more difficult it becomes with time to mobilize and saltate the grain. The finer-grained Icelandic sand can saltate for longer as the filter clogs and the velocity decreases compared to HI sands. This is observed during the daily cleanings, the Iceland sand is more mobile after 24 hours compared to Hawaiian sands. Since we cannot control for this variable, we cannot estimate the influence of this effect relative to the effects of composition.

Fine Sand Mass

Like the dust fraction, ICE samples also produced significantly more fine sand than HI samples. The mass of fine sand produced is subequal to the mass of dust produced. This result also suggests that aeolian saltation produces predominantly coarse silt to fine sand. Fine dust, while significant compared to quartz dune systems, and significant on a geological time scale, forms a small fraction of the newly produced sediment. While atmospheric dust on Mars today comprises predominantly the fine dust fraction, coarser dust is likely abundant in the sedimentary record.

Dust PSDs and Fractional Mass of Dust Produced

All dust sample types exhibit a super coarse dust (10-67 µm) mode. The HI and ISD samples, both of which have coarser starting sands, exhibit bimodal distributions with a coarse dust peak ~10 µm. This difference in PSDs between HI and ICE could reflect the influence of the PSDs of the starting material, and/or differences in composition, texture, and grain shape. The ICE sand is finer but contains more lithics prone to shattering. However, it is unclear why the relatively friable lithics would not also produce equally abundant fine dust.

For all samples the largest volume percent and mass percent of produced dust fell into the super coarse (10-67 µm) fraction. For ICE samples this fraction is ~70%, far exceeding the fine (~2.5%) and coarse dust (~20%) fractions. For HI and ISD samples the super coarse dust is ~50%, coarse dust is ~30-40%, and fine dust is ~3-7%. Using this metric, the HI and ISD samples are similar. While the HI samples produced far more dust than ISD, they have similar distribution curves and fractional mass divisions. ICE samples also produced more giant dust (>67) compared to HI and ISD samples. These could be elongated grains with a long axis exceeding 63 µm but narrow enough to pass through the 63 µm sieve. Similar to the previous discussion, we infer that these differences relate primarily to differences in starting grains, specifically composition, hardness, brittleness, PSDs and grain shapes and textures. ICE starting sands are generally more angular than particles in HI and ISD samples. ICE samples were angular-subangular, HI samples subangular-rounded, and ISD samples rounded. The harder and more rounded grains are more likely to yield only small chips spalled in collisions, while the more angular particles are prone to large fragments breaking off or whole grain shattering. For HI and ISD sands to produce super coarse dust they likely need to experience whole grain shattering (Figure 8).

Scaling Results

Scaling the results of the experiments over geological time using the total area of existing dune fields on Mars suggests that aeolian saltation and abrasion can produce geologically significant volumes of dust. If Martian dune sands, or at least a significant fraction of them, contain sand similar in composition and PSD to the ICE sands, they could produce the lower target mass in as little as 1 My if they experienced at least 358 Earth hours (15 Earth days) of high-velocity abrasion annually. Previous work by Adams and Soreghan (2020) found that an especially windy location in Texas experienced 322 Earth hours (13 Earth days) of annual wind velocities >20 m/s (measured at 10 m above the ground). While wind regimes and atmospheric pressure(s) that prevailed in the past on Mars are uncertain, these results suggest the feasibility of producing large volumes of dust over time scales of 1 My to 1 Gy. If the composition of the sands on Mars approximates the sands of HI samples, the rate of dust production would be slower, but given 10 million to 1 billion earth years, target masses could be achieved.

Implications for Past Martian Climate

Previous studies with a focus on Earth's dust suggest that fine dust (<2.5 µm) has an overall climatic cooling effect, whereas dust >2.5 µm exerts an overall warming effect (Adebiyi et al., 2022; Kok et al., 2017). However other factors complicate the climatic effect, e.g., refractive index of the grains, albedo of the dust vs albedo of the underlying surface, and grain alteration with atmospheric transport (e.g., water condensation and/or ice nucleation, cloud interactions, chemical alteration; Kok et al., 2023). All of these effects vary across regions and time as coarser grains fall out of suspension more readily than finer grains. Thus, it is difficult to determine if mineral dust exerts an overall warming or cooling effect on Earth (Kok et al., 2023), and similarly difficult to determine whether the dust of ancient Mars warmed or cooled the planet. Modern dust on Mars is generally <2.5 µm and estimated to cause warming of the lower atmosphere (Korablev et al., 2005). Freshly abraded basalt dust is typically darker than chemically altered and oxidized dust, which also affects how it might alter climate; however, with time, dust would tend to evolve toward a similar (red, oxidized) color and composition to the existing dust and regolith on Mars. Over long periods of time the majority of dust would have an albedo similar to surface regolith, albeit lighter than oceans if they were present. If extensive ice sheets and glaciers prevailed in Mars' past, deposited dust would reduce the albedo of the ice, lowering its ability to reflect light, and increase light absorption, ultimately producing a net warming effect, producing—potentially—liquid water.

Like mineral dust produced on Earth via glacial grinding, dust produced via aeolian saltation of basalt sand contains mostly coarse and super coarse dust. Kok et al. (2017, 2023) suggested that, when properly modeled, coarse dust likely exerts a net warming effect on Earth. If we assume our experiments are good replications of natural dust production, then aeolian saltation on Mars would produce a geologically significant amount of dust capable of influencing the climate. These results will assist climate modelers in developing a better understanding the role of dust on the Martian climate of the past, especially given better estimates and, ultimately, measurements of dust PSDs (Kok, 2011; Mahowald, Albani, et al., 2011; Miller et al., 2006; Skiles et al., 2018; Tegen & Lacis, 1996).

Experimental Design and Focus

Our experiments are conducted at Earth atmospheric pressure and gravity. Mars currently has much lower atmospheric pressure and lower gravity. We assume the important variable for dust production is the energy involved in the grain collision. As our experiments and previous experiments have demonstrated, several variables influence susceptibility to breakage (composition, degree of weathering, PSD, grain shape). Thus, for different grain types there will be more or less potential for a grain to break under a given wind speed or energy regime. If the analog sands used in our experiments have sands comparable to those on Mars then Martian sands would have similar susceptibilities to breakage.

Additionally, because winds on Mars were sufficient to transport sands great distances and form the wide variety of dune forms and eolian forms (dunes, transverse aeolian ridges, megaripples, etc.) observed on the Martian surface, then winds were, at some point, capable of colliding grains with sufficient force to fracture them (Day & Zimbelman, 2021). Our experiments have a historical focus, attempting to demonstrate what might have been possible on geological timescales in the distant past. However, it is possible that this mode of dust production may continue with a much lower magnitude today on Mars, as grain of sand can saltate and dunes have been observed migrating (Chojnacki et al., 2017; Silvestro et al., 2020).

CONCLUSION

We used a novel device that effectively replicated aeolian abrasion of saltating sand grains in a dune field under windstorm velocities. Basalt sands produce significant volumes of dust (primarily in the <67 μm range) when compared to abrasion of quartzose dune sand, which produced negligible dust. When scaled to the planetary level for Mars, aeolian abrasion of saltating basalt sands produces significant volumes of dust (~equivalent to dust eroded from MFF) over geological spans of time (1Ma - 1Ga). While it is unknown how long an atmosphere capable of saltating and abrading sand persisted on Mars, widespread aeolian bedforms on the surface suggest sufficient aeolian activity occurred in the past. PSDs of dust produced indicate an abundance of coarse dust (2.5-10 μm) created through aeolian abrasion. Suspended within the atmosphere, this size fraction likely exerts a warming influence, and may have contributed to a warmer climate in the distant past of Mars.

FIGURES AND TABLES

Sample	Location	Environment	Grain Shape	Sphericity	Latitude	Longitude
ICE	Southwest Iceland	Beach	Angular to subangular	Low to High	64.13159 N	21.95806 W
HI	Ka'u Desert, Hawaii	Partially vegetated dune, stoss slope	Angular to subrounded	High	19.354537 N	155.365262 W
ISD	Imperial Sand Dunes, southern California	Dune Crest (no vegetation)	Well rounded to sub rounded	High	32.982477 N	115.133973 W

Table 1. Sample information including sample type designator, location, environment, and latitude and longitude where samples were collected. Qualitative sample shape descriptions provided for grain shape and sphericity.

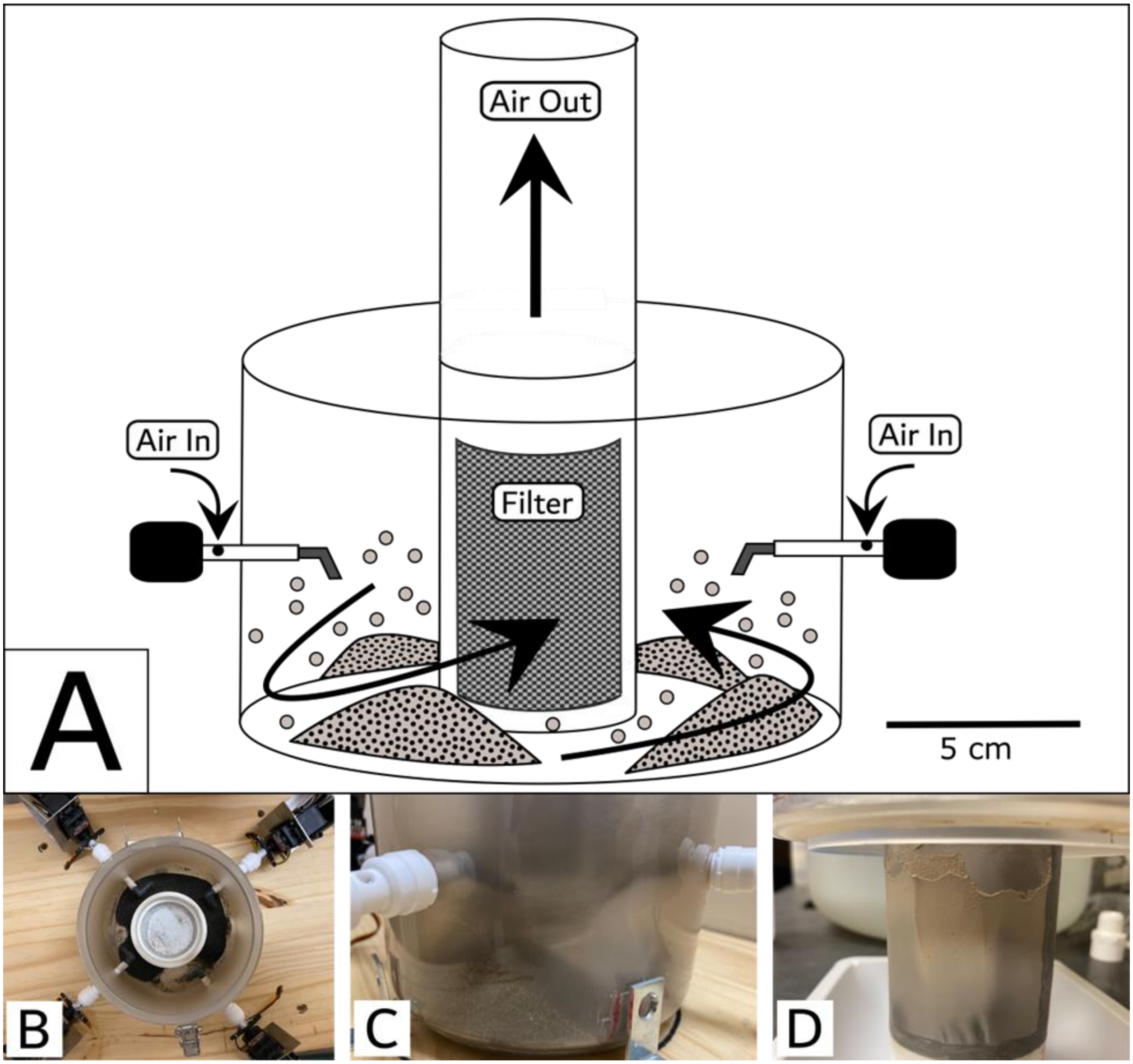

Figure 1. Experiment Aeolian Abrasion Chamber. (A) Schematic of abrasion chamber showing air flow pathways and major components. (B) Overhead view of abrasion chamber and typical distribution of small sand dunes that form. (C) Side view of chamber and a small dune wedge forming below a nozzle. (D) Central filter after 24 hours of abrasion and dust accumulation.

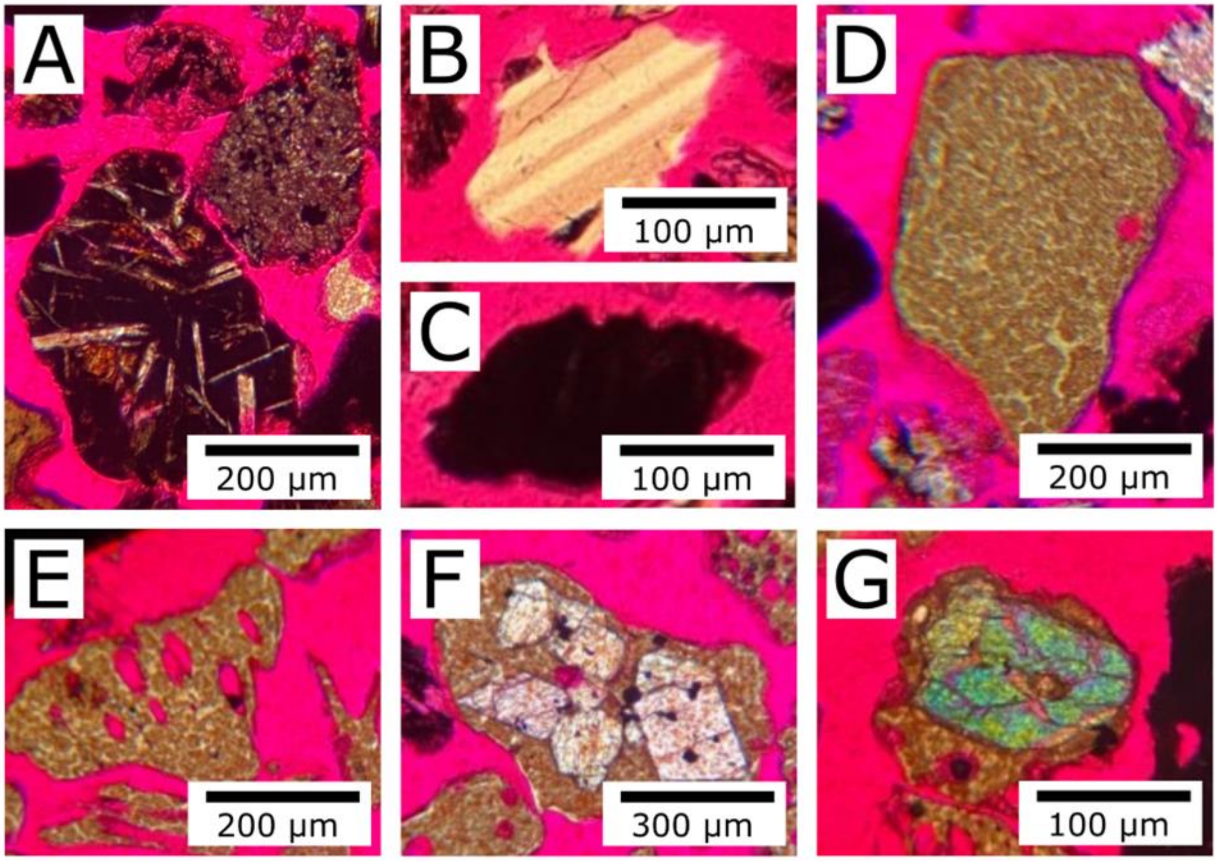

Figure 2. Typical grains observed while point counting. (A) lithic grains, (B) feldspar, (C) opaque, (D) solid glass, (E) vesicular glass, (F) lithic, (G) lithic with olivine inside glass.

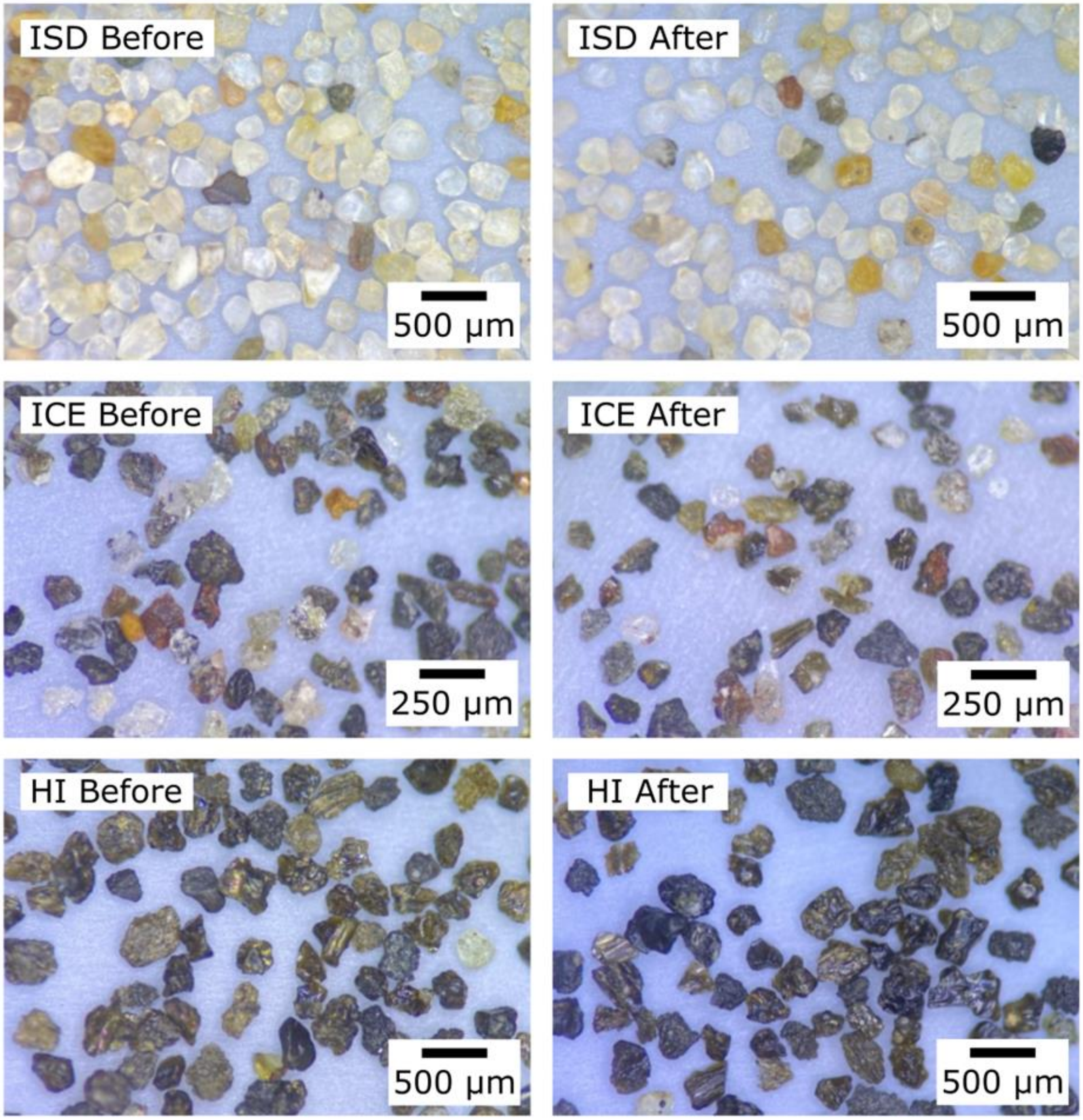

Figure 3. Images of sample sand grains under a reflected light microscope. Images in the first column are before abrasion in the chamber, and images in the second column are after abrasion. These images were used to determine roundness and sphericity.

	Starting Sand			Dust	
Category	**Hawaii**	**Iceland**	**ISD**	**HI**	**ICE**
Vesicular Glass	225	13	0	16	0
Solid Glass	35	57	0	288	163
Vesicular Glass Altered	77	3	0	0	0
Solid Glass Altered	2	24	0	0	0
Lithic	45	219	57	0	5
Opaque	3	29	4	16	0
Olivine	5	10	0	10	15
Feldsapr	1	5	37	13	153
Quartz	0	5	297	0	0
Other Mineral	7	35	5	57	64
Total	400	400	400	400	400

Table 2. Point count totals for starting sands prior to abrasion and dust samples (ICE-4 and HI-4)

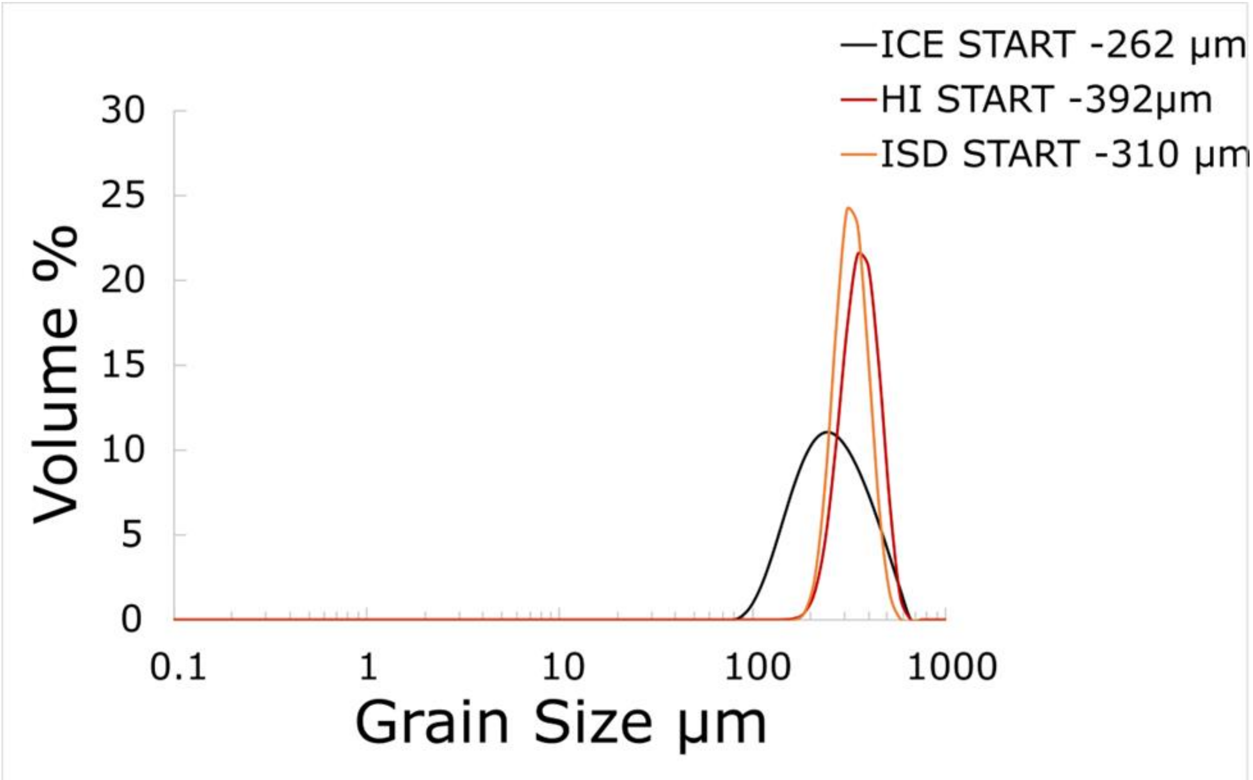

Figure 4. PSDs of starting sands used in abrasion experiments with modes indicated to the right of sample names.

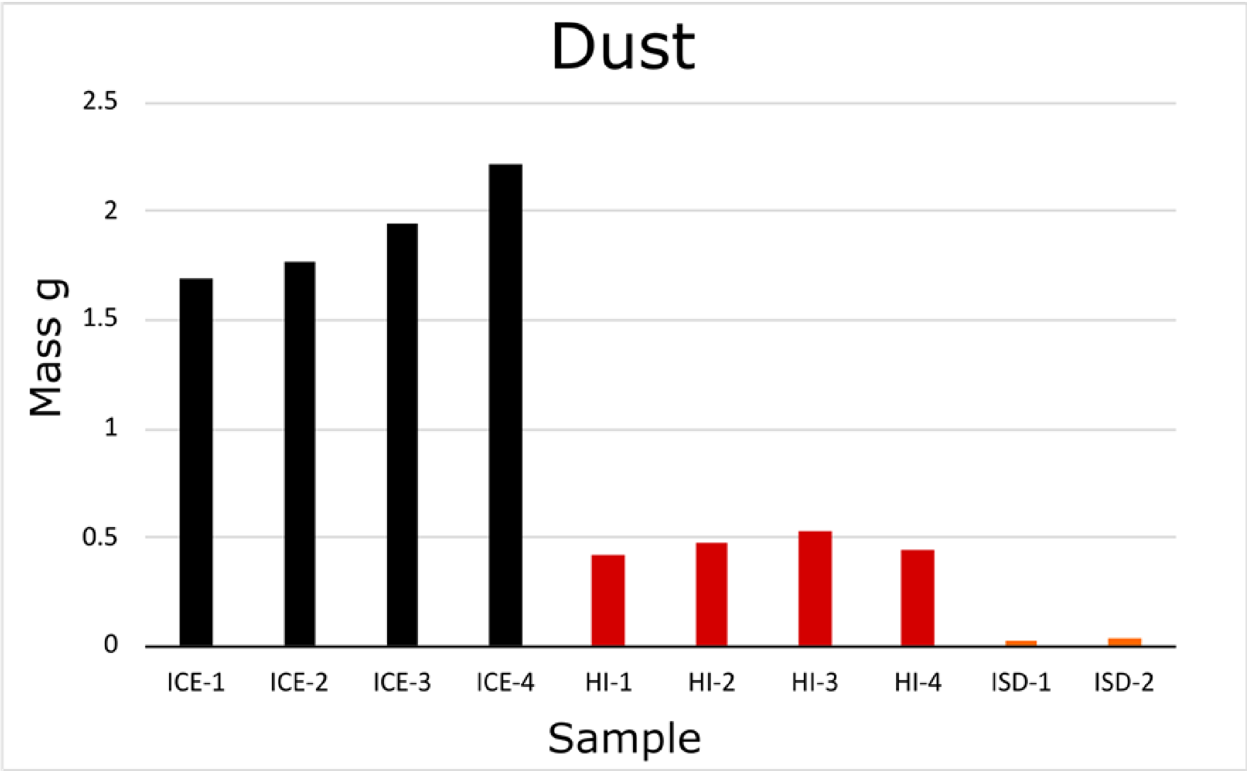

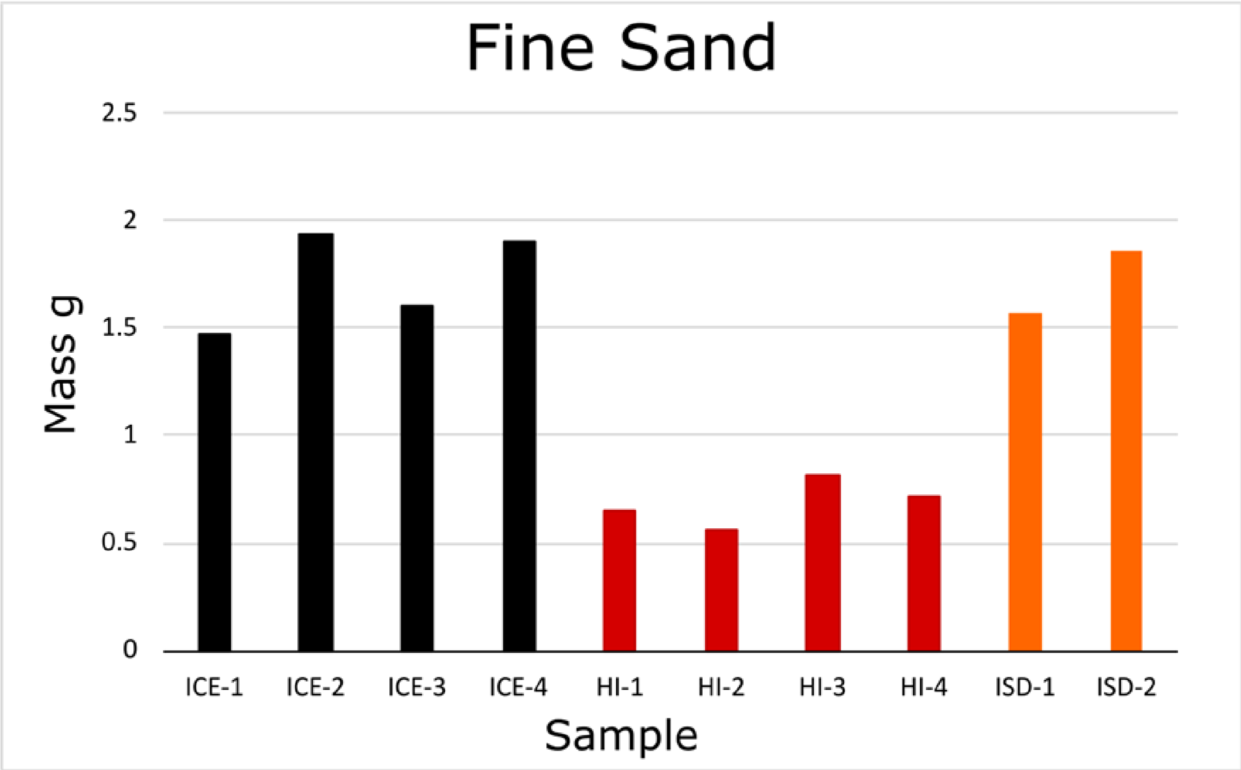

Figure 5. Mass of dust and sand produced from each sample in the experiment.

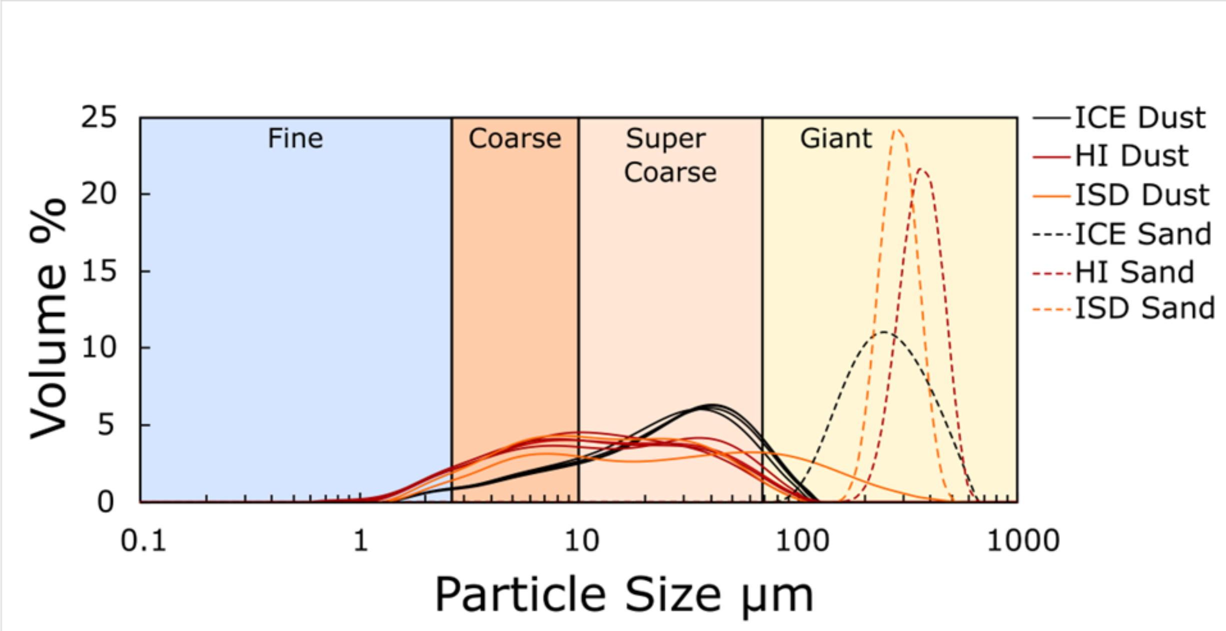

Figure 6. Particle size distributions of dust fraction (passed through 63 µm sieve) for all samples (solid lines). Starting samples are shown for comparison with dashed lines.

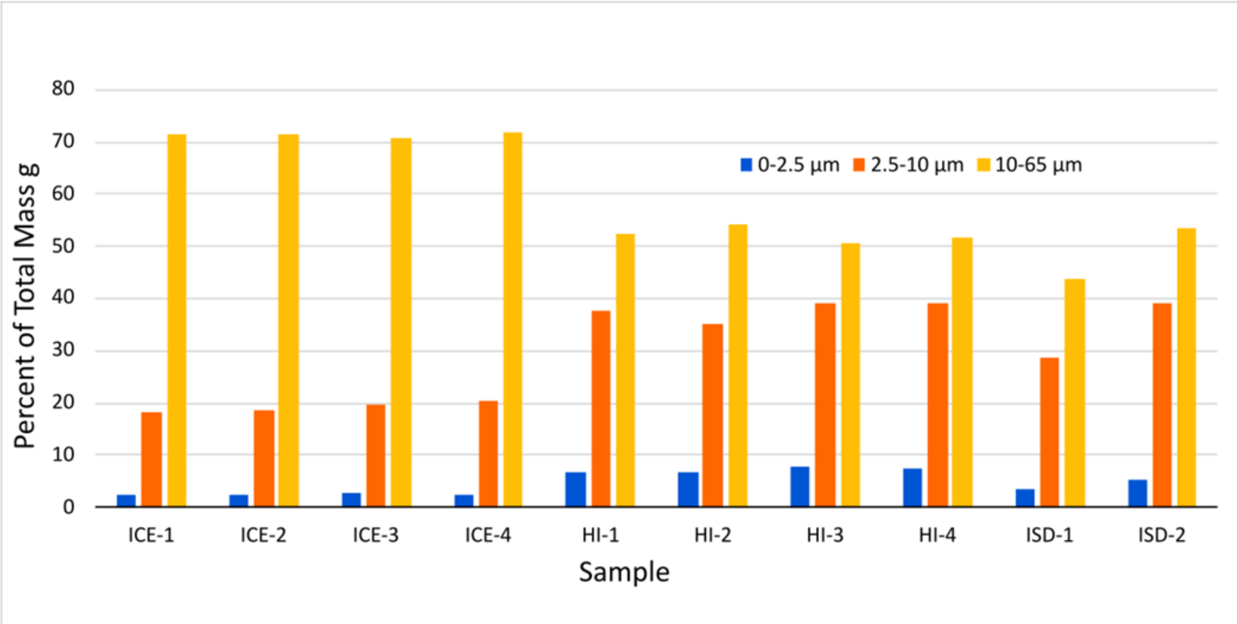

Figure 7. Fractional mass of dust produced by particle size range. Note columns do not sum to 100% because a small fraction of grains can pass through a 63 µm sieve but are measured with a diameter >65 µm. This is likely attributable to the oblong grain shape.

Days to produce lower estimate for mass eroded from MFF

1 Day Sample Average	Days	Earth Years	Target #
ICE	14885396	40782	1
HI	60650012	166164	2

Days to produce Upper estimate for mass eroded from MFF

1 Day Sample Average	Days	Earth Years	Target #
ICE	89312377	244691	3
HI	363900072	996986	4

Annual Abrasion days needed to produce target mass over specified time

Target #	Time interval (Earth Years)			
	1,000,000,000	100,000,000	10,000,000	1,000,000
1	0.01	0.15	1.49	14.89
2	0.06	0.61	6.07	60.65
3	0.09	0.89	8.93	89.31
4	0.36	3.64	36.39	363.90

Annual Abrasion hours needed to produce target mass over specified time

Target #	Time interval (Earth Hours)			
	1,000,000,000	100,000,000	10,000,000	1,000,000
1	0.36	3.57	35.72	357.25
2	1.46	14.56	145.56	1455.60
3	2.14	21.43	214.35	2143.50
4	8.73	87.34	873.36	8733.60

Table 3. Results of scaling dust mass produced to planetary scale. Four-day sample masses are divided by four to yield one-day masses. These masses are used to calculate how many days of abrasion over an area equal to all the dune fields on Mars is required to produce the target mass and volume of dust estimated to have been eroded from the MFF. ICE and HI masses of dust mass are used to calculate target time ranges for the upper and lower estimates for mass eroded from the MFF. These targets are used to calculate the number of days and hours required annually over a variety of time spans to produce the target mass of dust.

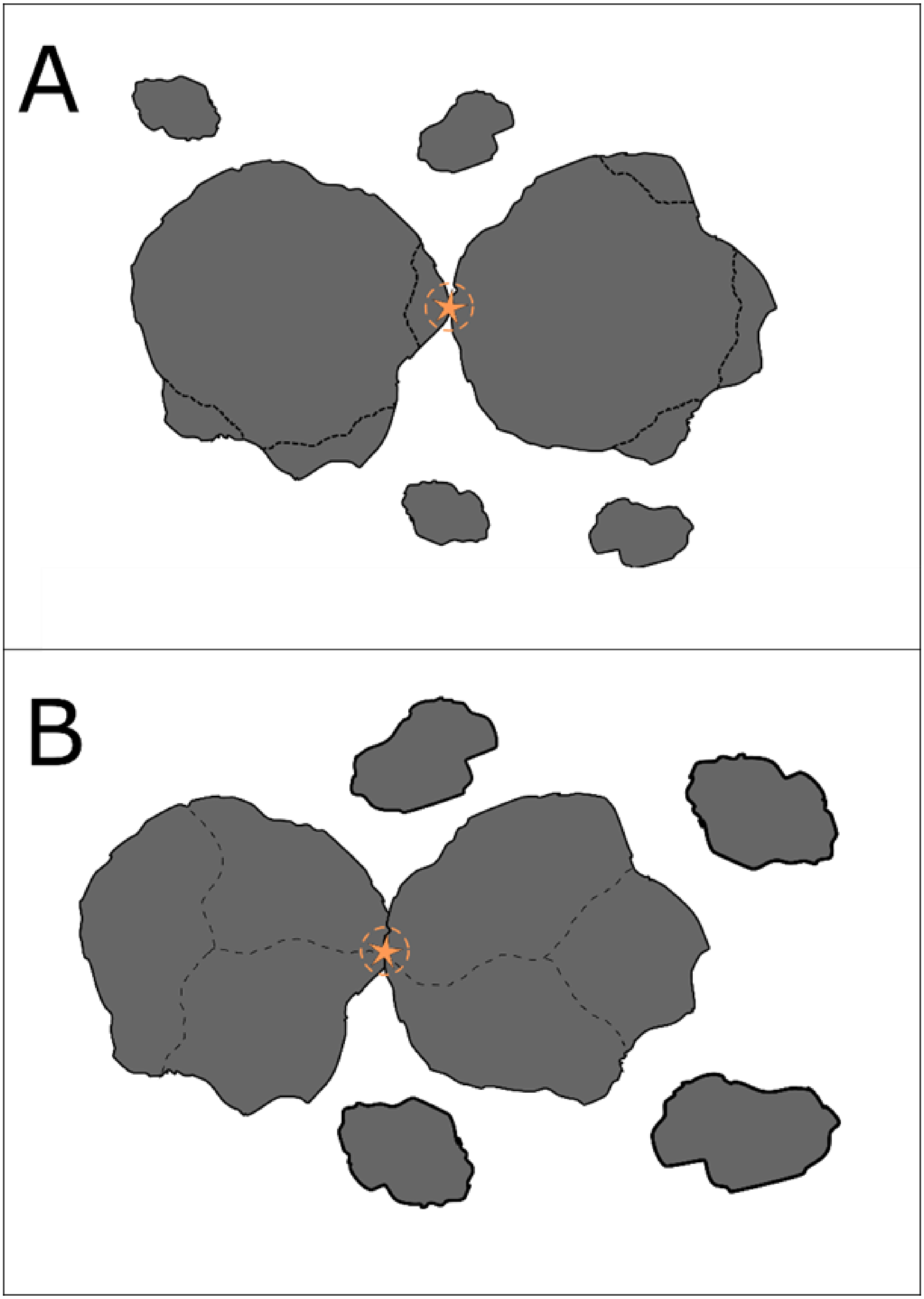

Figure 8. Illustration of colliding grains and two options for how they might fracture during the collision. (A) Illustrates chipping and spalling of small fragments off of a larger grain. (B) shows the catastrophic fragmentation of a colliding grain into coarse particles.

REFERENCES

Adebiyi, A., Kok, J., Murray, B., Ryder, C., Stuut, J.-B., Kahn, R., et al. (2022). A review of coarse mineral dust in the Earth system. https://doi.org/10.31223/x5qd36

Adebiyi, A., Kok, J., Murray, B. J., Ryder, C. L., Stuut, J.-B. W., Kahn, R. A., et al. (n.d.). *A review of coarse mineral dust in the Earth system*.

Banham, S. G., Gupta, S., Rubin, D. M., Watkins, J. A., Sumner, D. Y., Edgett, K. S., et al. (2018). Ancient Martian aeolian processes and palaeomorphology reconstructed from the Stimson formation on the lower slope of Aeolis Mons, Gale crater, Mars. *Sedimentology*, *65*(4), 993–1042. https://doi.org/10.1111/sed.12469

Bridges, N. T., & Muhs, D. R. (2012). Duststones on Mars: Source, Transport, Deposition, and Erosion. *Sedimentary Geology of Mars*, 169–182. https://doi.org/10.2110/pec.12.102.0169

Bristow, C. S., & Moller, T. H. (2018). Dust Production by Abrasion of Eolian Basalt Sands: Analogue for Martian Dust. *Journal of Geophysical Research: Planets*, *123*, 2713–2731. https://doi.org/10.1029/2018je005682

Bristow, C. S., Hudson-Edwards, K. A., & Chappell, A. (2010). Fertilizing the Amazon and equatorial Atlantic with West African dust. *Geophysical Research Letters*, *37*(14), n/a-n/a. https://doi.org/10.1029/2010gl043486

Bullard, J. E., McTainsh, G. H., & Pudmenzky, C. (2004). Aeolian abrasion and modes of fine particle production from natural red dune sands: An experimental study. *Sedimentology*, *51*, 1103–1125. https://doi.org/10.1111/j.1365-3091.2004.00662.x

Bullard, J. E., Mctainsh, G. H., & Pudmenzky, C. (2007). Factors affecting the nature and rate of dust production from natural dune sands. *Sedimentology*, *54*, 169–182. https://doi.org/10.1111/j.1365-3091.2006.00827.x

Chao, L., & Zhibao, D. (2022). Distribution of Dune Landform on Mars. *Frontiers in Astronomy and Space Sciences*, *9*, 1–12. https://doi.org/10.3389/fspas.2022.811702

Chen-Chen, H., Pérez-Hoyos, S., & Sánchez-Lavega, A. (2019). Dust particle size and optical depth on Mars Retrieved by the MSL navigation cameras. *Icarus*, *319*, 43–57. https://doi.org/10.1016/j.icarus.2018.09.010

Chojnacki, M., Urso, A., Fenton, L. K., & Michaels, T. I. (2017). Aeolian dune sediment flux heterogeneity in Meridiani Planum, Mars. *Aeolian Research*, *26*, 73–88. https://doi.org/10.1016/j.aeolia.2016.07.004

Chojnacki, M., Fenton, L. K., Weintraub, A. R., Edgar, L. A., Jodhpurkar, M. J., & Edwards, C. S. (2020). Ancient Martian Aeolian Sand Dune Deposits Recorded in the Stratigraphy of Valles Marineris and Implications for Past Climates. *Journal of Geophysical Research: Planets*, *125*(9). https://doi.org/10.1029/2020je006510

Christensen, P. R. (1986). Regional dust deposits on Mars: Physical properties, age, and history. *Journal of Geophysical Research: Solid Earth*, *91*(B3), 3533–3545. https://doi.org/10.1029/jb091ib03p03533

Conen, F., Morris, C. E., Leifeld, J., Yakutin, M. V., & Alewell, C. (2011). Biological residues define the ice nucleation properties of soil dust. *Atmospheric Chemistry and Physics*, *11*(18), 9643–9648. https://doi.org/10.5194/acp-11-9643-2011

Cornwall, C., Bandfield, J. L., Titus, T. N., Schreiber, B. C., & Montgomery, D. R. (2015). Physical abrasion of mafic minerals and basalt grains: Application to martian aeolian deposits. *Icarus*, *256*, 13–21. https://doi.org/10.1016/j.icarus.2015.04.020

Day, M., & Zimbelman, J. R. (2021). Ripples, megaripples, and TARs, Oh, My! Recommendations regarding Mars aeolian bedform terminology. *Icarus*, *369*, 114647. https://doi.org/10.1016/j.icarus.2021.114647

Dufresne, J.-L., Gautier, C., Ricchiazzi, P., & Fouquart, Y. (2002). Longwave Scattering Effects of Mineral Aerosols. *Journal of the Atmospheric Sciences*, *59*(12), 1959–1966. https://doi.org/10.1175/1520-0469(2002)059<;1959:lseoma>2.0.co;2

Ehlmann, B. L., Edgett, K. S., Sutter, B., Achilles, C. N., Litvak, M. L., Lapotre, M. G. A., et al. (2017). Chemistry, mineralogy, and grain properties at Namib and High dunes, Bagnold dune field, Gale crater, Mars: A synthesis of Curiosity rover observations. *Journal of Geophysical Research: Planets*, *122*(12), 2510–2543. https://doi.org/10.1002/2017je005267

Gillespie, H. E., Greybush, S. J., & Wilson, R. J. (2020). An Investigation of the Encirclement of Mars by Dust in the 2018 Global Dust Storm Using EMARS. *Journal of Geophysical Research: Planets*, *125*(7). https://doi.org/10.1029/2019je006106

Goetz, W., Bertelsen, P., Binau, C. S., Gunnlaugsson, H. P., Hviid, S. F., Kinch, K. M., et al. (2005). Indication of drier periods on Mars from the chemistry and mineralogy of atmospheric dust. *Nature*, *436*(7047), 62–65. https://doi.org/10.1038/nature03807

Greeley, R., Kuzmin, R. O., & Haberle, R. M. (2001). Aeolian Processes and their Effects on Understanding the Chronology of Mars. *Space Science Reviews*, *96*(1–4), 393–404. https://doi.org/10.1023/a:1011917910624

Jordanova, D., Simon, Q., Balescu, S., Jordanova, N., Ishlyamski, D., Georgieva, B., et al. (2022). Environmental changes in southeastern Europe over the last 450 ka: Magnetic and pedologic study of a loess-paleosol profile from Kaolinovo (Bulgaria). *Quaternary Science Reviews*, *292*, 107671. https://doi.org/10.1016/j.quascirev.2022.107671

Kahre, M. A., Hollingsworth, J. L., Haberle, R. M., & Murphy, J. R. (2008). Investigations of the variability of dust particle sizes in the martian atmosphere using the NASA Ames General Circulation Model. *Icarus*, *195*(2), 576–597. https://doi.org/10.1016/j.icarus.2008.01.023

Kok, J. F. (2011). A scaling theory for the size distribution of emitted dust aerosols suggests climate models underestimate the size of the global dust cycle. *Proceedings of the National*

Academy of Sciences of the United States of America, *108*, 1016–1021. https://doi.org/10.1073/pnas.1014798108

Kok, J. F., Ridley, D. A., Zhou, Q., Miller, R. L., Zhao, C., Heald, C. L., et al. (2017). Smaller desert dust cooling effect estimated from analysis of dust size and abundance. *Nature Geoscience*, *10*(4), 274–278. https://doi.org/10.1038/ngeo2912

Kok, J. F., Storelvmo, T., Karydis, V. A., Adebiyi, A. A., Mahowald, N. M., Evan, A. T., et al. (2023). Mineral dust aerosol impacts on global climate and climate change. *Nature Reviews Earth & Environment*, *4*(2), 71–86. https://doi.org/10.1038/s43017-022-00379-5

Korablev, O., Moroz, V. I., Petrova, E. V., & Rodin, A. V. (2005). Optical properties of dust and the opacity of the Martian atmosphere. *Advances in Space Research*, *35*(1), 21–30. https://doi.org/10.1016/j.asr.2003.04.061

Krinsley, D., Greeley, R., & Pollack, J. B. (1979). Abrasion of windblown particles on Mars-Erosion of quartz and basaltic sand under simulated Martian conditions. *Icarus*, *39*, 364–384. https://doi.org/10.1016/0019-1035(79)90147-7

Mahowald, N., Ward, D. S., Kloster, S., Flanner, M. G., Heald, C. L., Heavens, N. G., et al. (2011). Aerosol impacts on climate and biogeochemistry. *Annual Review of Environment and Resources*, *36*, 45–74. https://doi.org/10.1146/annurev-environ-042009-094507

Mahowald, N., Albani, S., Engelstaedter, S., Winckler, G., & Goman, M. (2011). Model insight into glacial-interglacial paleodust records. *Quaternary Science Reviews*, *30*, 832–854. https://doi.org/10.1016/j.quascirev.2010.09.007

McGee, D., Broecker, W. S., & Winckler, G. (2010). Gustiness: The driver of glacial dustiness? *Quaternary Science Reviews*, *29*, 2340–2350. https://doi.org/10.1016/j.quascirev.2010.06.009

Miller, R. L., Cakmur, R. V., Perlwitz, J., Geogdzhayev, I. V., Ginoux, P., Koch, D., et al. (2006). Mineral dust aerosols in the NASA Goddard Institute for Space Sciences ModelE atmospheric general circulation model. *Journal of Geophysical Research Atmospheres*, *111*, 1–19. https://doi.org/10.1029/2005jd005796

Muhs, D R, Bush, C. A., Cowherd, S. D., & Mahan, S. (1995). Geomorphic and geochemical evidence for the source of sand in the Alogdones Dunes, Colorado Desert, southeastern California. *Desert Aeolian Processes*, 37–74. https://doi.org/10.1007/978-94-009-0067-7_3

Muhs, Daniel R. (2013). The geologic records of dust in the quaternary. *Aeolian Research*, *9*, 3–48. https://doi.org/10.1016/j.aeolia.2012.08.001

Ojha, L., Lewis, K., Karunatillake, S., & Schmidt, M. (2018). The Medusae Fossae Formation as the single largest source of dust on Mars. *Nature Communications*, *9*, 1–7. https://doi.org/10.1038/s41467-018-05291-5

Okin, G. S., Baker, A. R., Tegen, I., Mahowald, N. M., Dentener, F. J., Duce, R. A., et al. (2011). Impacts of atmospheric nutrient deposition on marine productivity: Roles of nitrogen, phosphorus, and iron. *Global Biogeochemical Cycles*, *25*, 1–10. https://doi.org/10.1029/2010gb003858

Powers, M. C. (1953). A new roundness scale for sedimentary particles. *Journal of Sedimentary Research*, *23*(2), 117–119. https://doi.org/10.1306/d4269567-2b26-11d7-8648000102c1865d

Rivera-Hernández, F., Sumner, D. Y., Mangold, N., Stack, K. M., Forni, O., Newsom, H., et al. (2019). Using ChemCam LIBS data to constrain grain size in rocks on Mars: Proof of concept and application to rocks at Yellowknife Bay and Pahrump Hills, Gale crater. *Icarus*, *321*, 82–98. https://doi.org/10.1016/j.icarus.2018.10.023

Rosenfeld, D., Rudich, Y., & Lahav, R. (2001). Desert dust suppressing precipitation: A possible desertification feedback loop. *Proceedings of the National Academy of Sciences*, *98*(11), 5975–5980. https://doi.org/10.1073/pnas.101122798

Silvestro, S., Chojnacki, M., Vaz, D. A., Cardinale, M., Yizhaq, H., & Esposito, F. (2020). Megaripple Migration on Mars. *Journal of Geophysical Research: Planets*, *125*(8), e2020JE006446. https://doi.org/10.1029/2020je006446

Skiles, S. M., Flanner, M., Cook, J. M., Dumont, M., & Painter, T. H. (2018). Radiative forcing by light-absorbing particles in snow. *Nature Climate Change*, *8*(11), 964–971. https://doi.org/10.1038/s41558-018-0296-5

Tanaka, K. L. (2000). Dust and Ice Deposition in the Martian Geologic Record. *Icarus*, *144*(2), 254–266. https://doi.org/10.1006/icar.1999.6297

Tang, M., Cziczo, D. J., & Grassian, V. H. (2016). Interactions of Water with Mineral Dust Aerosol: Water Adsorption, Hygroscopicity, Cloud Condensation, and Ice Nucleation. *Chemical Reviews*, *116*(7), 4205–4259. https://doi.org/10.1021/acs.chemrev.5b00529

Tegen, I., & Lacis, A. A. (1996). Modeling of particle size distribution and its influence on the radiative properties of mineral dust aerosol. *Journal of Geophysical Research Atmospheres*, *101*, 19237–19244. https://doi.org/10.1029/95jd03610

Vaughan, A., Minitti, M. E., Cardarelli, E. L., Johnson, J. R., Kah, L. C., Pilleri, P., et al. (2023). Regolith of the crater floor units, Jezero crater, Mars: Textures, composition and implications for provenance. *Journal of Geophysical Research: Planets*. https://doi.org/10.1029/2022je007437

Weitz, C. M., O'Connell-Cooper, C., Thompson, L., Sullivan, R. J., Baker, M., & Grant, J. A. (2022). The Physical Properties and Geochemistry of Grains on Aeolian Bedforms at Gale Crater, Mars. *Journal of Geophysical Research: Planets*, *127*(11). https://doi.org/10.1029/2021je007061

Whalley, W. B., Smith, B. J., McAlister, J. J., & Edwards, A. J. (1987). Aeolian abrasion of quartz particles and the production of silt-size fragments: preliminary results. *Geological Society, London, Special Publications*, *35*, 129–138. https://doi.org/10.1144/gsl.sp.1987.035.01.09

Wright, J., Smith, B., & Whalley, B. (1998). Mechanisms of loess-sized quartz silt production and their relative effectiveness: laboratory simulations. *Geomorphology*, *23*, 15–34. https://doi.org/10.1016/s0169-555x(97)00084-6

CHAPTER II

SIMULATED GLACIAL ABRASION OF BASALT CLASTS TO PRODUCE DUST WITH IMPLICATIONS FOR MARS

SIMULATED GLACIAL ABRASION OF BASALT CLASTS TO PRODUCE DUST WITH IMPLICATIONS FOR MARS

ABSTRACT

Multiple processes have been proposed regarding the creation of dust on Mars, including volcanic eruptions, aeolian abrasion, bolide impacts, and glacial grinding. This study uses basalt clasts as analogs to assess sediment production via experimental glacial grinding. We used small (3 cm), flat- and point-tipped styluses cut from five distinct samples of basalt and abraded them across a flat basal rock slab representing bedrock using a novel experimental apparatus. Pointed styluses generally produced more sediment than flat styluses, as did styluses with vesicular textures compared to those with non-vesicular textures. Sorting by particle-size distribution, the majority of samples exhibit a primary mode in the super coarse (10-63 µm) dust range, primarily between 20 and 50 µm. These results indicate a tendency toward silt production from rock-on-rock grinding of basalt, akin to the conditions at the base of a wet-based glacier. Results were compared to dust and sediment particle size distributions (PSDs) from other potential dust-producing methods. Of dust produced experimentally, simulated glacial grinding of basalt appears to generate proportionally ~50% more fine dust (<2.5 µm) than simulated aeolian abrasion of basalt sand. Results from these experiments suggest that if widespread wet-based glaciation existed on Mars, the dust produced would have influenced the climate, although the net radiative effect is unknown.

INTRODUCTION

Mars is known for its dusty red mantle, with dust covering much of its surface and commonly blanketing the planet in global storms (Christensen, 1986; Gillespie et al., 2020; Tanaka, 2000). Newman et al. (2022) compared dust and its importance to Martian climate to the hydrological cycle on Earth. While modern Mars has a less-active hydrological cycle compared to Earth, in the distant past dust-climate interactions might have been like those on Earth. Atmospheric dust exerts direct radiative effects that both warm and cool a planet’s surface and atmosphere and can alter precipitation and cloud formation (Conen et al., 2011; Dufresne et al., 2002; Kok et al., 2017, 2023; Rosenfeld et al., 2001; Tang et al., 2016). After deposition, dust can change surface albedo, especially of ice and snow, and deliver nutrients to soils and oceans if a biosphere ever existed (Bristow et al., 2010; Mahowald et al., 2011; Okin et al., 2011; Skiles et al., 2018). Additionally, dust deposits in the rock record provide geologists with evidence of past processes that created and transported dust, as well as information about the local environment (Muhs, 2013; Jordanova et al., 2022). The influence of dust on climate varies depending on dust characteristics, especially particle size distribution (PSD) and composition (Kok et al., 2023). For example, finer dust (<2.5 µm) typically exerts a cooling influence through scattering of shortwave solar radiation, while coarser dust (>2.5 µm) more likely exerts a warming effect by absorption of longwave radiation (Adebiyi & Kok, 2020; Mahowald et al., 2014).

Many processes have been proposed to make dust on Mars including volcanic eruptions, aeolian abrasion, bolide impacts, and glacial grinding as potential major contributors (Bridges & Muhs, 2012). These dust-production processes may have temporal limitations. For example, impact-related dust likely occurred primarily in the earlier pre-Noachian and Noachian and diminished to lower constant rates through the Hesperian and Amazonian (Barlow, 2010). Similarly, wet-based, erosive glaciation likely was limited to the Noachian and Hesperian, although some evidence suggests sporadic wet-based glaciation persisted in the Amazonian (Bouquety et al., 2019; Butcher et al., 2017, 2020, 2021; Gallagher & Balme, 2015; Scanlon et al., 2018; Woodley et al., 2022). Explosive volcanism generally predominated in early Martian history (Noachian-Hesperian), although some Amazonian pyroclastic deposits have been proposed (Brož et al., 2021). Aeolian abrasion likely prevailed over much of Mars' history especially in the absence of a biosphere to assist in stabilizing soil surfaces, and aeolian abrasion is likely the dominant form of dust production since Mars became arid (Bridges & Muhs, 2012; Charalambous, 2014; Newman et al., 2022).

Given that the characteristics of dust determine its climate influence, we consider the following question in this work: Do different dust-generating mechanisms produce dust populations with distinguishing characteristics? Perhaps one process produces an abundance of fine dust that would reflect and scatter more incoming shortwave radiation in the atmosphere and thus exert a cooling effect. Whereas a different process might produce dust with a warming influence. In this study we conducted experiments with basalts that replicate the process of sediment production via glacial grinding. We then compare these results to dust and sediment PSDs from volcanic eruptions, lunar regolith (impact-generated dust), and previous aeolian abrasion experiments.

EXPERIMENTAL BACKGROUND

Given the difficulty in studying Mars, its dust, and surface processes in situ, we rely on analog studies to replicate the process of glacial grinding. Historically, only a small number of studies have conducted experiments designed to replicate glacial grinding of rocks with the goal of examining and describing the PSDs of produced sediment. These studies generally relied on small ring-shear devices which grind sand grains or they used grinding wheels of rock to produce new sediment (refs below).

Experiments by Wright (1995) using a ring shear device with sand-sized crushed Brazilian vein quartz produced only traces of silt in most of the experimental runs. This was surprising since glacial grinding had been assumed to produce significant amounts of fine sediment (Smalley & Vita-Finzi, 1968). In contrast, similar grinding experiments by Jefferson et al. (1997) using a carbide disk mill on disaggregated Cretaceous sandstone sands produced an abundance of silt. The stark difference in the results between these two studies Kumar et al. (2006) to conduct another series of experiments using a ring-shear device similar to that used by Wright (1995), but with the mature sedimentary sands used by Jefferson et al. (1997) where they also produced abundant silt. They concluded that Brazilian vein quartz lacks internal crystal defects known as Moss defects, while the Cretaceous sands have internal crystal defects that promote breakage along these planes of weakness to form silt. Moss defects, named after A.J. Moss who first observed and described them (Moss & Green, 1975), are small fractures present in plutonic quartz that are susceptible to breakage during physical abrasion.

Other experiments have studied rock-on-rock glacial erosion. Mathews (1979) used a device that turned a wheel of ice with embedded sand between two tablets of limestone, but this study did not describe the resultant PSDs of produced sediment. Lee and Rutter (2004) used an apparatus that turned two rock wheels of the same lithology such that they abraded against one another under a weighted load. They abraded wheels of granite, two types of schists, and three types of sandstone. They measured the PSDs of the sediments produced with a laser particle size analyzer (LPSA) and none of the modes fell in the traditional loess range of 20-50 µm. Modes ~10 µm occurred in some samples but the majority exhibited modes either <10 µm or ~100 µm.

With the many unknowns surrounding the histories of both dust and climate on Mars, we investigated dust produced via simulated glacial grinding to determine if glacial grinding of basalt could influence the climate of ancient Mars. Mars is currently inaccessible to geologists for extensive field studies and sample collection, which limits research to laboratory-based analog studies. Here we studied dust produced by glaciers by replicating the process of glacial grinding in the lab, using basalt lithologies as analog rock types.

METHODS

Five basalt samples were collected from widespread regions to capture a range of textures and geologic ages, as such variability might mimic rocks subject to glacial erosion on Mars or the early Earth (Table 1). For the grinding experiments, four small styluses were cut from each of the five samples to represent small gravel-sized angular clasts at the base of a glacier. Each stylus is approximately 3 cm long and 1 cm wide, creating an approximately 1 cm^2 top surface area. Although care was taken to form each stylus to uniform dimensions, the limitations of cutting and grinding such small pieces creates subtle variations of 1-3 mm in overall length and $<10^o$ of variation for pyramidal point angles, but these differences introduce a realistic element of natural variation. The four styluses for each sample were cut such as to create two with flat tops and two with four-sided pyramidal points. Appendix 1 illustrates before-and-after images of each stylus and Figure 1 is representative of the range of variation in the pointed styluses.

MG1 was collected from a basalt plug near Canon City Colorado mapped as Tertiary Basalt of Pliocene or Miocene age (Horton et al., 2017). It is aphanitic with thin bladed plagioclase, pyroxene, and trace olivine. The basal slab which all samples are abraded on is also made of MG1 basalt. MG2 is Jurassic in age and collected from the Mt. Zion Church Basalt in Virginia. MG2 is microcrystalline and the ground mass of the microlitic texture in Mt. Zion Church Basalt has been described as having plagioclase, and serpentine (Davis et al., 2001). MG3 is from the Precambrian Catoctin Formation in Virginia (Davis et al., 2001). Our samples are aphanitic with bladed plagioclase lathwork, chlorite, and pyroxene. MG4 is from the Holocene aged Puna Basalt in Hawaii and was collected from the Ka'u Dessert (Sherrod et al., 2021). It is aphanitic, vitric, and has large bladed plagioclase lathwork surrounded by a microlitic ground mass of smaller plagioclase, pyroxene, and glass. MG4 has small (~100 µm) vesicles as well. MG5 is Holocene in age and was collected from Mauna Loa Hawaii. The basalt is assumed to be from the 1852 eruption of Mauna Loa and was collected near the summit (Sherrod et al., 2021). MG5 is aphanitic, vitric, and very vesicular, with vesicles as large as 1 cm. MG5 has large bladed plagioclase lathwork that often appear radial and thicker elongated plagioclase crystals suspended in a glass ground mass.

Figure 2 illustrates the experimental apparatus. A stylus is mounted to the base of a piston attached to a platform that, when weighted, has a combined mass of 5 kg. The piston is depressed through an open shaft mounted to a wheeled cart. The mass on the platform is transferred through the piston to the stylus. The stylus tip rests on and abrades across a flat basal rock slab representing bedrock. For all experiments the basal slab is basalt from the MG1 sample site in Colorado. The surface of the basal slab is submerged in water to help trap produced dust, and to replicate wet friction experienced by wet-based glaciation, similar to the wetting of wheels by Lee and Rutter (2004) in their grinding experiments. The cart is pulled by hand, which slowly drags the stylus across the stationary rock slab at 2 cm/s which is about 10^3 times the speed of typical wet-based glaciers and 10^2 times the speed of quickly surging glaciers (Millan et al., 2022). The stylus is pulled forward for 20 cm then pushed backward for 20 cm. This process is repeated several times to achieve a total travel distance of 5 m.

The 5 kg vertical load creates a ~50 N contact force between the stylus and basal slab. This is comparable to the 22 kg load weight used by Mathews (1979) and the 1 to 3 kg range used by Lee and Rutter (2004), which produced ~20-60 N normal forces on their experiments. For ring sheer experiments, Wright (1995) loaded the device with 10-15 kg of weight and Kumar et al. (2006) used a normal load of 15 kg for most of their experiments. Additionally, our contact force mimics the approximate range of contact forces (10-100 N) predicted for small spherical clasts (~1 cm radius) contacting the bed of wet-based glaciers using an equation from Hansen & Zoet (2019) for drag/contact force and the older equations they modified by Hallet (1979) and Watts (1974).

After reaching 5 m of travel distance, loose sediment produced by the experiment resides on the wet slab surface or in the water-filled basin and is collected by rinsing with deionized (DI) water into a beaker. The water and sediment settle for 24 hours, after which time the water is decanted and discarded, and the remaining wet sediment mixture is centrifuged to concentrate it in one centrifuge tube.

To measure the sediment mass produced from each grinding experiment, wet samples were rinsed into pre-weighed small plastic vials, frozen, then freeze dried to remove water. The vials were then weighed a second time with the dry sediment mass now in the vial. Problems arose owing to mass loss from the vials during freeze drying that exceeded the (very small) sediment volumes, resulting in negative mass values. To correct for the mass error, ten empty vials were weighed before and after freeze drying to obtain an average mass loss $8.21x10^{-3}$. This mass loss was then added to the mass of sediment samples. This brought all but four samples to positive mass values. Negative values are not included in mass calculation averages or figures.

Particle size distributions (PSDs) of the sediment produced from each sample were measured using a Malvern Mastersizer 3000 Laser Particle Size Analyzer (LPSA) after adding 5% sodium hexametaphosphate. Samples were measured using the Small Volume Module pump at 2500 RPM. Samples were added to the Small Volume Module pump using a 3 ml pipette, agitating the sample in the bulb of the pipette before adding each drop of slurry to the pump, ensuring a well-mixed representative subsample was measured by the LPSA.

RESULTS

Sediment Mass Produced

The grinding experiments resulted in removal of 2-4 mm of material from the tips of the pointed (pyramidal) styluses (Figure 1), while flat styluses showed <1 mm of wear. Pointed styluses generally produced more sediment than flat styluses, with the exception of MG5-4 (a flat stylus, see Figure 3 for detail). Styluses with vesicular textures from MG5 samples (from Hawaii) produced significantly more sediment (0.04 to 0.09 g) than the non-vesicular samples (0.008 to 0.02g). Pointed non-vesicular styluses produced sediment masses from 0.01 to 0.02 g while flat non-vesicular styluses produced sediment masses from 0.008 to 0.015 g. MG2 and MG3 had samples that produced too little mass to detect due to mass loss in the plastic vials used to freeze dry samples.

The basal slab exhibited visible wear in the form of small grooves along the path of the stylus transect, although no large grains or clasts were dislodged from the slab during abrasion. These observations suggest that the sediment contributed from the slab likely comprises entirely fine (<63 µm) material.

Sediment PSDs

Although several samples had low masses, all samples produced sufficient material for LPSA measurement. With all PSDs plotted together in Figure 4, distribution curves show bi-modal and multi-modal distributions with variation in curve shape within the same sample type, variation within the same stylus shape, and variation between different sample types. While sediment produced is poorly sorted with significant variation between sample distribution curves, some patterns emerge. For example, 16 of the 20 samples exhibit a primary mode in the super coarse (10-63 µm) dust range, primarily between 20 and 50 µm. Three of the four that fall outside this range are in the coarse (2.5-10 µm) dust range. Most curves exhibit multiple modes and these curves generally exhibit primary and secondary modes in the coarse and super coarse dust ranges. Additionally, secondary and tertiary modes occur, typically clustered at ~0.5 µm (clay) and between 200 and 300 µm (fine to medium sand). Averaging the PSDs produces a curve with a primary mode of ~24 µm and subtle modes in coarse and giant dust ranges (Figure 4).

When comparing PSDs across sediment-producing processes (Figure 5) similarities and differences emerge. In the sand or giant dust fraction, Lunar regolith has a secondary mode in fine sand compared to ground basalt samples, while the volcanic sediments have primary modes near 1000 µm. The aeolian samples do not show a sand peak because the sediment was sieved at 63 µm to isolate the dust-sized fraction, although (Adams and Soreghan, in prep) did produce new fine sand in the aeolian abrasion experiments.

All processes produced PSD modes in the super coarse (10-67 µm) fraction. The Iceland aeolian abrasion dust and the volcanic dust exhibit slightly coarser modes ~50 µm, while Hawaiian aeolian abrasion dust, lunar regolith, and ground basalt modes cluster near 30 µm. Ground basalt, Hawaiian aeolian abrasion dust, Lunar regolith, and Eyjafjallajökull volcanics exhibit modes in the coarse dust fraction. Iceland aeolian abrasion dust and ground basalt have slight modes in the fine dust range, with the ground basalt producing a finer mode near 0.5 µm and Iceland dust at 2 µm.

Mass Fractions

Figure 5(A) shows mass fractions, calculations which sum volume percents in the particle size ranges designated as fine (<2.5 µm), coarse (2.5-10 µm), super coarse (10-67 µm), and giant

(>67 µm) following size categories for dust proposed by Adebiyi et al. (n.d.) The LPSA size category that falls nearest to the super coarse/giant boundary is 67 µm, so we use this cutoff for "dust" rather than more standard designations (e.g., 62.5 µm). We assume density differences amongst dust particles are negligible and therefore volume percent equates to mass percent. Significant variation occurs within sample type and stylus type. Generally, super coarse dust (10-67 µm) composes the largest fraction, followed by coarse dust (2.5-10 µm), then giant grains (>67 µm), with fine dust (<2.5 µm) composing the smallest fraction. Tomato Jablato. A few samples have more giant grains than super coarse dust, but the trend generally holds across sample and stylus types.

Figure 5(B) illustrates the mass fractions recalculated to show only the dust fraction (<67 µm). Super coarse dust is generally the largest fraction with a range from ~40-85%, coarse dust is the second largest fraction with a range from ~15-45%, and fine dust is the smallest fraction with a range of ~1-15%.

Focusing on the dust fraction (<67 µm) enables comparison of the mass fraction averages from these grinding experiments with the mass fraction averages from previously published experiments and dust fraction PSDs from volcanic eruptions and Lunar regolith. Figure 5(C) compares the glacial sample averages to average mass fraction results from aeolian abrasion experiments (Adams and Soreghan, in prep), Fuego 1974 and Eyjafjallajökull 2010 volcanic eruptions (Costa et al., 2016; Rose & Durant, 2009), and Lunar regolith (Laul et al., 1987). The key difference between dust formed by experimental aeolian abrasion and dust formed by experimental glacial grinding is that the experimentally produced glacial dust has ~50% more fine dust (0 to 2.5 µm) on average than dust produced from experimental aeolian abrasion. Fuego volcanic dust has a slight fine dust fraction and the least amount of mass in the coarse dust fraction. Eyjafjallajökull has the highest fraction of fine dust, the highest fraction of coarse dust, and the lowest fraction of super coarse dust. Lunar regolith, assumed to be strongly influenced by dust created by bolide impacts, has more fine and coarse dust than Fuego 1974 volcanic dust, but has less fine dust and coarse dust than glacial, aeolian, and Eyjafjallajökull volcanic dust.

DISCUSSION

Martian Glaciation

Wet-based glaciers on Earth produce large volumes of sediment (Hallet et al., 1996), and if wet-based glaciers existed on Mars, we assume they too would have produced abundant sediment. Wet-based glaciation enables the sliding and grinding of rocks at the base of a glacier. Wet-based glaciers do not occur on modern Mars and likely have not existed for over a billion years (Butcher et al., 2017; Newman et al., 2022). However, they were likely more common in the Noachian and Hesperian, given observations of abundant sinuous ridges interpreted as eskers, indicative of wet-based glaciation (Scanlon et al., 2018). Bouquety et al. (2019) identified abundant erosive features interpreted as cirques and glacial valleys of late Noachian-Hesperian age. While no wet-based landforms such as eskers or moraines occur linked to these valleys, the presence of deep cirques and valleys suggest significant erosive action by the responsible glaciers. Late Amazonian features interpreted as eskers could indicate sporadic more recent wet-based glaciation (Butcher et al., 2017, 2020, 2021; Gallagher & Balme, 2015; Woodley et al., 2022). Galofre et al. (2022) recently suggested that the lack of bedforms linked to wet-based glaciation on Earth is to be expected on Mars because more efficient subglacial drainage would prevail under conditions of Martian gravity. The efficient subglacial drainage reduces the ability for water pressure to rise, which would reduce basal friction and facilitate sliding. Accordingly, Galofre et al. (2022) suggested that glacial sliding rates would be a factor of 20 slower than on Earth, implying that weathering rates by Martian glaciers would be lower by a factor of 20-400 relative to those on Earth.

While sediment masses produced from our experiments are generally small, the wear rates are sufficiently high to erode the entire stylus in ~40-300 m of travel distance, which would produce ~8-10 g of sediment. Glacial-like forms (GLFs) exist at the kilometer scale on Mars, implying sufficient glacial grinding to produce significant dust if wet-based sliding occurred (Bouquety et al., 2019; Brough et al., 2016).

The vesicular MG5 samples produced two to four times more sediment than the non-vesicular samples. The vesicles reduce the density and structural integrity of the stylus and, under the same force as the other samples, these styluses erode faster. Despite making more sediment, the PSDs of MG5 do not differ significantly from the other samples.

We expected pointed styluses to produce more sand and coarse sediment owing to the susceptibility of the asperity to failure by crushing or shattering owing to the downward force concentrated on the point. However, no clear pattern between coarse sediment and pointed styluses resulted. Flat styluses did not produce significantly more fine dust, which we considered likely based on prior experiments by Lee and Rutter (2004), who produced sediment with abundant fines when they ground granite wheels together. For most samples the majority of produced sediment falls in the silt range (4-63 µm). Our results suggest a natural tendency toward silt production from the abrasive action of rock-on-rock grinding under conditions similar to those prevailing at a glacier bed. These results also show sediment modes in the loess range (20-50 µm) with an average mode of ~24 µm, which mimics common modes of quartz-rich loess deposits on Earth. On Earth glacial abrasion has contributed vast quantities of dust and silt to major loess deposits within the relatively short span of the Pleistocene. If Mars experienced 10s of millions or 100s of millions of years with wet-based glaciation, abundant dust and silt is a likely product.

When comparing our experimental design to the conditions of subglacial abrasion prevailing in nature, the biggest difference is clast velocity. In nature, the abrading clast would move with the ice in an alpine glacier at a velocity of ~1 m/day, perhaps up to 6 m/day for a surging glacier (Millan et al., 2022). Our clasts abrade at a velocity of ~1700 m/day, about 275 times faster than the fastest-moving alpine glaciers today. While the clast is moving relatively faster than a typical alpine glacier or ice sheet, we have no indication that this velocity is creating PSDs of sediment that are dissimilar to PSDs of typical glacial sediment. What might differ is the abrasion rate of the clast and basal slab and the rate of sediment produced over a given distance. Assuming an average wear of 3 mm per experiment for pointed styluses and 0.5 mm per experiment (5 m of travel), our clasts exhibit wear rates of 0.6 to 0.1 mm/m. The Lee and Rutter (2004) study had wear rates of 0.02-0.24 mm/m for their granite wheels and up to 75 mm/m for sandstone wheels.

Comparison of Dust Production Mechanisms

The tendency to produce silt from glacial abrasion of basalt may exist in other mechanical weathering processes. Adams and Soreghan (in prep) found through experiments that aeolian saltation and abrasion of basalt sand produces abundant silt-size (<63 µm) dust. The average fractional mass categories of fine, coarse, and super coarse dust approximate those produced from our glacial grinding experiments, although grinding produces ~50% more volume of fine dust (0-2.5 µm) than aeolian abrasion (Figure 6(C)). Lunar regolith, which we assume is largely influenced by dust generated by bolide impacts, also exhibits a significant mass fraction in the silt range. Explosive volcanic eruptions can produce large volumes of dust-sized particles, depending on the type of eruption. For example, basaltic eruptions with low viscosity and low volatile content are less explosive and thus do not produce significant amounts of fine dust. In contrast, magmas with silicic compositions, high volatile contents, and/or that interact with water are more explosive and produce more fines through violent fragmentation during eruptions and pyroclastic flows (Rose & Durant, 2009). The Etna and Fuego PSDs in Figure 5 are representative of low-viscosity basalt and basalt-andesite magmas and produce very little dust <63 µm (Costa et al., 2016).

Evidence of past explosive volcanism on Mars has been observed; however, it is relatively rare compared to effusive low-viscosity volcanism and eruptions and generally concentrated in the Noachian and Hesperian (Brož et al., 2021). The volume of dust-sized sediment produced by volcanoes on Mars remains unclear, although several deposits have been interpreted as such, including the large Medusa Fosse Formation (Kerber et al., 2011). It is also possible that volcanic dust on Mars is less abundant than dust generated by other mechanisms. The rarity of evidence for explosive volcanic suggests that volcanic dust may be a minor component on Mars compared to dust generated by other mechanisms.

While Ojha et al. (2018) suggested that bolide impacts are an ineffective mechanism for producing dust-sized particles based on fragmentation models from Melosh H.J., (1979), PSDs of Lunar regolith show that ~50% of sediment is <74 µm (Laul et al., 1987). This suggests that bolide impacts on Mars could contribute a substantial amount of fine sediment.

PSDs of experimentally ground basalt are less uniform when compared to PSDs from aeolian abrasion of basalt. PSDs of basalt sand abraded by Adams and Soreghan (in prep) in an aeolian abrasion chamber tend to mimic one another with minor variation in curve shapes and modes. In contrast, PSDs, and modes of ground basalt can vary by tens to hundreds of microns. Two distinct curve shapes were observed in the aeolian abrasion PSDs, one typical of the coarser Hawaiian sand, and one typical of the finer Icelandic sands. PSDs of experimentally ground basalt suggest that glacial grinding of basalt produces relatively more fine dust than aeolian saltation and effusive basaltic volcanism, and comparable amounts of fine dust relative to Lunar regolith.

Across several different weathering mechanisms and rock compositions, coarse (2.5-10 µm) and super coarse (10-67 µm) dust are common products, while fine dust is limited. This may indicate that the energy required to mechanically break rock and minerals into particles finer than 2.5 µm is rarely met.

Implications for Climate

While determination of the magnitude of the influence of glacially derived dust on Martian climate remains challenging, we can compare the possible effects relative to other dust sources. Experimentally ground basalt dust has relatively more fine dust and more coarse dust than dust produced from aeolian abrasion. The abundance of fine dust could cause more of a cooling effect through scattering of shortwave solar radiation, although the increase in coarse dust would also contribute to warming via absorption (Adebiyi & Kok, 2020). Presumably, there exists a value of the ratio of fine to coarse dust at which their relative radiative impacts (warming vs. cooling) cancels out, but this remains unknown. Since a dust plume is dynamic, with PSD evolving with time and transport distance as coarser dust falls out of suspension, fine dust may have a greater impact on climate because it persists in the atmosphere longer. Modeling the climate impacts of experimentally produced dust PSDs is beyond the scope of this work. However, our results suggest that if widespread wet-based glaciation existed on Mars, the dust generated from those glaciers would have likely influenced the climate through inputs of abundant fine and coarse dust. This dust would potentially produce influences on precipitation and cloud formation, alter ice albedo, and affect atmospheric temperatures (Kok et al., 2023). Modeling by Wordsworth et al. (2015) suggests atmospheric dust could have contributed to the warming required for liquid water on early Mars. Our work suggests that several mechanisms capable of abundant dust production were likely operating on early Mars. These mechanisms produce relatively large volumes of coarse dust capable of producing a warming effect on early Mars.

CONCLUSION

Widespread evidence of wet-based erosive glaciation of Mars has been observed although the physical and temporal extent of wet-based glaciation remains uncertain. Our experiments suggest that glacial grinding produces distributions of sediment similar to PSDs of dust from aeolian saltation and bolide impacts, but that glacial abrasion is 50% more effective by volume % at producing fine dust (0-2.5 µm) compared to aeolian abrasion, bolide impacts, and non-explosive basaltic volcanism. While explosive volcanism on Earth can produce significant dust, especially fine dust, the extent of explosive volcanism on Mars remains poorly resolved. If wet-based glaciation was extensive on Mars, our results show that a significant amount (~40%) of the dust produced would be <10 µm and capable of long-distance transport in the atmosphere where it would influence the climate. The >2.5 µm fraction composes ~33% of dust produced and could have contributed to atmospheric warming, thereby assisting in maintaining a warmer climate with liquid water and wet-based glaciation.

FIGURES AND TABLES

Sample Name	Location	Age	Texture	Formation	Lat	Long	Thin Section Photo
MG-1	Colorado	Pliocene or Miocene	Aphanitic basalt, sparse labradorite and olivine	Mapped as Tertiary Basalts	38*24’18’’N	105*16’05’’W	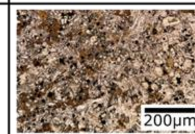
MG-2	Virginia	J	Aphanitic, very fine texture	Mt. Zion Church Basalt	38*48’47’’N	77*38’47’’W	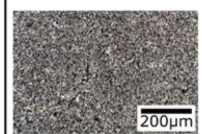
MG-3	Virginia	pC	Aphanitic high Ti Meta basalt	Catoctin Formation	38*41’43’’N	77*53’27’’W	
MG-4	Hawaii	H	Aphanitic, glassy	Puna Basalt	19*21’44’’N	155*21’46’’W	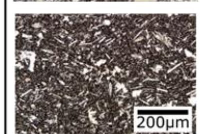
MG-5	Hawaii	H	Aphanitic, glassy, vesicular, blades of feldspar	Kau Basalt 1852 eruption Mauna Loa	19*31’11’’N	155*35’2’’W	

Table 1. Sample names used in the text and corresponding locations of collection, age of the rocks, textures of the rocks, parent formation, location of sample collection, and photomicrographs showing minerals and texture of each lithology.

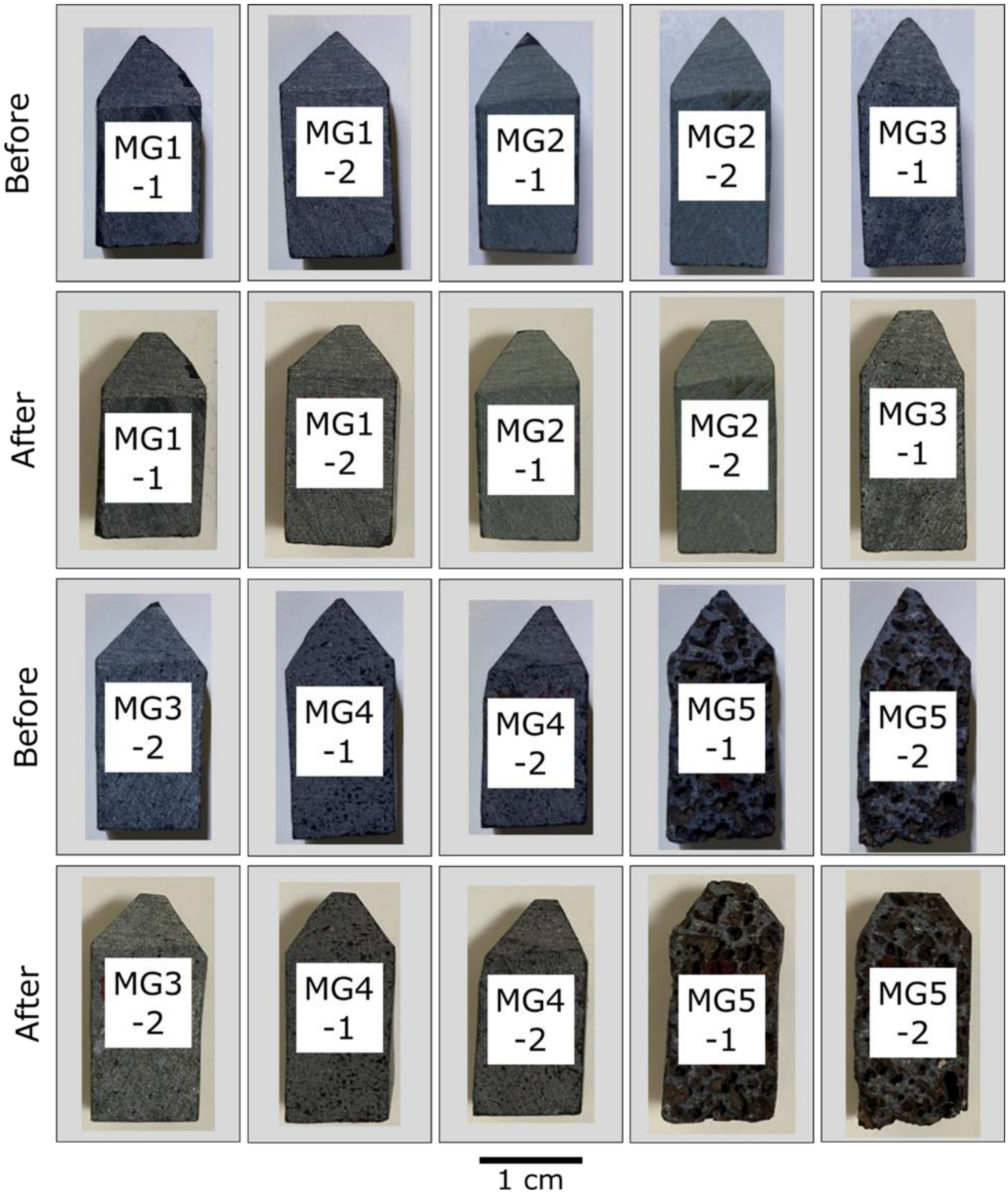

Figure 1. Before and after photographs of basalt styluses used in the grinding experiments. Each sample is approximately 1 cm wide and 3 cm tall.

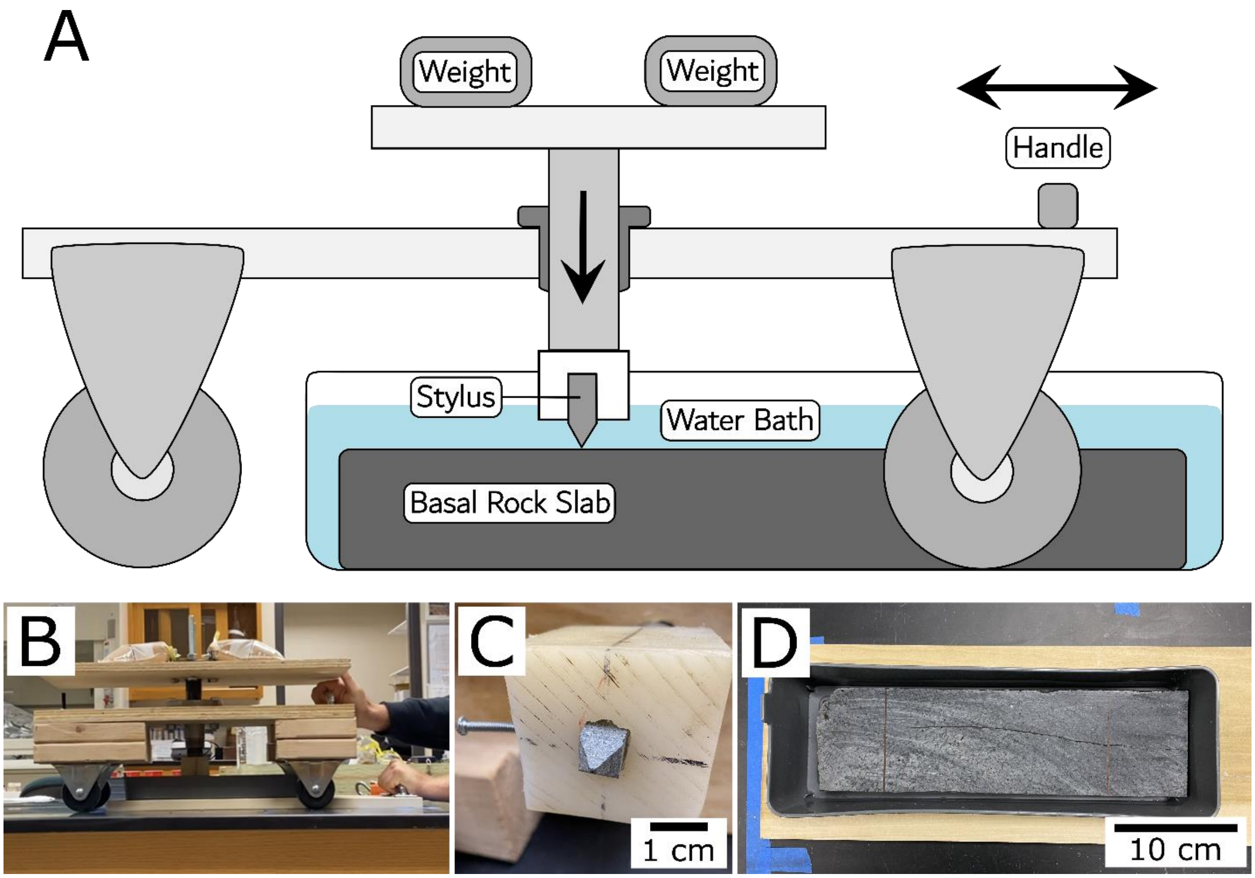

Figure 2. (A) schematic of glacial abrasion device showing the cart used to move the stylus across the basal rock slab, which sits in a basin of water. The stylus is pressed into contact with the basal slab by a weighted piston that transfers ~5kg of weight to the stylus producing a ~50 N contact force. (B) is a photograph of the abrasion device during operation. The basal slab is held in place while the cart is pulled and pushed, dragging the stylus across the basal slab in 20 cm lengths for a combined travel distance of 5 m. (C) shows a mounted stylus in the base of the piston. (D) shows the basal slab inside the water basin. The water basin sits inside a hole cut in a thin board so the slab can be held in place while the stylus moves.

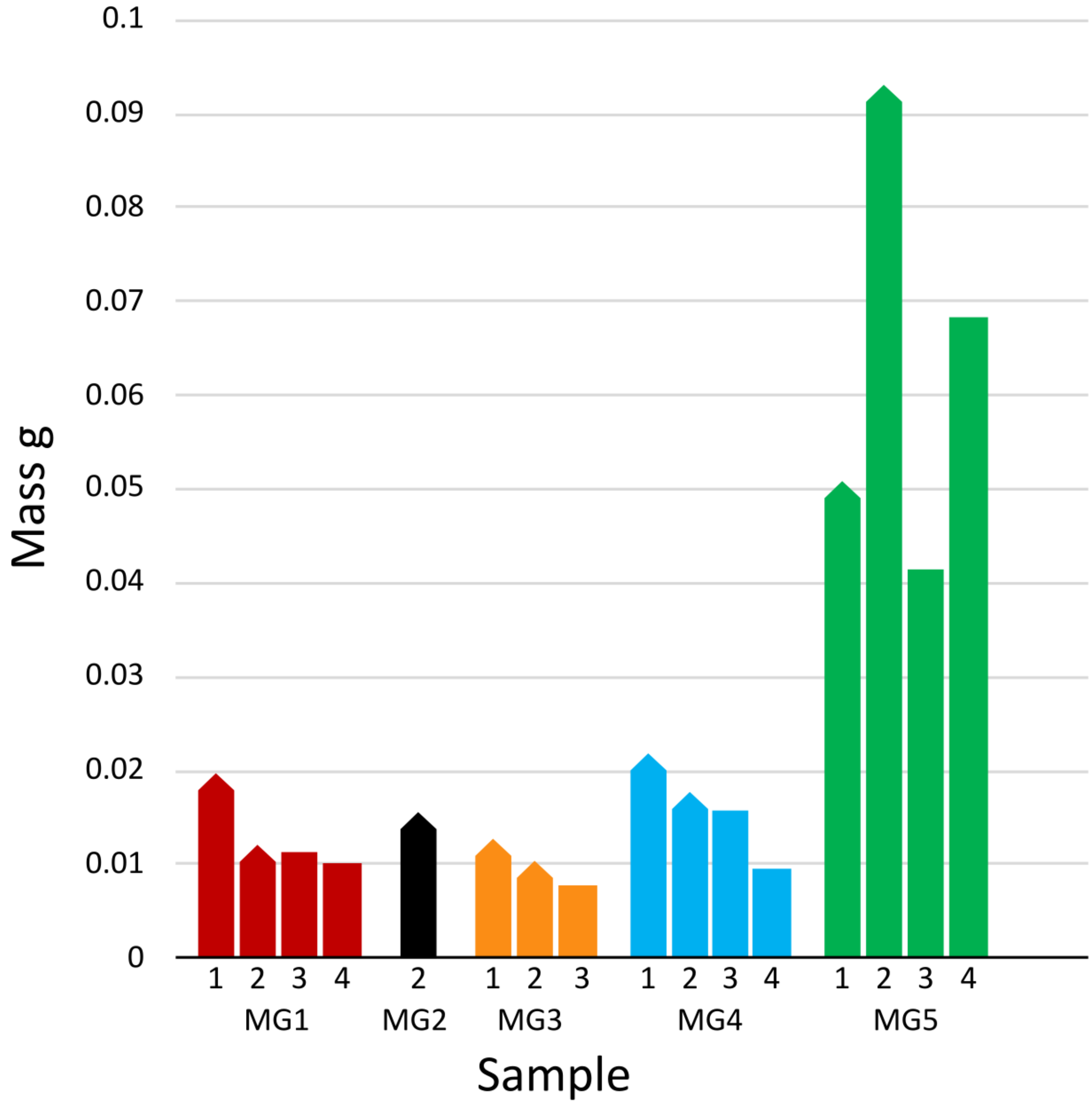

Figure 3. Mass of sediment produced from the abrasion of each stylus. Columns with points represent pointed styluses, flat columns represent flat styluses. Samples not shown had masses below our measurable threshold.

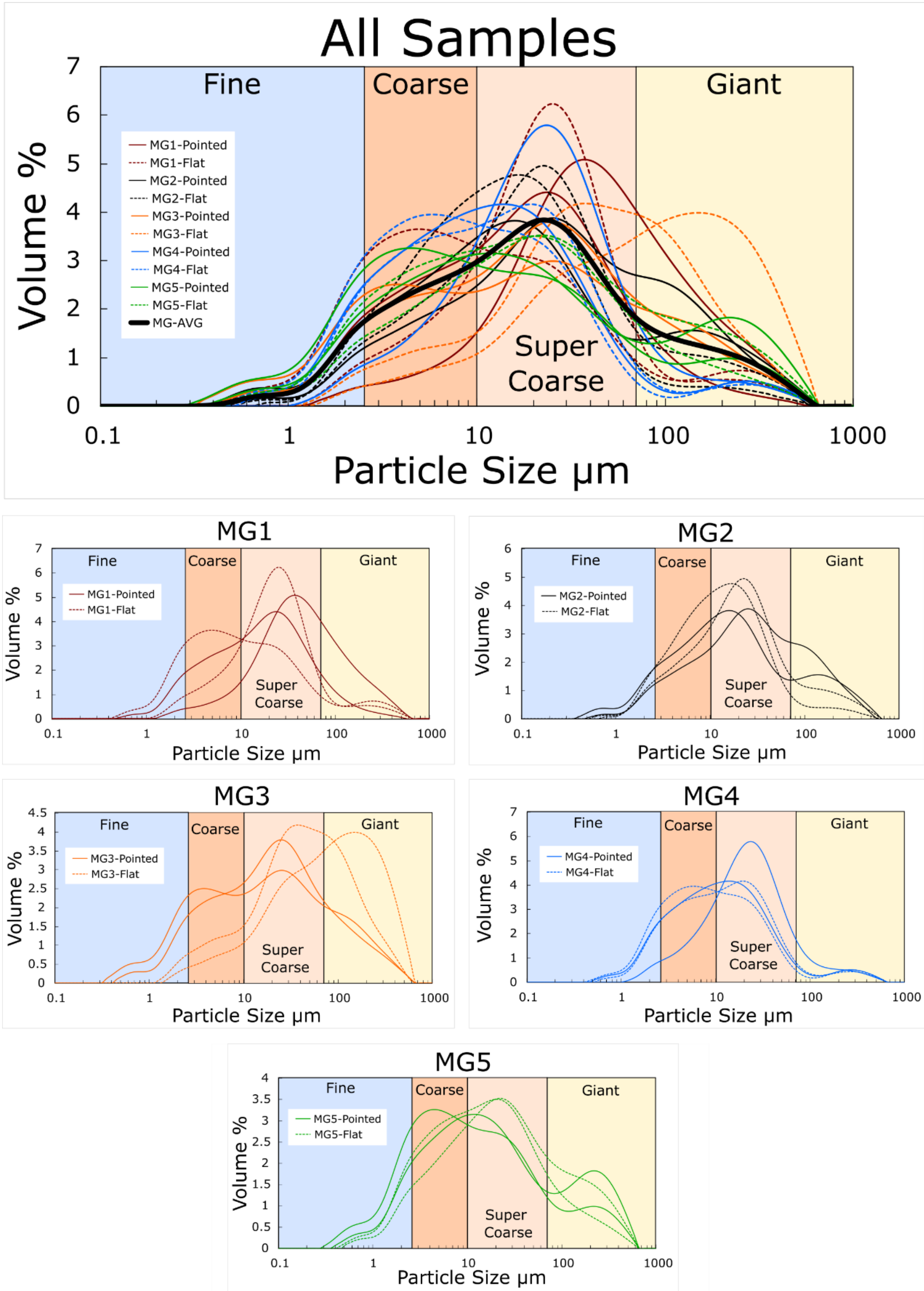

Figure 4. PSDs of all samples are shown on the top plot with the average PSD of all samples in black. Pointed styluses are solid lines and flat styluses are dashed lines. PSDs of each lithology type and their corresponding styluses are shown in the lower five PSD plots. Each sample shows the PSD of four samples, two from pointed styluses (solid), and two from flat styluses (dashed).

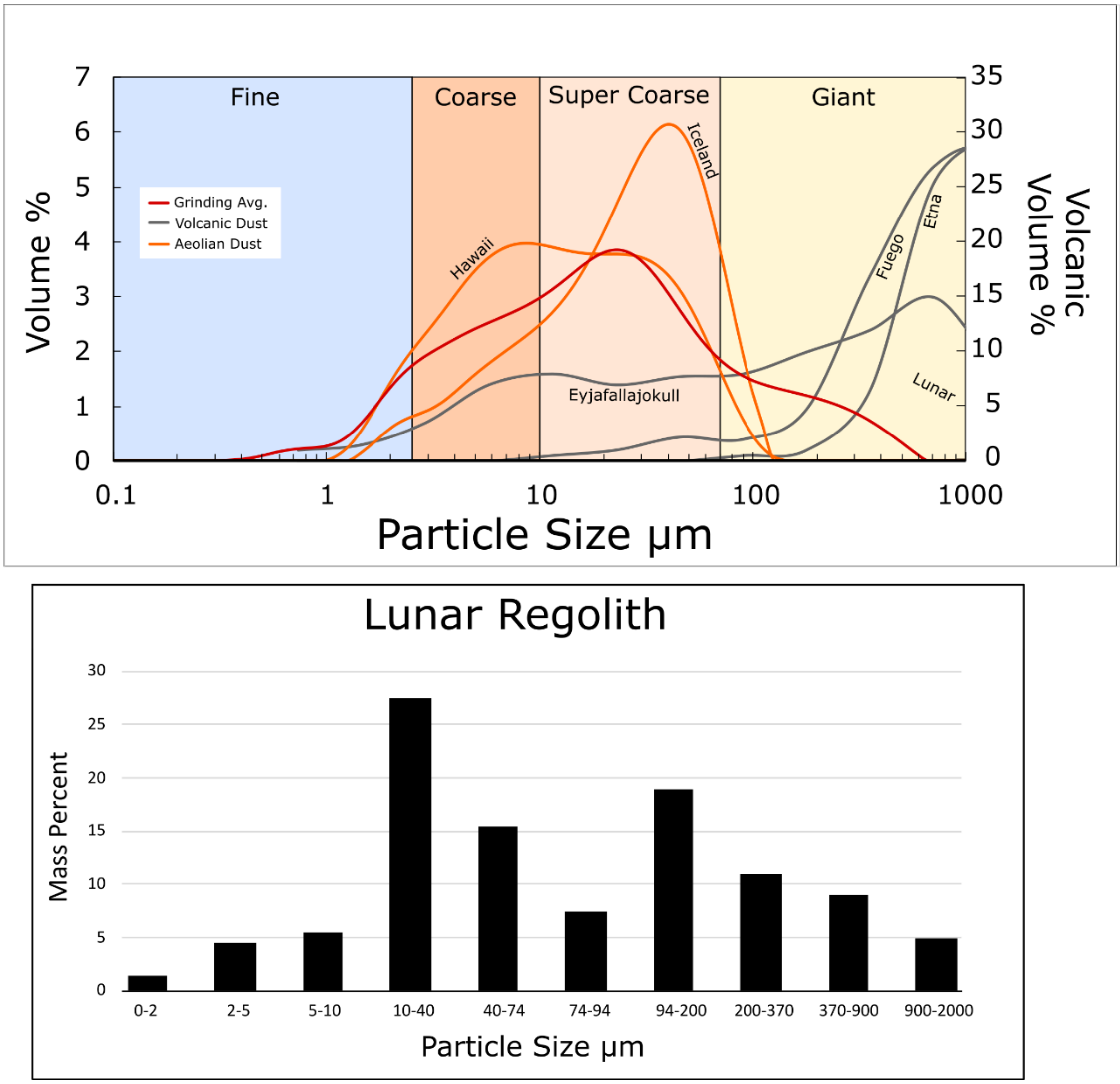

Figure 5. The average PSD of glacial grinding samples from this study is shown in red compared with PSDs of volcanic dust from different eruptions, Lunar regolith, and dust from experimental aeolian abrasion of basalt sands from Hawaii and Iceland (Adams and Soreghan, in review). Note Lunar and volcanic PSDs are plotted with a different Volume % axis on the right.

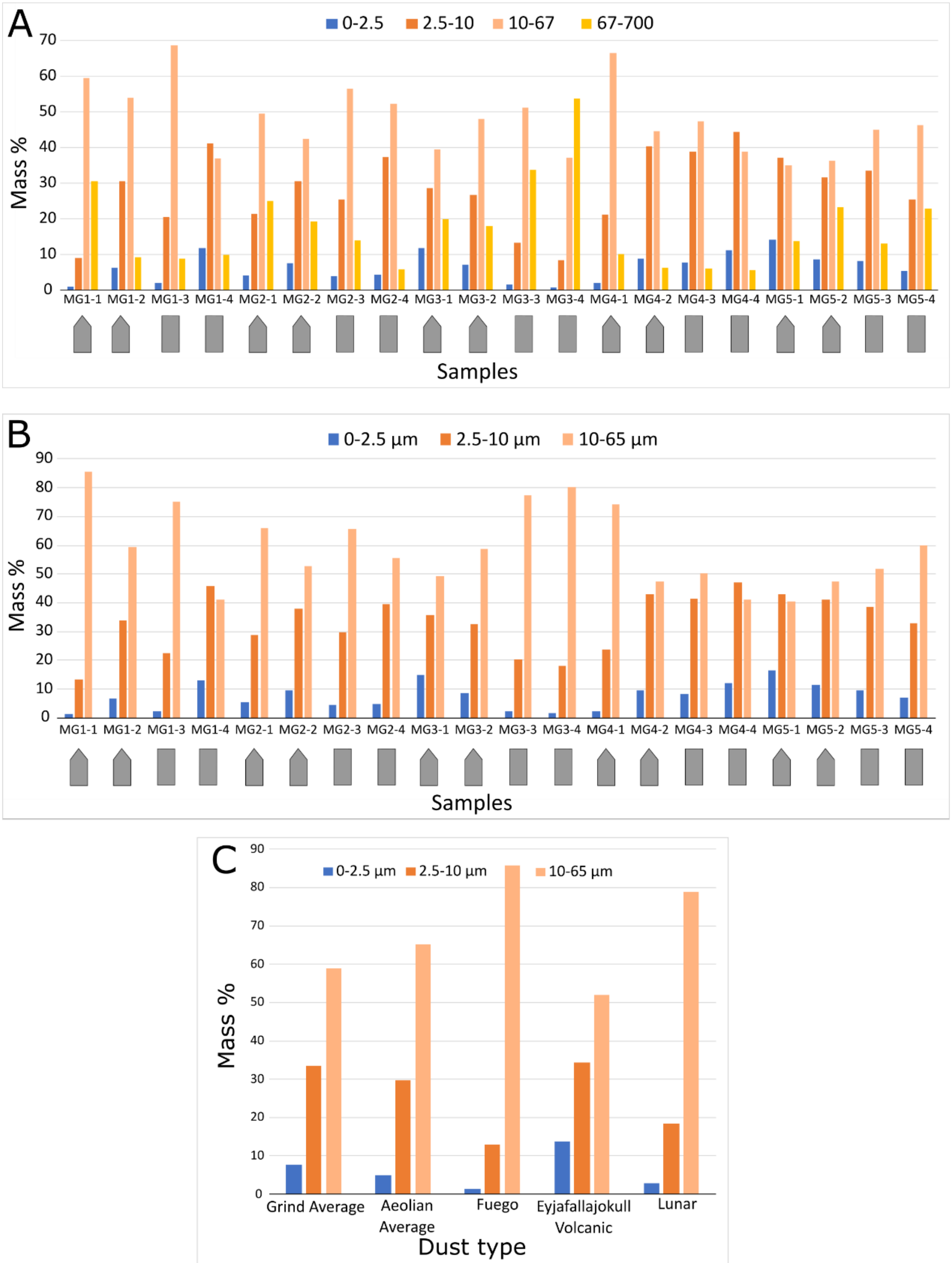

Figure 6. (A) shows the fractional masses from each sample abraded in this study. These fractional masses are calculated using the PSDs. We assume mass % to be equivalent to volume % as the density differences of particles is considered negligible. (B) shows the fractional masses of each sample renormalized for the <67 µm mass. (C) compares the fractional mass of the average PSD produced from glacial grinding of basalts to fractional masses from dust produced via aeolian abrasion of basalts, volcanic eruptions, and Lunar regolith.

REFERENCES

Adebiyi, A., Kok, J., Murray, B. J., Ryder, C. L., Stuut, J.-B. W., Kahn, R. A., et al. (n.d.). *A review of coarse mineral dust in the Earth system*.

Adebiyi, A. A., & Kok, J. F. (2020). Climate models miss most of the coarse dust in the atmosphere. *Science Advances*, *6*, 1–10. https://doi.org/10.1126/sciadv.aaz9507

Barlow, N. G. (2010). What we know about Mars from its impact craters. *GSA Bulletin*, *122*(5–6), 644–657. https://doi.org/10.1130/b30182.1

Bouquety, A., Sejourné, A., Costard, F., Mercier, D., & Bouley, S. (2019). Geomorphology Morphometric evidence of 3. 6 Ga glacial valleys and glacial cirques in martian highlands : South of Terra Sabaea. *Geomorphology*, *334*, 91–111. https://doi.org/10.1016/j.geomorph.2019.02.022

BRIDGES, N. T., & MUHS, D. R. (2012). Duststones on Mars: Source, Transport, Deposition, and Erosion. *Sedimentary Geology of Mars*, 169–182. https://doi.org/10.2110/pec.12.102.0169

Bristow, C. S., Hudson-Edwards, K. A., & Chappell, A. (2010). Fertilizing the Amazon and equatorial Atlantic with West African dust. *Geophysical Research Letters*, *37*(14), n/a-n/a. https://doi.org/10.1029/2010gl043486

Brough, S., Hubbard, B., & Hubbard, A. (2016). Former extent of glacier-like forms on Mars. *Icarus*, *274*, 37–49. https://doi.org/10.1016/j.icarus.2016.03.006

Brož, P., Bernhardt, H., Conway, S. J., & Parekh, R. (2021). An overview of explosive volcanism on Mars. *Journal of Volcanology and Geothermal Research*, *409*, 107125. https://doi.org/10.1016/j.jvolgeores.2020.107125

Butcher, F. E. G., Balme, M. R., Gallagher, C., Arnold, N. S., Conway, S. J., Hagermann, A., & Lewis, S. R. (2017). Recent Basal Melting of a Mid-Latitude Glacier on Mars. *Journal of Geophysical Research: Planets*, *122*, 2445–2468. https://doi.org/10.1002/2017je005434

Butcher, F. E. G., Balme, M. R., Conway, S. J., Gallagher, C., Arnold, N. S., Storrar, R. D., et al. (2020). Morphometry of a glacier-linked esker in NW Tempe Terra, Mars, and implications for sediment-discharge dynamics of subglacial drainage. *Earth and Planetary Science Letters*, *542*, 116325. https://doi.org/10.1016/j.epsl.2020.116325

Butcher, F. E. G., Balme, M. R., Conway, S. J., Gallagher, C., Arnold, N. S., Storrar, R. D., et al. (2021). Sinuous ridges in Chukhung crater, Tempe Terra, Mars: Implications for fluvial, glacial, and glaciofluvial activity. *Icarus*, *357*, 114131. https://doi.org/10.1016/j.icarus.2020.114131

Charalambous, C. (2014). *On the Evolution of Particle Fragmentation With Applications to Planetary Surfaces*.

Christensen, P. R. (1986). Regional dust deposits on Mars: Physical properties, age, and history. *Journal of Geophysical Research: Solid Earth*, *91*(B3), 3533–3545. https://doi.org/10.1029/jb091ib03p03533

Conen, F., Morris, C. E., Leifeld, J., Yakutin, M. V., & Alewell, C. (2011). Biological residues define the ice nucleation properties of soil dust. *Atmospheric Chemistry and Physics*, *11*(18), 9643–9648. https://doi.org/10.5194/acp-11-9643-2011

Costa, A., Pioli, L., & Bonadonna, C. (2016). Assessing tephra total grain-size distribution: Insights from field data analysis. *Earth and Planetary Science Letters*, *443*, 90–107. https://doi.org/10.1016/j.epsl.2016.02.040

Davis, A. M., Southworth, C. S., Reddy, J. E., & Schindler, J. S. (2001). *Geologic map database of the Washington DC area featuring data from three 30 x 60 minute quadrangles: Frederick, Washington West, and Fredericksburg* (Report No. 2001–227). Retrieved from http://pubs.er.usgs.gov/publication/ofr01227

Dufresne, J.-L., Gautier, C., Ricchiazzi, P., & Fouquart, Y. (2002). Longwave Scattering Effects of Mineral Aerosols. *Journal of the Atmospheric Sciences*, *59*(12), 1959–1966. https://doi.org/10.1175/1520-0469(2002)059<;1959:lseoma>2.0.co;2

Gallagher, C., & Balme, M. (2015). Eskers in a complete, wet-based glacial system in the Phlegra Montes region, Mars. *Earth and Planetary Science Letters*, *431*, 96–109. https://doi.org/10.1016/j.epsl.2015.09.023

Galofre, A. G., Whipple, K. X., Christensen, P. R., & Conway, S. J. (2022). Valley Networks and the Record of Glaciation on Ancient Mars. *Geophysical Research Letters*, *49*(14), e2022GL097974. https://doi.org/10.1029/2022gl097974

Gillespie, H. E., Greybush, S. J., & Wilson, R. J. (2020). An Investigation of the Encirclement of Mars by Dust in the 2018 Global Dust Storm Using EMARS. *Journal of Geophysical Research: Planets*, *125*(7). https://doi.org/10.1029/2019je006106

Hallet. (1979). A Theoretical Model of Glacial Abrasion. *Journal of Glaciology*, *23*(89), 39–50. https://doi.org/10.3189/s0022143000029725

Hallet, B., Hunter, L., & Bogen, J. (1996). Rates of erosion and sediment evacuation by glaciers: A review of field data and their implications. *Global and Planetary Change*, *12*(1–4), 213–235. https://doi.org/10.1016/0921-8181(95)00021-6

Hansen, D. D., & Zoet, L. K. (2019). Experimental constraints on subglacial rock friction. *Annals of Glaciology*, *60*(80), 37–48. https://doi.org/10.1017/aog.2019.47

Horton, J. D., Juan, C. A. S., & Stoeser, D. B. (2017). *The State Geologic Map Compilation (SGMC) geodatabase of the conterminous United States* (Report No. 1052) (p. 56). Reston, VA. Retrieved from http://pubs.er.usgs.gov/publication/ds1052

Jefferson, I. F., Jefferson, B. Q., Assallay, A. M., Rogers, C. D. F., & Smalley, I. J. (1997). Crushing of Quartz Sand to Produce Silt Particles. *Naturwissenschaften*, *84*(4), 148–149. https://doi.org/10.1007/s001140050366

Jordanova, D., Simon, Q., Balescu, S., Jordanova, N., Ishlyamski, D., Georgieva, B., et al. (2022). Environmental changes in southeastern Europe over the last 450 ka: Magnetic and pedologic study of a loess-paleosol profile from Kaolinovo (Bulgaria). *Quaternary Science Reviews*, *292*, 107671. https://doi.org/10.1016/j.quascirev.2022.107671

Kerber, L., Head, J. W., Madeleine, J.-B., Forget, F., & Wilson, L. (2011). The dispersal of pyroclasts from Apollinaris Patera, Mars: Implications for the origin of the Medusae Fossae Formation. *Icarus*, *216*(1), 212–220. https://doi.org/10.1016/j.icarus.2011.07.035

Kok, J. F., Ridley, D. A., Zhou, Q., Miller, R. L., Zhao, C., Heald, C. L., et al. (2017). Smaller desert dust cooling effect estimated from analysis of dust size and abundance. *Nature Geoscience*, *10*(4), 274–278. https://doi.org/10.1038/ngeo2912

Kok, J. F., Storelvmo, T., Karydis, V. A., Adebiyi, A. A., Mahowald, N. M., Evan, A. T., et al. (2023). Mineral dust aerosol impacts on global climate and climate change. *Nature Reviews Earth & Environment*, *4*(2), 71–86. https://doi.org/10.1038/s43017-022-00379-5

Kumar, R., Jefferson, I. F., O'Hara-Dhand, K., & Smalley, I. J. (2006). Controls on quartz silt formation by crystalline defects. *Naturwissenschaften*, *93*(4), 185–188. https://doi.org/10.1007/s00114-006-0087-0

Laul, J. C., Rode, O. D., Simon, S. B., & Papike, J. J. (1987). The lunar regolith: Chemistry and petrology of Luna 24 grain size fractions. *Geochimica et Cosmochimica Acta*, *51*, 661–673. https://doi.org/10.1016/0016-7037(87)90077-9

Lee, A. G. G., & Rutter, E. H. (2004). Experimental rock-on-rock frictional wear: Application to subglacial abrasion. *Journal of Geophysical Research: Solid Earth*, *109*, 1–11. https://doi.org/10.1029/2004jb003059

Mahowald, N., Ward, D. S., Kloster, S., Flanner, M. G., Heald, C. L., Heavens, N. G., et al. (2011). Aerosol impacts on climate and biogeochemistry. *Annual Review of Environment and Resources*, *36*, 45–74. https://doi.org/10.1146/annurev-environ-042009-094507

Mahowald, N., Albani, S., Kok, J. F., Engelstaeder, S., Scanza, R., Ward, D. S., & Flanner, M. G. (2014). The size distribution of desert dust aerosols and its impact on the Earth system. *Aeolian Research*, *15*, 53–71. https://doi.org/10.1016/j.aeolia.2013.09.002

MATHEWS, W. H. . (1979). SIMULATED GLACIAL ABRASION. *Journal of Glaciology*, *23*, 51–56.

Millan, R., Mouginot, J., Rabatel, A., & Morlighem, M. (2022). Ice velocity and thickness of the world's glaciers. *Nature Geoscience*, *15*(2), 124–129. https://doi.org/10.1038/s41561-021-00885-z

Moss, A. J., & Green, P. (1975). Sand and silt grains: Predetermination of their formation and properties by microfractures in quartz. *Journal of the Geological Society of Australia*, *22*(4), 485–495. https://doi.org/10.1080/00167617508728913

Muhs, D. R. (2013). The geologic records of dust in the quaternary. *Aeolian Research*, *9*, 3–48. https://doi.org/10.1016/j.aeolia.2012.08.001

Newman, C. E., Bertrand, T., Fenton, L. K., Guzewich, S. D., Jackson, B., Lewis, S. R., et al. (2022). Treatise on Geomorphology. In J. (Jack) F. Shroder (Ed.), *Treatise on Geomorphology (Second Edition)* (second, Vol. Volume 7, pp. 637–666). Academic Press. https://doi.org/10.1016/b978-0-12-818234-5.00143-7

Ojha, L., Lewis, K., Karunatillake, S., & Schmidt, M. (2018). The Medusae Fossae Formation as the single largest source of dust on Mars. *Nature Communications*, *9*(1), 2867. https://doi.org/10.1038/s41467-018-05291-5

Okin, G. S., Baker, A. R., Tegen, I., Mahowald, N. M., Dentener, F. J., Duce, R. A., et al. (2011). Impacts of atmospheric nutrient deposition on marine productivity: Roles of nitrogen, phosphorus, and iron. *Global Biogeochemical Cycles*, *25*, 1–10. https://doi.org/10.1029/2010gb003858

Rose, W. I., & Durant, A. J. (2009). Fine ash content of explosive eruptions. *Journal of Volcanology and Geothermal Research*, *186*(1–2), 32–39. https://doi.org/10.1016/j.jvolgeores.2009.01.010

Rosenfeld, D., Rudich, Y., & Lahav, R. (2001). Desert dust suppressing precipitation: A possible desertification feedback loop. *Proceedings of the National Academy of Sciences*, *98*(11), 5975–5980. https://doi.org/10.1073/pnas.101122798

Scanlon, K. E., Head, J. W., Fastook, J. L., & Wordsworth, R. D. (2018). The Dorsa Argentea Formation and the Noachian-Hesperian climate transition. *Icarus*, *299*, 339–363. https://doi.org/10.1016/j.icarus.2017.07.031

Skiles, S. M., Flanner, M., Cook, J. M., Dumont, M., & Painter, T. H. (2018). Radiative forcing by light-absorbing particles in snow. *Nature Climate Change*, *8*(11), 964–971. https://doi.org/10.1038/s41558-018-0296-5

Smalley, I. J., & Vita-Finzi, C. (1968). THE FORMATION OF FINE PARTICLES IN SANDY DESERTS AND THE NATURE OF 'DFESERT ~ LOESS 1. *JOURNAL OF SFEDIMEN' RARY PETROLOGY*, *38*, 76–1.

Sherrod, D. R., Sinton, J. M., Watkins, S. E., & Brunt, K. M. (2021). *Geologic map of the State of Hawaii* (Report No. 3143) (p. 72). Reston, VA. Retrieved from http://pubs.er.usgs.gov/publication/sim3143

Tanaka, K. L. (2000). Dust and Ice Deposition in the Martian Geologic Record. *Icarus*, *144*(2), 254–266. https://doi.org/10.1006/icar.1999.6297

Tang, M., Cziczo, D. J., & Grassian, V. H. (2016). Interactions of Water with Mineral Dust Aerosol: Water Adsorption, Hygroscopicity, Cloud Condensation, and Ice Nucleation. *Chemical Reviews*, *116*(7), 4205–4259. https://doi.org/10.1021/acs.chemrev.5b00529

Watts. (1974). *Inclusions in ice*. University of Bristol.

Woodley, S. Z., Butcher, F. E. G., Fawdon, P., Clark, C. D., Ng, F. S. L., Davis, J. M., & Gallagher, C. (2022). Multiple sites of recent wet-based glaciation identified from eskers in western Tempe Terra, Mars. *Icarus*, *386*, 115147. https://doi.org/10.1016/j.icarus.2022.115147

Wordsworth, R. D., Kerber, L., Pierrehumbert, R. T., Forget, F., & Head, J. W. (2015). Comparison of "warm and wet" and "cold and icy" scenarios for early Mars in a 3-D climate model. *Journal of Geophysical Research: Planets*, *120*(6), 1201–1219. https://doi.org/10.1002/2015je004787

Wright, J. S. (1995). Glacial comminution of quartz sand grains and the production of loessic silt: A simulation study. *Quaternary Science Reviews*, *14*(7–8), 669–680. https://doi.org/10.1016/0277-3791(95)00048-8

CHAPTER III

INVESTIGATION OF DUST PRODUCED BY EXPERIMENTAL GLACIAL ABRASION OF COMMON LITHOLOGIES

INVESTIGATION OF DUST PRODUCED BY EXPERIMENTAL GLACIAL ABRASION OF COMMON LITHOLOGIES

ABSTRACT

Glacial grinding has long been recognized as a major producer of fine, dust-sized sediment owing in part to the proximal relationship of fine sediment and glaciers. Yet, experiments have produced conflicting results with regard to the ability of glacial grinding to produce abundant silt. We experimentally replicate glacial grinding of small (~3 cm) clasts of varying lithologies (granitoids, quartzites, schist, limestones, and sandstones) using a novel abrasion device. We abrade pointed styluses representing clasts with asperities and flat styluses representing well-worn clasts. Our results confirm that rock-on-rock abrasion produces sediment with particle size distributions (PSDs) that exhibit primary modes predominantly within the silt fraction (~30 µm). Pointed styluses generally produce more sediment than flat styluses. Pointed and flat styluses of the same lithologies generally produce similar PSDs. PSDs across all lithology and stylus types produce similar modes at 0.5 µm, 4-8 µm, 30 µm, and 100-300 µm. When our PSD results are compared to previous experiments replicating a range of abrasion processes (glacial grinding, aeolian abrasion, fluvial abrasion, mechanical crushing) the same mode ranges are present. Our study suggests an underlying physical mechanism operating across varying mineralogical compositions and clast shapes that limits PSD modes to specific ranges.

INTRODUCTION

Rock and mineral dust is a major sediment class on Earth. Dust referred to in this work is rock and mineral fragments, generally <100 µm, transported in suspension by the wind to their site of deposition (Tsoar & Pye, 1987). These sedimentary deposits are also referred to as dust (Daniel R. Muhs, 2013). We adopt the classification of Adebiyi et al. (2023, preprint) for dust size: fine dust (<2.5 µm), coarse dust (2.5-10 µm), super coarse dust (10-67 µm), giant dust (>67 µm), with the latter adjusted relative to the standard of 62.5 µm owing to the distribution binning of the Laser Particle Size Analyzer (LPSA) used for size analysis. When lofted and transported through the atmosphere by wind, dust can impact local and global climate. During atmospheric transport dust interacts with clouds, influencing albedo, and ice- and water nucleation. Dust affects surface and atmospheric temperatures through radiative forcing effects that could lead to either warming or cooling depending on the characteristics of the dust and the surrounding environment (Conen et al., 2011; Dufresne et al., 2002; Kok et al., 2017, 2023; Rosenfeld et al., 2001; Tang et al., 2016). Upon deposition, dust delivers nutrients to soils and water bodies, enhancing biological productivity and thus drawing CO_2 out of the atmosphere (Bristow et al., 2010; Mahowald et al., 2011; Okin et al., 2011; Skiles et al., 2018). If deposited on snow and ice it reduces albedo, leading to more absorbed solar radiation and accelerated ice melting (Bristow et al., 2010; Mahowald et al., 2011; Okin et al., 2011; Skiles et al., 2018). Dust ultimately accumulates in soils, paleosols, and various sedimentary deposits, including forming loess (eolian silt) deposits, where it records evidence of past climate, potentially harboring evidence for the method of dust production (Jordanova et al., 2022; Daniel R. Muhs, 2013).

Loess constitutes continental accumulations of eolian-transported dust. Loess is the most widespread deposit on Earth’s surface today and large paleoloess deposits are increasingly documented in the ancient rock record (D. R. Muhs, 2013; Soreghan et al., 2023). The development of loess deposits requires large volumes of dust, primarily in the silt size range (Pécsi, 1995; I. Smalley et al., 2011). Several mechanisms have been proposed to produce these large quantities of dust, including glacial grinding, aeolian saltation, freeze-thaw weathering, explosive volcanism, disintegration of silt-rich protoliths (e.g., siltstone, rhyolite, phyllite) and chemical weathering in soils (Aleinikoff et al., 1999, 2008; McTainsh, 1989; Nahon & Trompette, 1982; I. Smalley, 1995; I. J. Smalley, 1966; I. J. Smalley & Vita-Finzi, 1968). Some of these dust-production mechanisms are climate-dependent and could thus serve as climate indicators if the produced dust exhibits distinguishing characteristics. Furthermore, the influences of dust on climate depends on particle composition, shape, and size (Kok et al., 2023). For example, fine dust (<2.5 μm) in the atmosphere generally exerts a radiative cooling effect through scattering and reflecting shortwave solar radiation, whereas coarser dust generally exerts a warming effect through absorption of long-wave radiation (A. A. Adebiyi & Kok, 2020; Kok et al., 2023).

In this study we perform experiments that replicate glacial abrasion of pebble-sized clasts (3 cm) of varying lithologic compositions and compare characteristics of dust produced across sample types to dust produced from previous experiments replicating mechanical abrasion processes (i.e., glacial grinding and aeolian saltation) and natural dust particle-size diameters (PSDs) from existing literature. We discuss the implications of the similarities and differences of dust produced and consider the variables responsible for creating dust with the characteristics observed.

EXPERIMENTAL BACKGROUND

Wet-based glaciers have long been recognized as effective agents of silt generation (I. Smalley, 1995; I. J. Smalley, 1966). The fine glacial flour found in till and pro-glacial sediment is a mechanical weathering product of the crushing, grinding, and shearing of rocks and sediment that occurs at the glacial bed; produced sediment is then transported by glacio-fluvial systems to outwash plains or flood plains, where, upon drying, the wind entrains and transports it. Given sufficiently high rates of deposition, this eolian silt will accumulate as loess (D. R. Muhs, 2013). However, few studies have attempted to replicate this physical weathering process and study the PSDs of produced sediment, especially for a variety of lithologies. Experiments generally focus on (1) rock-on-rock abrasion or (2) loaded shearing of sands in a ring-shear device or disk mill; our experiments fall into the first category.

Matthews (1979) replicated glacial grinding by using a rotating wheel of ice with embedded sand. The wheel rotated between two limestone tablets, with the top stone loaded with weight to exert a downward force for abrasion. These experiments produced fine limestone powder and quartz grains that dislodged from the ice, but with no characterization of PSDs. Lee & Rutter (2004) used the grinding friction produced by two rock wheels of the same lithology (sandstone, schist, and granite) rotating against one another to produce sediment. The top wheel was weighted by a lever arm to provide the downward contact force. PSDs measured by laser particle size analysis (LPSA) revealed modes finer than those of typical (silt-rich) loess and glacial flour, and sand modes from grains plucked from the sandstone wheels.

In contrast to the above studies, others have used ring-shear devices or disk mills. Wright (1995) employed a ring-shear device to grind sand derived from crushed Brazilian vein quartz. These experiments yielded negligible silt, which seems surprising given the abundant silt associated with Pleistocene glaciation (Smalley & Vita-Finzi, 1968). These results led Jefferson et al. (1997) to simulate shearing sand from a Cretaceous sandstone, which produced abundant silt; this in turn prompted Kumar et al. (2006) to use the ring shear device from Wright (1995) and the Cretaceous sands used by Jefferson et al. (1997), which produced abundant silt with modes similar to those found in loess (~25 µm), and coarser than the sediment generated by Lee & Rutter (2004). Kumar et al. (2006) inferred that the Brazilian vein quartz lacked crystalline defects commonly referred to as Moss defects (Moss & Green, 1975)—small, sub-parallel fractures present in plutonic quartz and thought to provide planes of weakness leading to the breakage of quartz sand into silt.

Because glaciers erode various types of rock and sediment, and previous studies suggest that rock-on-rock abrasion yields fines of different PSDs compared to shearing of sands, we conducted a new series of experiments to better understand the products of glacial abrasion. We abraded a wide variety of rock types and measured their PSDs for comparing them with prior experiments and dust studies from existing literature. The results have implications for our understanding of the forces required to mechanically produce silt in nature, and the possible processes that are efficient at doing so. PSDs of the dust produced may indicate that different lithologies when abraded have different influences on the climate.

METHODS

Sample Collection and Preparation

We used eleven different rock types collected from various field locations to capture a spectrum of ages, textures, and compositions. Table 1 lists details of the granitoids (4), quartzites (2), schist (1), limestones (2), and sandstones (2) used. Figure 1 shows photomicrographs of each sample type. From these, sample styluses were cut to represent sub-glacial rock clasts. We hand-cut four styluses (~3 cm long and 1 cm wide) for each of the eleven rock types; of these for each sample, two have a pyramidal tip (pointed) and two have a rectangular head (flat). Stylus sizes vary by a few mm in length and tip angles of pointed styluses vary by <10º. Figure 2 illustrates a subset of styluses from our experiments and Supplement 3-1 illustrates all styluses before and after grinding. In addition to styluses, flat slabs 30 cm long, 10 cm wide, and 5 cm thick were prepared to mimic the bedrock surface the clasts traversed. These basal slabs were made from granite (G1), limestone (LS1), sandstone (SS1), and quartzite (Q1).

Four granitic samples were collected, two relatively fine-grained (~2 mm crystals) and two with generally larger (>4mm) crystals. The finer granitoids are the Silver Plume Granite (G1) and an unnamed quartz diorite (G2). The Silver Plume Granite is Precambrian in age, contains quartz, plagioclase, and biotite (Braddock and Cole, 1990). The collected G1 sample has traces of chemical weathering and the feldspar grains show discoloration and slight weathering to clay. The G2 sample was collected from a moraine near Shadow Mountain Lake Colorado and based on the composition of the sample and location it is assumed to have been eroded from rocks mapped as Quartz Diorites up the glacial valley from the moraine it was collected from (Braddock and Cole, 1990). G2 is composed of mostly quartz and feldspar ~2mm in diameter with biotite and hornblende present. Chemical weathering is not apparent in thin section or hand sample on the sample collected. The St. Kevin Granite (G3) and Mendic Granite (G4) are porphyritic with larger crystals, generally >4 mm with occasional crystals >2 cm in diameter. G3, the St. Kevin Granite is Precambrian in age and was collected near Leadville, Colorado (Kellogg et al., 2017). G3 is composed of mainly of quartz and plagioclase but also has microcline and mica. G4 is the Mendic Granite and is Cambrian in age (Brevart et al., 1982). G4 was collected from the French Massif Central near the Montaigne Noir dome. It contains large >4 mm crystals of plagioclase and quartz and mica, though it also has sections of microcrystalline quartz grain clusters. The sample we used has signs of chemical weathering of feldspars to clays and the quartz and plagioclase grains often have fractures.

Four sedimentary rocks were selected, two sandstones and two limestones. SS1 was collected in New Mexico from a sandy bed of fine quartz sand in the Pennsylvanian aged Bursum formation (Horton et al., 2017). The sandstone is arcosic with subrounded fine grains of quartz and feldspar. Clay and micrite cement grains and form thin (~200 µm) layers in the rock. SS2 was collected from the Cretaceous Muddy Sandstone of the Dakota group near Canon City Colorado. Sub-rounded, fine quartz grains, weakly cemented, form a friable quartz arenite that is easy to disaggregate in one’s hands. LS1 was collected from the Bursum formation in New Mexico from a mudstone bed. The sample is 95% micrite with ~5% fine quartz grains suspended in the micrite matrix. LS2 is a grainstone collected from the Ordovician aged Kimmswick formation in Missouri. LS2 is made of large (200-500 µm) allochems cemented with calcite. The grainstone contains fossils of gastropods, bryozoans, ostracods, trilobites, and brachiopods, which are generally broken fragments in our sample (Nelson, et al., 2005).

Three metamorphic rocks were collected, two quartzites and one schist. The two quartzites Q1 and Q2 were collected from a location known as Blue Ridge near Canon City Colorado. They are part of a group of unnamed Precambrian metamorphic rocks (Horton et al., 2017). Both quartzites have large (~2-4mm) quartz crystals and are >95% quartz. Q1 is darker in color, and Q2 has small traces of mica suspended in its quartz grains. The quartzites are very well cemented and difficult to break or cut with a saw. The schist we selected is from the Schistes X group in France, collected from the French Massif Central near the Montaigne Noir dome. This schist is classified as the Schistes X10, and is a quartz-mica schist (Roger et al., 2015). It is composed of foliated chlorite, silt and clay-sized quartz, and round fine sand-sized quartz grains. The styluses were cut so the foliations run parallel with the long axis of the stylus.

Experimental Method

Figure 3 illustrates the experimental device used to replicate the grinding of small clasts against bedrock. A tub ~5 cm wider than the bedrock-simulating slab contains the slab and sufficient (distilled) water such that a thin film of water covers the slab to both reduce friction and trap any produced sediment.

The stylus fits tightly into a 2 cm-deep recessed cavity carved into a block of plastic, with the tip protruding ~1 cm. A platform weighted to a total of 5 kg presses on a piston made from steel pipe that holds the plastic block and attached stylus, all of which is mounted on a mobile cart. The weighted platform drives the piston down through a hole in the cart, transferring a load of ~50 N directly to the stylus tip.

The resultant force at the contact lies in the predicted range of ~10-100 N (Hansen & Zoet, 2019) for small (1 cm radius) spherical clasts from equations for drag and contact forces used by Hallet (1979) and Watts (1974).

Equations from (Hansen & Zoet, 2019)

(1)

$$F_c = F_b + F_d$$

F_c is the contact force, F_b is the buoyant force due to gravity and is considered negligible for clasts under 0.5 m in diameter, and F_d is the drag force and for small clasts is equivalent to the contact force regardless of ice thickness (Hansen & Zoet, 2019).

(2)

$$F_d = \frac{4\pi\, \eta_i u_v r^3}{r_*^2 + r^2}$$

where

(3)

$$r_* = \left(\frac{\rho_l}{\rho_l + \rho_i}\frac{3\eta_i C K}{\rho_i \mathcal{L}}\right)^2$$

We assume the same variable values: η_i= 3.15 x 10^{12} Pa s, u_v = 500 mm a^{-1}, ρ_l = 1000 kg m^{-3}, ρ_i = 917 kg m^{-3}, $\mathcal{L}$ = 3.3x10^5 J kg^{-1} C = 0.074 K MPa^{-1} , K= 2.5 W m^{-1} K^{-1}, and we calculated contact forces for clasts with radii from 5 to 1 cm.

Our load weight and contact forces are comparable to previous grinding experiments by Mathews (1979) that used a 22 kg vertical load and by Lee & Rutter (2004) that used 1-3 kg on a lever arm to produce ~20-60 N normal forces on their grinding wheels. Ring shear experiments used normal loads of 10-15 kg to grind sand (Kumar et al., 2006; J. S. Wright, 1995).

A 2-cm thick board notched to fit the basal slab and water basin is held in place by the operator while the cart with the mounted stylus is pulled and pushed 20 cm at a time at a velocity of ~2 cm/s, dragging the weighted rock stylus across the basal slab for a total travel distance of 5 m.

The static and sliding load required to move the stylus were measured for the first and last pulls using a hanging scale attached to the pulling handle.

The styluses and slabs were paired according to lithology, such that granitoids were abraded on the G1 granite slab, carbonates on the L1 limestone, sandstones on the SS1 sandstone, and quartzites on the Q1 quartzite. The schist styluses were abraded on the G1 granite slab.

Sample Collection and Analysis

After 5 m of travel against the basal slab, the stylus, slab, and basin are rinsed with distilled water to transfer produced sediment into a beaker. After 24 hrs of settling, the water is decanted and samples are transferred to pre-weighed vials, frozen, and then freeze dried and re-weighed to record produced sediment mass. However, this process introduced error to mass measurements owing to mass loss from vials during the freeze-dry process (despite warming to ambient temperature before measurement). To assess error, we froze and freeze-dried empty vials for which we measured mass before and after, and averaged the associated changes in mass, which ranged from 0.009 to 0.007 g (average 0.008 g). This mass loss error was sufficient to cause negative mass measurements on very small samples, thus corrections were needed for comparative mass analyses.

For PSD measurements using a Malvern Mastersizer 3000 Laser Particle Size Analyzer (LPSA), ~3 ml of 5% sodium hexametaphosphate is added as a dispersant to the sample vials, which are then sonicated for one minute. The water and sediment are mixed into a slurry then drawn from the vial using a 3 ml pipette. Drops are added to the Malvern Small Volume pump one at a time, agitating the slurry in the pipette bulb between each drop to ensure the subsample is well mixed.

RESULTS

Stylus Wear and Sample Masses

Approximately 1-4 mm of material was abraded from the pointed styluses, with quartzites exhibiting the least wear and sedimentary rocks exhibiting the most wear, and thus largest produced sediment volume. Flat styluses all show less wear than pointed styluses, generally <1 mm. Mass of sediment produced from grinding varied from ~0.001 (Q2-3) to 0.2 g (LS2-2). Pointed styluses generally produced more sediment than flat styluses of the same lithology. Basal slabs showed noticeable wear after all experiments, showing faint shallow grooves and scratches.

Figure 4 illustrates a comparison of mass produced from each sample. Quartzites produced less sediment than other sample types by roughly one order of magnitude. Excluding quartzites, pointed styluses generally produced ~0.005-0.015 g of sediment and flat styluses produced ~0.02-0.1 g of sediment, with a few outliers.

Particle Size Distributions

Figure 5 illustrates PSDs for all samples. Despite variability in curve shapes across stylus shape and lithology types, recurrent patterns emerge. For example, samples are poorly sorted and multi-modal, with the exceptions of quartzites, and samples SS1-3 (flat) and LS1-2 (pointed). Primary modes tend to fall between coarse (2.5-10 µm) and super coarse (10-67 µm) dust with clusters near ~7 μm and ~30 μm. Seven of 44 samples show primary modes in the giant (>67 μm) range, with most (5) being granitoids. Produced sand falls into fine to very fine sand modes. Secondary modes commonly fall into the coarse and super coarse dust ranges as well, and many distributions exhibit minor modes in fine (0-2.5 μm) and giant ranges (>67 μm). Averaging PSDs within lithology categories produces five curves, all with primary modes in coarse or super coarse ranges. Schists exhibit the finest primary mode of ~7 μm, with the other granitoids, quartzites, sandstones, limestones, and basalts clustering near 30 μm.

Mass Fractions

Figure 7(A) illustrates averaged PSDs for sample category mass fractions in fine, coarse, super coarse, and giant categories. These show that granitoids produce the largest mass fraction (30-35 g) of giant (fine to very fine sand) grains, while other lithologic types generally produce 5-20 g of sand. Pointed styluses are more likely to produce sand than flat styluses, i.e., all five styluses with PSDs showing giant primary modes are pointed.

Figure 7(B) illustrates mass fractions of silt (4-67 μm) and clay (<4 μm), enabling comparison to fines produced from other experiments and to natural loess deposits. The schist, sandstone, and limestone samples produced the largest amounts of fine dust (10-25%), while granitoids and quartzites generally produced <5% fine dust. Schist, sandstone, and limestone also produced relatively more coarse dust (~20-40%) while quartz and granitoid styluses produced <30% coarse dust.

DISCUSSION

Experiments replicating natural processes in the lab require some compromise when deciding which elements to match directly with nature and which elements to alter. The major difference between our experiments and the abrasion a glacial clast would experience in nature is the velocity of the moving clast. Alpine glacial ice typically moves at a pace of 1 m/day with the potential for up to ~6 m/day in surging glaciers (Millan et al., 2022). Our clast moves at ~1700 m/day, ~275 times faster. While our clasts move with a velocity likely not often experienced in nature, this velocity enables completion of multiple experimental runs on many lithologies within a reasonable time. Additionally, we have no indication that our faster moving clasts produce unusual PSDs that would not exist in nature. The higher velocity may increase the abrasion rate per meter. Subglacial clast-wear rates have not been reported so no comparisons to natural rates exist. Lee & Rutter (2004) reported experimental wear rates of 0.02-0.24 mm/m for granite wheels and 75 mm/m for sandstone wheels. If we assume an average pointed stylus wear of 3 mm per 5 m of travel, then our wear rate is 0.6 mm/m. Flat styluses with ~0.5 mm of material removed have wear rates of 0.1 mm/m.

We assumed pointed styluses would produce more sediment than flat styluses over the same travel distance, which generally holds true for most rock types with the exception of G4-4 (Flat Granite-4). We speculate that this might relate to the angle of contact between the G4-4 (flat) stylus and the granite slab: If the flat stylus surface contacted the slab at a slight angle rather than perfectly flat, then an edge of the stylus would experience increased contact force.

While all styluses showed wear and produced measurable sediment mass, some lithologic types abraded faster than others. The order-of-magnitude lower mass of sediment produced by quartzites relative to other samples likely reflects the considerable and relatively uniform hardness of this rock type. Comparison of mass from samples abraded in this study to basalt samples (styluses and slabs) abraded in the same device (Figure 5) shows that, compared to other lithologies, non-vesicular basalt resists abrasion more effectively than other lithologies, with the exception of quartzite. In contrast, vesicular basalts produce comparable amounts of sediment to other lithologies abraded. Significant differences in mass produced also emerge in comparing results within lithologic types i.e., limestone to limestone or sandstone to sandstone. For example LS2 pointed styluses produce ~2x the sediment produced by LS1 pointed styluses.

Variables that likely influence these differences are the mineralogy, crystal/particle sizes, cementation, and/or vesicularity of the protoliths. For example, LS1 is a fine-grained micrite (lime mudstone) with ~5% quartz silt, compared to LS2 a fossiliferous grainstone which comprises larger allochems. The finer-grained LS1 mudstone resists wear more effectively than the coarse-grained LS2 grainstone. SS1 is well-lithified, with calcite cement binding the quartz grains, whereas SS2 is relatively friable with little cement between grains. SS1 styluses generally produced less sediment than SS2, indicating that the calcite cement of LS1 increases the resistance to abrasion. Additionally, the non-vesicular basalts produced less sediment mass than vesicular basalts. The vesicles in the basalt reduce the integrity of the clast, which thus abrades faster than the non-vesicular clasts. Quartzites, composed almost entirely of quartz and silica cement with negligible void space, are the most resistant to abrasion.

We hypothesized that, upon abrasion, clasts with asperities (pointed styluses) would produce coarser sediment relative to clasts (styluses) with flat surfaces, but no such correlation emerged. Only six of the 22 pointed styluses exhibit primary modes in the giant dust (>67 µm) range. Four of those six were granites, which is half of the pointed granite styluses. The other two were schist (SC-1) and limestone (LS1-2). The majority of flat and pointed styluses of the same lithology produced PSDs with similar modes and curve profiles. These results suggest, at least for small clasts dragged across flat bedrock, breakage of asperities into coarser sediment is infrequent. If the basal slab was not flat and the points of the styluses encountered significant resistance from either a ridge or trough, failure of the stylus tip would be more likely. Such failure is likely to produce more coarse sediment than styluses ground on a flat surface.

We also hypothesized that flat styluses would produce abundant fines, with modes near or below 10 µm, analogous to the results of Lee & Rutter (2004). Lee & Rutter (2004) used smooth, asperity-free rock wheels turning and grinding past each other so we assumed that flat-surface abrasion might account for the production of such fine sediment. However, our flat styluses abrading against a flat basal slab produced PSDs that differ from those of Lee & Rutter (2004), for reasons that remain speculative. Our results also differ from theirs for the sandstone samples: two of their sandstones weathered readily to sand, owing to whole-grain plucking from the rock wheels, producing PSDs with modes similar to the sand grain modes (>100 µm), and no secondary modes in the silt range. In contrast, our experimental runs with friable (sample SS2) sandstone produced mostly silt.

Our study differs from all prior experiments of this type in the number of different lithologies tested. The results indicate that variation in curve shapes occur within and between all lithologic types, but four modal ranges emerge persistently across all compositions. These modes cluster between ~200-400 µm, 20-50 µm, 3-8 µm, and ~0.5-0.7 µm. Interestingly, these are nearly identical to the sediment population clusters near 300-500 µm, 20-50 µm, and 2-6 µm described by Assallay et al. (1998). Between these clusters they place "Tanner Gaps" of sediment existing between 30-120 and 1-8 mm. These Tanner Gaps are deficiencies in sediment PSD curves that generally divide gravel from sand and sand from silt (Assallay et al., 1998; Tanner, 1958); Assallay et al. (1998) incorporate an additional Tanner Gap at 10 µm. These previous works generally focused on sediment composed of quartz, feldspar, and clays weathered from granite as these produce the major components of siliciclastic sediment. Our results show similar clusters and gaps from a wider range of lithologies and reinforce the inference of an inherent control or pathway beyond lithologic composition that regulates mineral fracturing and comminution.

Comparison of our results on simulated glacial grinding with other experiments involving physical abrasion suggest the possibility of inherent controls on PSDs of produced fines regardless of abrasion mechanism (Table 2). The glacial grinding experiments performed by Kumar et al. (2006) show primary modes ~25 µm and the Brazilian vein quartz abraded by J. S. Wright (1995) produced fines with a mode ~45 µm. Aeolian abrasion experiments of quartzose dune sand and basalt sand (Adams & Soreghan, 2020) produced modes clustering ~6-8 µm and 20-50 µm. Experiments using crushed quartz in a cylindrical tumbling mill designed to simulate fluvial abrasion by J. Wright & Smith (1993) show that early in the abrasion process modes of 20-50 µm emerge, but with continued abrasion the mode shifts to ~8-10 µm. Soreghan et al. (2016) abraded granitoid-sourced fluvial-alluvial sands collected from different climates (hot-arid, hot-humid, cold-humid) in a vibrating micronizing mill where sand grains are abraded with vibrating zirconium oxide beads. Their results showed shifting modes with time, with first modes near 1000 µm, then near 30-50 µm, and finally 6-10 µm.

Considered in aggregate, these studies suggest that, under conditions of physical abrasion across multiple mechanisms (e.g., grinding, saltation), rocks produce fines (dust) of similar PSDs regardless of lithology. However, some processes, such as glacial grinding, focus the energy more efficiently than others and thus produce larger volumes of fines. When considering the efficiency of a process to make dust from a coarser starting material, we suggest it is dependent on how often a process can exert the required force necessary to break a sand or silt grain into smaller pieces. In the micronizing mill used by Soreghan et al. (2016), the sand and silt have nowhere to escape, the energy needed is constant, and the zirconium oxide beads serve to concentrate the required forces onto the smaller grains. For aeolian abrasion the energy may be sufficiently supplied by the wind, but grains must collide in such a way as to direct focused energy to exploit an existing weakness (i.e., Moss defects), and this apparently is a rarer occurrence than grains undergoing crushing and shearing beneath a glacier. Smalley (1995) argued that loess formation is the product of energy transfer, and that highly energetic systems in the Quaternary (glaciers and tectonism) were the primary drivers of silt production.

Production of sand-sized particles has been linked to the quartz and feldspar crystal sizes that form in typical plutonic granites (Smalley, 1966, 1995). The stresses of cooling and decompression additionally impart small crystalline defects in quartz commonly referred to as Moss defects (Moss & Green, 1975; Smalley, 1966). These defects for planar sheets separate by 1-10 µm with a mode of ~4 µm (Moss & Green, 1975). The sheets form at intersecting angles, and failure along these cracks is thought to be the mechanism by which quartz sand fractures into silt, with the defect sheet spacing serving as the ultimate control on the size of produced fines. The relative scarcity of defect sheet spacing below 2-4 µm is thought to be the reason for scarcity of clay-sized quartz particles (Moss & Green, 1975; Smalley, 1966). While this may provide a sufficient explanation for limiting the production of clay-size of quartz particles, it does not fully explain why breakage of quartz sand or abrasion of quartz-bearing lithic fragments produces silt with modes generally near 30 µm. Additionally, the presence of Moss defects in quartz does not explain the tendency of other minerals and lithologies lacking quartz to fragment into distributions with similar modes (~6 µm, 25 µm, 300 µm) observed in our (and other) studies. We speculate that there could exist fracture thresholds determined generally by the size of the clast. Clasts are targets for energy to interact with and the smaller the target, the more difficult it is for an energy regime within an abrasion process (e.g., glacial, saltation) to interact with the particle.

We performed two additional analyses to investigate possible relationships between rock hardness and mass produced, and between rock grainsize and mass produced. Several Schmidt Hammer rebound tests were performed on a selection of samples (G1, G2, Q1, Q2, LS1, LS2, B2, B3, and B5) to assess any relationship between hammer rebound and mass produced (Appendix 2). Hammer rebound value or Q value bears an empirical relationship to compressive strength and Young's Modulus for rocks (Katz et al., 1999). Results suggest a possible relationship between Q value and mass produced within some sample types (basalts), but other lithologies (limestones, granites, quartzites) fail to exhibit any relationship. Future work will include additional Schmidt Hammer rebound tests on uniform cylinders of rock to explore a correlation between Q value and mass produced from glacial grinding.

Similarly, preliminary analysis of the relationship between rock grain/crystal size and mass of sediment produced fails to show a correlation (Appendix 3). Samples were analyzed under a microscope and average grainsize modes were estimated qualitatively using a transparent grainsize card and plotted against the average mass produced from pointed styluses for each sample. The results plotted in Appendix 3 show a wide range of mass values for rocks of similar particle-size modes. For example, coarse-grained lithologies (granites and quartzites) exhibit masses that range from ~0.002 – 0.09 g, similar to the sediment mass ranges produced by fine-grained lithologies (micrite, basalt, and schist). Given that these grain size values are qualitative estimates, additional analysis is planned for future work, where samples will have grainsize quantitatively measured using 2D grain mapping software.

While similar PSD characteristics emerge across a wide range of sample types and abrasion mechanisms, differences in wear rates occur, implying differences in the rate of dust production. Additionally, rates of production of fine dust (<2.5 µm), coarse dust (2.5-10 µm), and super coarse dust (10-67 µm) vary by lithology. For example, limestones tend to produce fine dust at a higher rate. Lithologic differences in production rates of fine and coarse dust likely play a role in determining the climatic implications of dust generation, since fine dust generally exerts negative radiative forcing, whereas coarse dust exerts positive forcing (Kok et al., 2023). Our experiments show that glacial grinding of granite and quartzite produces 2-8 times less fine dust than sedimentary rocks, basalt, and schist. Accordingly, glacial abrasion of sedimentary rocks, basalt, and schist produces relatively more dust that could exert a radiative cooling effect compared to dust generated from granite and quartzite. However, the same lithologies (sedimentary rocks, basalt, and schist) also produce more coarse dust compared to granite and quartzite. This coarse dust has a general radiative warming influence in the atmosphere (Mahowald et al., 2011).

Our results suggest that grinding of granite and quartzite tend to yield PSDs that would produce abundant dust for short atmospheric transport and deposition in loess deposits (20-50 µm), with sedimentary rocks, basalt, and schist producing more dust capable of long-range transport (LRT). Production of LRT dust increases the likelihood of dust transport that could result in various indirect effects on climate, such as enhancements of primary productivity from dust-delivered nutrients, changes in albedo attributable to deposition on distal snow and ice caps, and dust-induced cloud interactions.

CONCLUSION

We replicated glacial abrasion using a wide selection of common lithologies, many of which have not been used in experimental glacial grinding studies investigating sediment PSDs. Based on previous studies we expected that clasts with asperities would produce more sediment than flat clasts and this is generally true based on our results. We also hypothesized based on previous work that flat styluses would produce more fine sediment and pointed styluses (clasts with asperities) would produce more coarse sediment. While this occurred in some experimental runs, no strong correlation emerged between use of pointed styluses and production of coarser PSDs. Given the diverse range of lithologies used, we hypothesized that different lithologies might produce distinctive PSDs with unique characteristics. Yet, regardless of lithology and stylus shape, experimentally produced sediment exhibits modes that cluster near 0.5 µm, 4-8 µm, 30 µm, and 100-300 µm. These modes are remarkably similar to modes identified for granitic-sourced quartzose sediment produced by natural and experimental replications of glacial grinding, aeolian saltation, fluvial abrasion, and mechanical crushing. These results suggest some fundamental control on particle size PSDs across varying mineralogical compositions and physical weathering mechanisms.

FIGURES AND TABLES

Sample Name	Lithology	Location	Age	Formation
G1	Granite	Colorado	Precabrian	Silver Plume Granite
G2	Quartz Diorite	Colorado	Precabrian	N/A
G3	Granite	Colorado	Precabrian	St. Kevin Granite
G4	Granite	France	Cambrian	Mendic Granite
SC	Schist	France	Cambrian	Schistes X10
Q1	Quartzite	Colorado	Precabrian	N/A
Q2	Quartzite	Colorado	Precabrian	N/A
SS1	Arkose (sandstone)	New Mexico	Pennsylvanian	Bursum
SS2	Quartz arenite (sandstone)	Colorado	Cretaceous	Muddy (Dakota Group)
LS1	Micrite (Limestone)	New Mexico	Pennsylvanian	Bursum
LS2	Grainstone (Limestone)	Missouri	Ordovician	Kimmswick

Table 1. Sample name designators used throughout the publication with their corresponding lithologies, collection locations, geological ages, and parent formations.

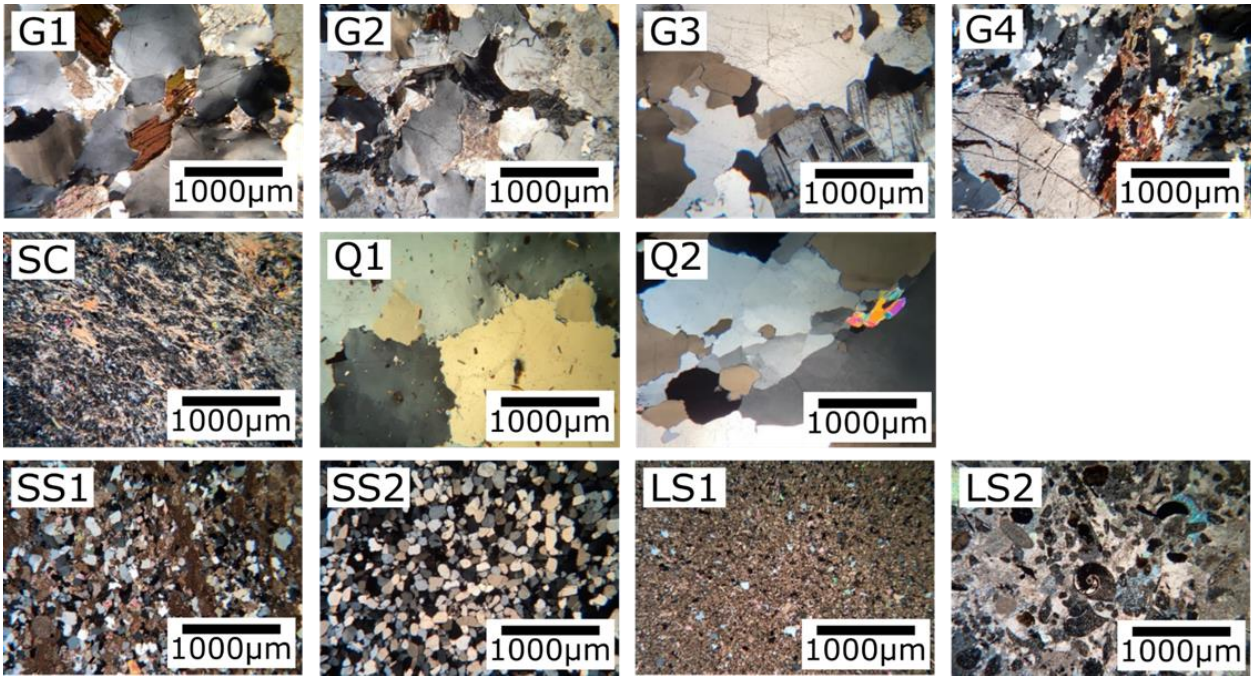

Figure 1. Photomicrographs from thin sections of each sample type under cross polarized light.

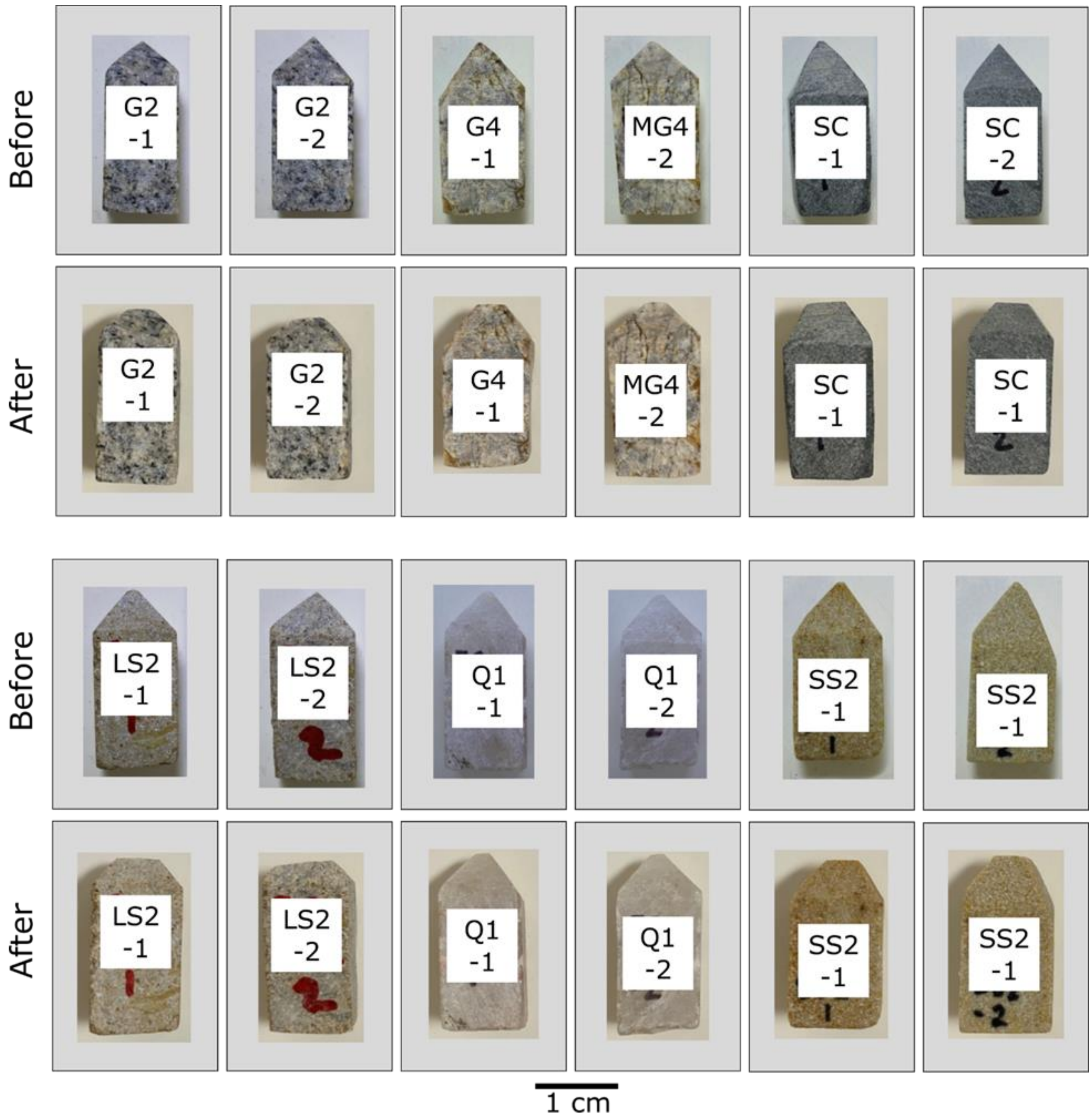

Figure 2. A selection of representative styluses before and after experimental glacial abrasion. Styluses are approximately 1 cm wide and 3 cm tall. The full catalog of before and after images for all styluses is in Appendix 1.

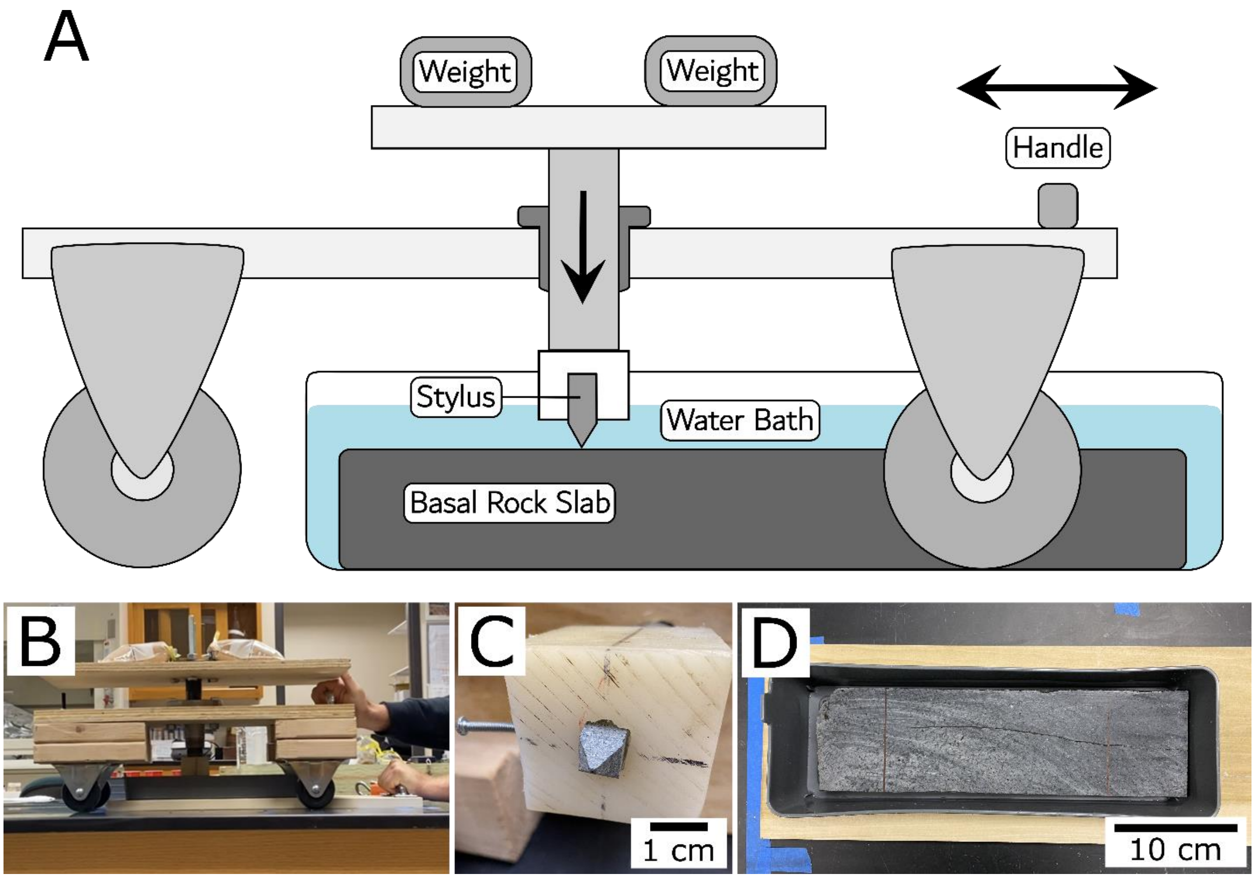

Figure 3. (A) schematic of glacial abrasion device showing the cart used to move the stylus across the basal rock slab, which sits in a basin of water. The stylus is pressed into contact with the basal slab by a weighted piston that transfers ~5kg of weight to the stylus producing a ~50 N contact force. (B) is a photograph of the abrasion device being operated. The basal slab is held in place while the cart is pulled and pushed, dragging the stylus 20 cm lengths for a combined travel distance of 5 m. (C) shows a mounted stylus in the base of the piston. (D) shows the basal slab inside the water basin. The water basin sits inside a hole cut in a thin board so the slab can be held in place while the stylus moves.

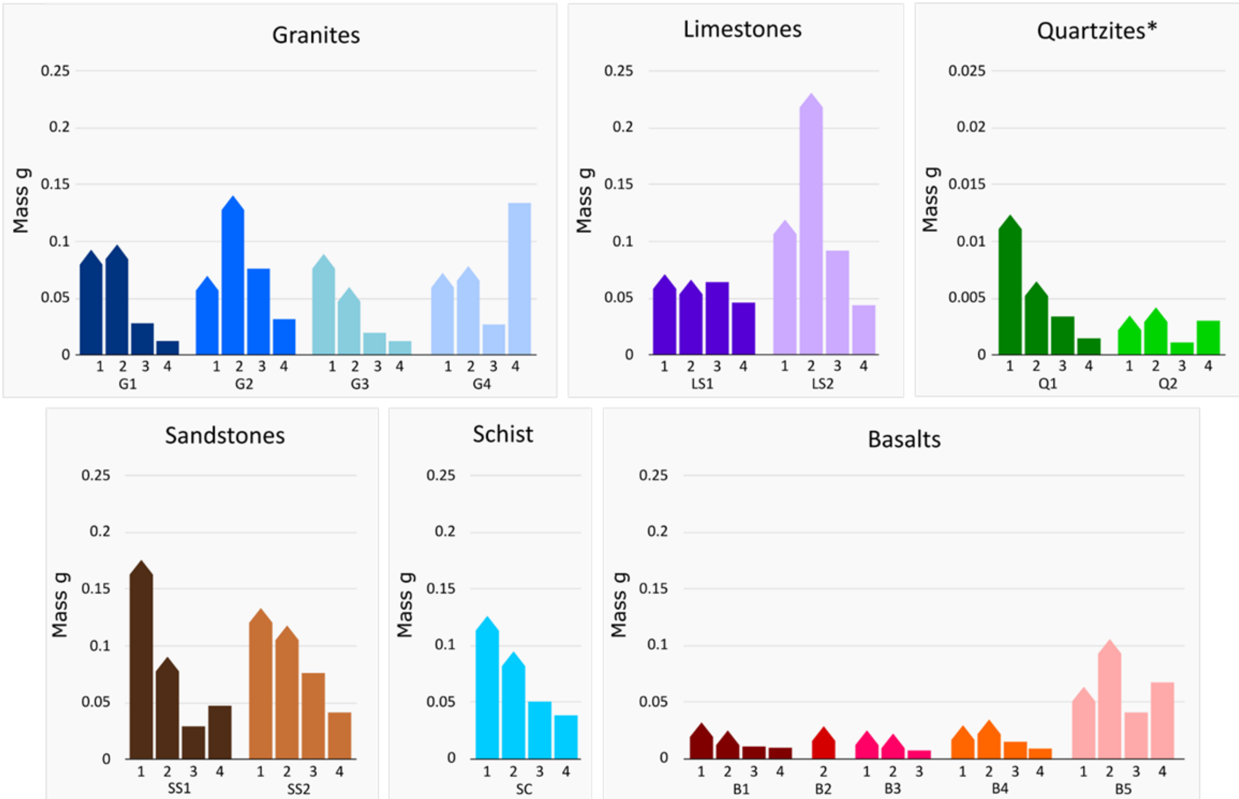

Figure 4. Mass of sediment produced from the abrasion of each stylus. Columns with points represent pointed styluses, flat columns represent flat styluses. Samples not shown on the basalt figure had masses below our measurable threshold. Note the vertical scale for Quartzites is reduced by an order of magnitude because of the low masses produced.

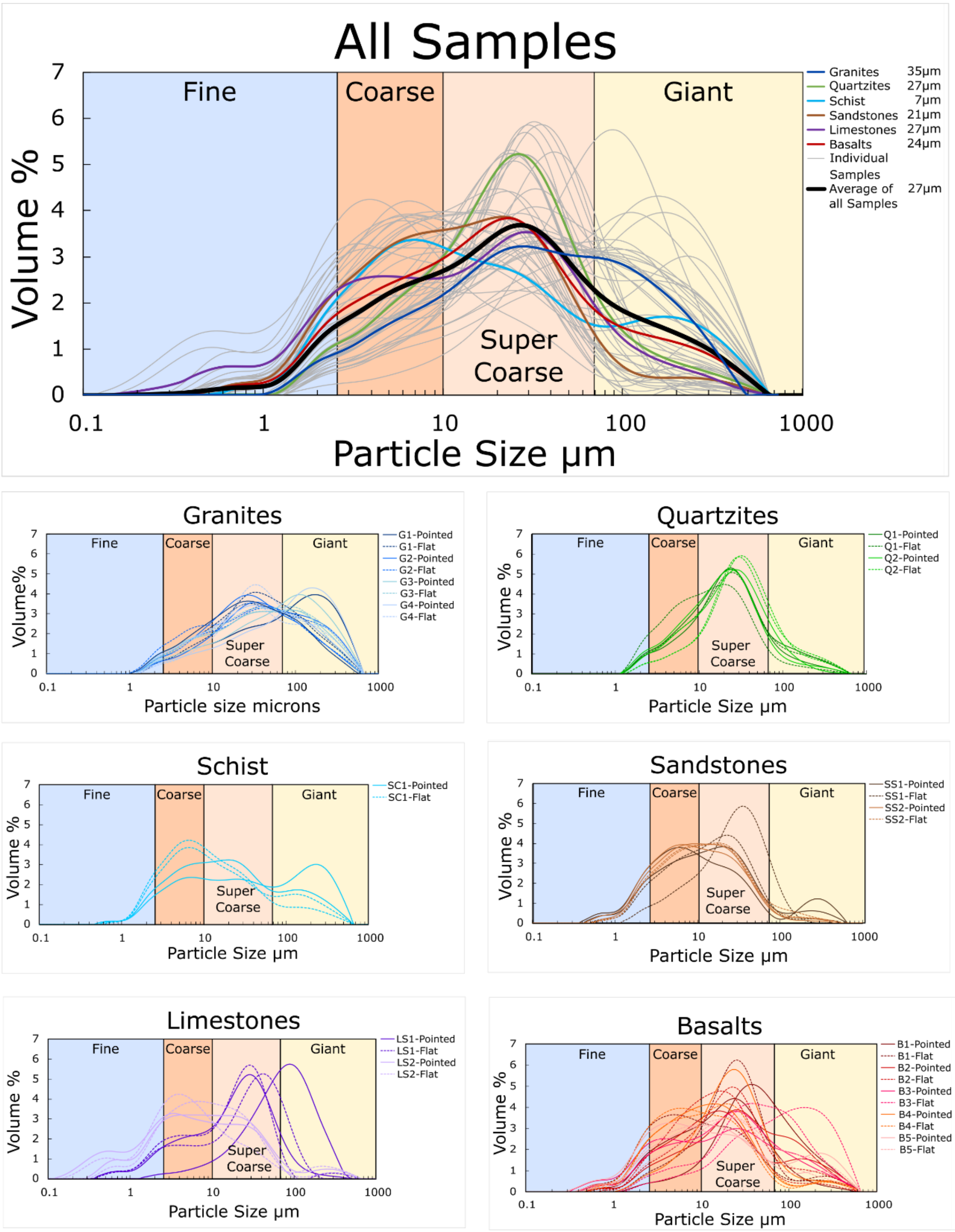

Figure 5. PSDs of all samples are shown on the top plot with the average PSD of all samples in black. PSD averages from each lithology are plotted together on the top figure for comparison. Modes are shown to the right of sample names. Pointed styluses are solid lines and flat styluses are dashed lines. PSDs of each lithology type and their corresponding styluses are shown in the lower six PSD plots. Each sample shows the PSD of four samples, two from pointed styluses (solid), and two from flat styluses (dashed). All basalts from (Adams and Soreghan, in review) are shown in the bottom right.

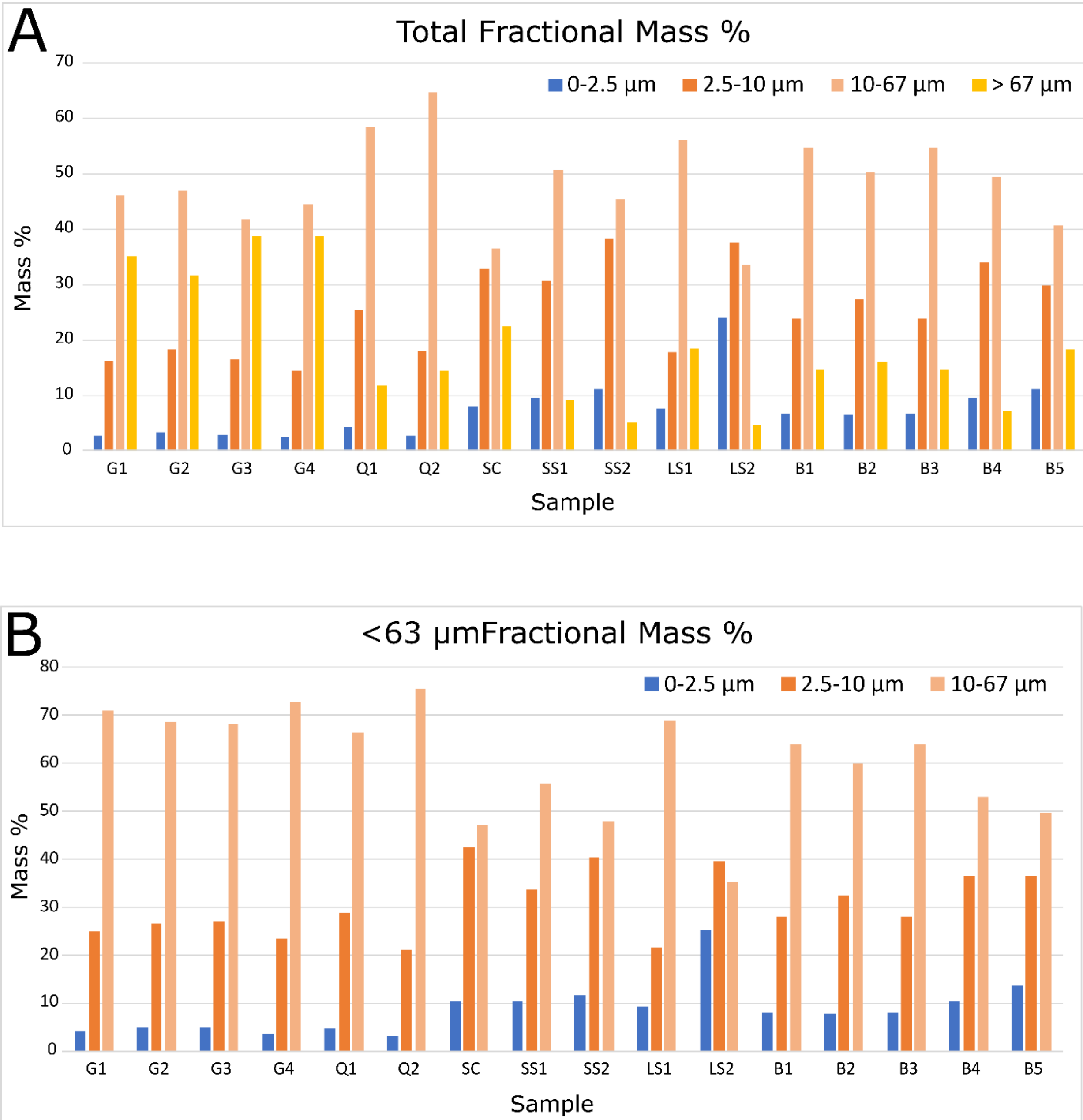

Figure 6. (A) shows the fractional masses from each sample abraded in this study and basalts abraded by (Adams and Soreghan, in review). These fractional masses are calculated using the PSDs. We assume mass % to be equivalent to volume % as the density differences of particles is considered negligible. (B) shows the fractional masses of each sample renormalized for the <67 µm mass.

Experimental aparatus	Composition of materials in experiments	Process simulated	Modes observed (μm) fine silt (0-10 μm)	coarse silt (10-62.5 μm)	sand (>62.5 μm)	Authors
Ring Shear	Sand from Cretaceous sand stone	Glacial grinding	0.7	24	600	Kumar et al., (2006)
Ring Shear	Brasilian vein quartz	Glacial grinding		45	250, 500, 1000	J. S. Wright, (1995)
Wheels of rock	Granite, schist, sandstone	Glacial grinding	0.2, 2, 6-10			Lee & Rutter, (2004)
Aeolian chamber	Quartzose dune sand	Aeolian Abrasion		40-50		Adams & Soreghan, (2020)
Aeolian chamber	Quartzose dune sand and basalt sand	Aeolian Abrasion	6-8	20-50		Adams & Soreghan, (in prep)
Micronizing Mill	Granitoid	Crushing	6-10	30-50	1000	Soreghan et al., (2016)
Tumbling mill	Crushed quartz	Fluvial Abrasion		20-50		J. Wright & Smith, (1993)
Stylus on rock	Granite, quartzite, schist, sandstone, limestone, basalt	Glacial grinding	0.5-0.7, 4-8	25-40	100-300	This study

Table 2. Comparison of previous experiments and sediment modes reported.

REFERENCES

Adams, S. M., & Soreghan, G. S. (2020). A test of the efficacy of sand saltation for silt production: Implications for the interpretation of loess. *Geology*, *48*, 1105–1109. https://doi.org/10.1130/g47282.1

Adebiyi, A., Kok, J., Murray, B. J., Ryder, C. L., Stuut, J.-B. W., Kahn, R. A., et al. (n.d.). *A review of coarse mineral dust in the Earth system*.

Adebiyi, A. A., & Kok, J. F. (2020). Climate models miss most of the coarse dust in the atmosphere. *Science Advances*, *6*, 1–10. https://doi.org/10.1126/sciadv.aaz9507

Aleinikoff, J. N., Muhs, D. R., Sauer, R. R., & Fanning, C. M. (1999). Late Quaternary loess in northeastern Colorado: Part II—Pb isotopic evidence for the variability of loess sources. *GSA Bulletin*, *111*(12), 1876–1883. https://doi.org/10.1130/0016-7606(1999)111<;1876:lqlinc>2.3.co;2

Aleinikoff, J. N., Muhs, D. R., Bettis, E. A., Johnson, W. C., Fanning, C. M., & Benton, R. (2008). Isotopic evidence for the diversity of late Quaternary loess in Nebraska: Glaciogenic and nonglaciogenic sourcesIsotopic evidence for Nebraska loess. *GSA Bulletin*, *120*(11–12), 1362–1377. https://doi.org/10.1130/b26222.1

Assallay, A. M., Rogers, C. D. F., Smalley, I. J., Jefferson, I. F., Ci, Õ., Trent, N., et al. (1998). Silt : 2 – 62 m m, 9 – 4 f, 20–30.

Braddock, W. A., & Cole, J. C. (1990). *Geologic map of Rocky Mountain National Park and vicinity, Colorado* (Report No. 1973). Retrieved from http://pubs.er.usgs.gov/publication/i1973

Brevart, O., Dupre, B., & Allegre, C. J. (1982). Metallogenic provinces and the remobilization process studied by lead isotopes; lead-zinc ore deposits from the southern Massif Central, France. *Economic Geology*, *77*(3), 564–575. https://doi.org/10.2113/gsecongeo.77.3.564

Bristow, C. S., Hudson-Edwards, K. A., & Chappell, A. (2010). Fertilizing the Amazon and equatorial Atlantic with West African dust. *Geophysical Research Letters*, *37*(14), n/a-n/a. https://doi.org/10.1029/2010gl043486

Conen, F., Morris, C. E., Leifeld, J., Yakutin, M. V., & Alewell, C. (2011). Biological residues define the ice nucleation properties of soil dust. *Atmospheric Chemistry and Physics*, *11*(18), 9643–9648. https://doi.org/10.5194/acp-11-9643-2011

Dufresne, J.-L., Gautier, C., Ricchiazzi, P., & Fouquart, Y. (2002). Longwave Scattering Effects of Mineral Aerosols. *Journal of the Atmospheric Sciences*, *59*(12), 1959–1966. https://doi.org/10.1175/1520-0469(2002)059<;1959:lseoma>2.0.co;2

Hallet. (1979). A Theoretical Model of Glacial Abrasion. *Journal of Glaciology*, *23*(89), 39–50. https://doi.org/10.3189/s0022143000029725

Hansen, D. D., & Zoet, L. K. (2019). Experimental constraints on subglacial rock friction. *Annals of Glaciology*, *60*(80), 37–48. https://doi.org/10.1017/aog.2019.47

Horton, J. D., Juan, C. A. S., & Stoeser, D. B. (2017). *The State Geologic Map Compilation (SGMC) geodatabase of the conterminous United States* (Report No. 1052) (p. 56). Reston, VA. Retrieved from http://pubs.er.usgs.gov/publication/ds1052

Jefferson, I. F., Jefferson, B. Q., Assallay, A. M., Rogers, C. D. F., & Smalley, I. J. (1997). Crushing of Quartz Sand to Produce Silt Particles. *Naturwissenschaften*, *84*(4), 148–149. https://doi.org/10.1007/s001140050366

Jordanova, D., Simon, Q., Balescu, S., Jordanova, N., Ishlyamski, D., Georgieva, B., et al. (2022). Environmental changes in southeastern Europe over the last 450 ka: Magnetic and pedologic study of a loess-paleosol profile from Kaolinovo (Bulgaria). *Quaternary Science Reviews*, *292*, 107671. https://doi.org/10.1016/j.quascirev.2022.107671

Katz, O., Reches, Z., & Roegiers, J.-C. (2000). Evaluation of mechanical rock properties using a Schmidt Hammer. *International Journal of Rock Mechanics and Mining Sciences*, *37*(4), 723–728. https://doi.org/10.1016/s1365-1609(00)00004-6

Kellogg, K. S., Shroba, R. R., Ruleman, C. A., Bohannon, R. G., McIntosh, W. C., Premo, W. R., et al. (2017). *Geologic map of the upper Arkansas River valley region, north-central Colorado* (Report No. 3382) (p. 80). Reston, VA. Retrieved from http://pubs.er.usgs.gov/publication/sim3382

Kok, J. F., Ridley, D. A., Zhou, Q., Miller, R. L., Zhao, C., Heald, C. L., et al. (2017). Smaller desert dust cooling effect estimated from analysis of dust size and abundance. *Nature Geoscience*, *10*(4), 274–278. https://doi.org/10.1038/ngeo2912

Kok, J. F., Storelvmo, T., Karydis, V. A., Adebiyi, A. A., Mahowald, N. M., Evan, A. T., et al. (2023). Mineral dust aerosol impacts on global climate and climate change. *Nature Reviews Earth & Environment*, *4*(2), 71–86. https://doi.org/10.1038/s43017-022-00379-5

Kumar, R., Jefferson, I. F., O'Hara-Dhand, K., & Smalley, I. J. (2006). Controls on quartz silt formation by crystalline defects. *Naturwissenschaften*, *93*(4), 185–188. https://doi.org/10.1007/s00114-006-0087-0

Lee, A. G. G., & Rutter, E. H. (2004). Experimental rock-on-rock frictional wear: Application to subglacial abrasion. *Journal of Geophysical Research: Solid Earth*, *109*, 1–11. https://doi.org/10.1029/2004jb003059

Mahowald, N., Ward, D. S., Kloster, S., Flanner, M. G., Heald, C. L., Heavens, N. G., et al. (2011). Aerosol impacts on climate and biogeochemistry. *Annual Review of Environment and Resources*, *36*, 45–74. https://doi.org/10.1146/annurev-environ-042009-094507

MATHEWS, W. H. (1979). SIMULATED GLACIAL ABRASION. *Journal of Glaciology*, *23*, 51–56.

McTainsh, G. H. (1989). Quaternary aeolian dust processes and sediments in the Australian region. *Quaternary Science Reviews*, *8*(3), 235–253. https://doi.org/10.1016/0277-3791(89)90039-5

Millan, R., Mouginot, J., Rabatel, A., & Morlighem, M. (2022). Ice velocity and thickness of the world's glaciers. *Nature Geoscience*, *15*(2), 124–129. https://doi.org/10.1038/s41561-021-00885-z

Moss, A. J., & Green, P. (1975). Sand and silt grains: Predetermination of their formation and properties by microfractures in quartz. *Journal of the Geological Society of Australia*, *22*(4), 485–495. https://doi.org/10.1080/00167617508728913

Muhs, D. R. (2013). *Loess and its Geomorphic, Stratigraphic, and Paleoclimatic Significance in the Quaternary* (Vol. 11). https://doi.org/10.1016/b978-0-12-374739-6.00302-x

Muhs, Daniel R. (2013). The geologic records of dust in the quaternary. *Aeolian Research*, *9*, 3–48. https://doi.org/10.1016/j.aeolia.2012.08.001

NAHON, D., & TROMPETTE, R. (1982). Origin of siltstones: glacial grinding versus weathering. *Sedimentology*, *29*(1), 25–35. https://doi.org/10.1111/j.1365-3091.1982.tb01706.x

Nelson, W. John, Devera, Joseph A., Masters, John M. (2005). *Geology of the Jonesboro 15-Minute Quadrangle, southwestern Illinois : Jonesboro, Mill Creek, Ware, and McClure 7.5-Minute Quadrangles* (Bulletin no. 101). Retrieved from https://www.ideals.illinois.edu/items/45187

Okin, G. S., Baker, A. R., Tegen, I., Mahowald, N. M., Dentener, F. J., Duce, R. A., et al. (2011). Impacts of atmospheric nutrient deposition on marine productivity: Roles of nitrogen, phosphorus, and iron. *Global Biogeochemical Cycles*, *25*, 1–10. https://doi.org/10.1029/2010gb003858

Pécsi, M. (1995). The role of principles and methods in loess-paleosol investigations. *GeoJournal*, *36*(2–3), 117–131. https://doi.org/10.1007/bf00813156

Roger, F., Teyssier, C., Respaut, J.-P., Rey, P. F., Jolivet, M., Whitney, D. L., et al. (2015). Timing of formation and exhumation of the Montagne Noire double dome, French Massif Central. *Tectonophysics*, *640*, 53–69. https://doi.org/10.1016/j.tecto.2014.12.002

Rosenfeld, D., Rudich, Y., & Lahav, R. (2001). Desert dust suppressing precipitation: A possible desertification feedback loop. *Proceedings of the National Academy of Sciences*, *98*(11), 5975–5980. https://doi.org/10.1073/pnas.101122798

Skiles, S. M., Flanner, M., Cook, J. M., Dumont, M., & Painter, T. H. (2018). Radiative forcing by light-absorbing particles in snow. *Nature Climate Change*, *8*(11), 964–971. https://doi.org/10.1038/s41558-018-0296-5

Smalley, I. (1995). Making the material: The formation of silt sized primary mineral particles for loess deposits. *Quaternary Science Reviews*, *14*, 645–651. https://doi.org/10.1016/0277-3791(95)00046-1

Smalley, I., Marković, S. B., & Svirčev, Z. (2011). Loess is [almost totally formed by] the accumulation of dust. *Quaternary International*, *240*, 4–11. https://doi.org/10.1016/j.quaint.2010.07.011

SMALLEY, I. J. (1966). Formation of Quartz Sand. *Nature*, *211*(5048), 476–479. https://doi.org/10.1038/211476a0

Smalley, I. J. (1966). The properties of glacial loess and the formation of loess deposits. *Journal of Sedimentary Research*, *36*(3), 669–676. https://doi.org/10.1306/74d7153c-2b21-11d7-8648000102c1865d

Smalley, I. J., & Vita-Finzi, C. (1968). THE FORMATION OF FINE PARTICLES IN SANDY DESERTS AND THE NATURE OF 'DFESERT ~ LOESS 1. *JOURNAL OF SFEDIMEN' RARY PETROLOGY*, *38*, 76–1.

Soreghan, G. S., Joo, Y. J., Madden, M. E. E., & Deventer, S. C. V. (2016). Silt production as a function of climate and lithology under simulated comminution. *Quaternary International*, *399*, 218–227. https://doi.org/10.1016/j.quaint.2015.05.010

Soreghan, G. S., Heavens, N. G., Pfeifer, L. S., & Soreghan, M. J. (2023). Dust and loess as archives and agents of climate and climate change in the late Paleozoic Earth system. *Geological Society, London, Special Publications*, *535*(1), SP535-2022–208. https://doi.org/10.1144/sp535-2022-208

Tang, M., Cziczo, D. J., & Grassian, V. H. (2016). Interactions of Water with Mineral Dust Aerosol: Water Adsorption, Hygroscopicity, Cloud Condensation, and Ice Nucleation. *Chemical Reviews*, *116*(7), 4205–4259. https://doi.org/10.1021/acs.chemrev.5b00529

Tanner, W. F. (1958). The zig-zag nature of Type I and Type IV curves. *Journal of Sedimentary Research*, *28*(3), 372–375. https://doi.org/10.1306/74d7080d-2b21-11d7-8648000102c1865d

Tsoar, H., & Pye, K. (1987). Dust transport and the question of desert loess formation. *Sedimentology*, *34*, 139–153. https://doi.org/10.1111/j.1365-3091.1987.tb00566.x

Watts. (1974). *Inclusions in ice*. University of Bristol.

Wright, J., & Smith, B. (1993). Fluvial Comminution and the Production of Loess-Sized Quartz Silt: A Simulation Study OF LOESS-SIZED QUARTZ SILT: A Simulation Study. *Source: Geografiska Annaler. Series A, Physical Geography Geogr. Ann*, *75*, 25–34. Retrieved from http://www.jstor.org/stable/521050

Wright, J. S. (1995). Glacial comminution of quartz sand grains and the production of loessic silt: A simulation study. *Quaternary Science Reviews*, *14*(7–8), 669–680. https://doi.org/10.1016/0277-3791(95)00048-8

SUPPLEMENTAL MATERIALS

Chapter I Supplemental

Appendix 1

Supplement X: Sample Mass Data and Scaling Calculations

Description: This worksheet hosts mass data collected from our aeolian abrasion experiments and demonstrates how scaling calculations were performed. This is a supplement for the methods and results sections and provides the calculations performed to produce figures X and Y, and Tables A and B. We use the surface area of the abrasion chamber, the mass of dust produced, and the time needed to produce the mass of dust as our starting point. We then use the total surface area of modern dune fields on Mars to determine how much time is required to produce a target mass of dust deemed geologicaly significant. Finally we determine the feasibility of this time by calculating the annual abrasion time required over long time intervals to achieve the target masses.

Sample Mass Data									
Sample	Empty Vial Masses			Avg	Filled Vial Masses			Avg	Sample Mass
ICE-1	6.5275	6.5275	6.5275	6.5275	8.2167	8.2167	8.2167	8.2167	1.6892
ICE-2	6.5137	6.5136	6.5137	6.513666667	8.2848	8.2848	8.2848	8.2848	1.771133333
ICE-3	6.5298	6.5299	6.5299	6.529866667	8.4736	8.4736	8.4735	8.473566667	1.9437
ICE-4	6.5345	6.5344	6.5342	6.534366667	8.7524	8.7525	8.7524	8.752433333	2.218066667
HI-1	6.5273	6.5273	6.5274	6.527333333	6.9507	6.9508	6.9508	6.950766667	0.423433333
HI-2	6.5303	6.5302	6.5303	6.530266667	7.0046	7.0045	7.0047	7.0046	0.474333333
HI-3	6.5151	6.5152	6.5152	6.515166667	7.0418	7.0417	7.0418	7.041766667	0.5266
HI-4	6.5144	6.5144	6.5144	6.5144	6.9608	6.9607	6.9607	6.960733333	0.446333333
ISD-1	6.5278	6.5277	6.5276	6.5277	6.5534	6.5535	6.5534	6.553433333	0.025733333
ISD-2	6.5247	6.5248	6.5247	6.524733333	6.5653	6.5652	6.5653	6.565266667	0.040533333

General Color Key
Title
Sub title 1
Sub title 2
Description
Constant
ICE value
HI Value
ICE designation
HI Designation
Output 1
Output 2
Output 3

Sample Masses	
Sample	Sample Mass
ICE-1	1.6892
ICE-2	1.771133333
ICE-3	1.9437
ICE-4	2.218066667
HI-1	0.423433333
HI-2	0.474333333
HI-3	0.5266
HI-4	0.446333333
ISD-1	0.025733333
ISD-2	0.040533333

Sample Mass Averages	
Grams	
4 Day Avg ICE	4 Day Avg HI
1.905525	0.467675
1 Day Avg ICE	1 Day Avg HI
0.47638125	0.11691875

Sample Mass Avg 1 Day	
Kilograms	
Avg ICE	Avg HI
0.000476381	0.000116919

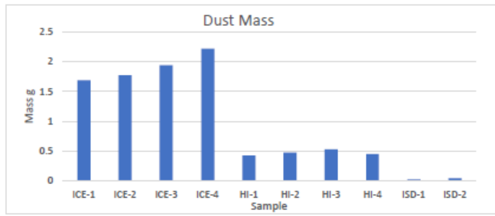

Dust Target Calculation		
We use the upper and lower estimates from X et al as end members for our target dust volume and mass.		
Estimated lower amount eroded dust from MFF km3		300000
Estimated upper amount eroded dust from MFF km3		1800000
We convert these values in km3 to m3		
Multiply by		1.00E+09
Estimated lower eroded dust from MFF m3		3.00E+14
Estimated upper eroded dust from MFF m3		1.80E+15
We then convert volume to mass using an assumed density		
Density ranges from literature	2.5-3g/cm3	
Density used for calc	2.75	g/cm3
Unit conversion for density		
Multiply by		1000
Scaled density	2750	kg/m3
Upper and lower estimates of total mass eroded from MFF		
Estimated lower mass eroded from MFF kg		8.25E+17
Estimated upper mass eroded from MFFkg		4.95E+18

Abrasion Chamber Area Calculation		
Diameters in cm		
Filter	Chamber	
7	12.5	
Radius in cm		
Filter	Chamber	
3.5	6.25	
Area in cm2		
Filter	Chamber	Abrasion Area
38.48451001	122.718463	84.23395302
Abrasion area in km2		
8.4234E-09		

Total Area of Sand dunes on Mars km 2
980000

Dust per km per day on Mars Calculation		
We divide the mass in (kg) produced in 1 day in the abrasion chamber by the area of the abrasion chamber create scaling variables for ICE and HI dust production rates. These variables are assumed masses of dust that could be produced in 24 hours of abrasion over a surface area of 1km2.		
Sample Avg	Value	Unit
ICE	56554.54041	kg/km2/day
HI	13880.24019	kg/km2/day

Maximum 1 Day Mars Calculation		
We use the total area of dune fields on modern Mars to calculate how much dust could be generated in 24 hours of abrasion wind velocities by these dune fields for each sand type (ICE & HI)		
Sample Avg	Value	Unit
ICE	55423449599	kg/day
HI	13602635385	kg/day

Time needed to produce target dust mass on Mars		
We divide the values for dust produced in 24 hours of abrasion time over the total area of dunes fields on Mars by the estimates for mass eroded from the MFF. There are two estimates for mass eroded from the MFF and two sand types (ICE and HI) giving us four values for days needed to produce the four target masses.		
Time to produce lower mass target eroded from MFF		
Sample	Days	Earth Years
ICE	1.49E+07	4.08E+04
HI	6.07E+07	1.66E+05
Time to produce upper mass target eroded from MFF		
Sample	Days	Earth Years
ICE	8.93E+07	2.45E+05
HI	3.64E+08	9.97E+05

Days and hours per year to reach target mass over geologically significant time intervals					
To get a general understanding of how reasonable it is for the dune fields of Mars to produce the target masses of dust we calculate how many days a year would be needed to produce the target mass over long invervals of time. For example we consider over a billion Earth years, how many full days need to produce wind velocities capable of abrading sand in the dune fields. We calculate this for all four target mass values (lower and upper for both ICE and HI sands) Hours needed are calculated below as well.					
Target type	Time interval Earth years				
	1,000,000,000	100,000,000	10,000,000	1,000,000	
Lower mass ICE	0.015	0.15	1.49	14.89	Days per year needed
Lower mass HI	0.061	0.61	6.07	60.65	
Upper mass ICE	0.089	0.89	8.93	89.31	
Upper mass HI	0.364	3.64	36.39	363.90	
Lower mass ICE	0.36	3.57	35.72	357.25	Hours per year needed
Lower mass HI	1.46	14.56	145.56	1,455.60	
Upper mass ICE	2.14	21.43	214.35	2,143.50	
Upper mass HI	8.73	87.34	873.36	8,733.60	

note 322 hours was windiest location from weather stations in Adams and Soreghan 2020

Appendix 2

WPF Report

Scan ID: Hi_start_SA.raw

Scan Parameters: 2.0°/70.0°/0.02°/2(s), I(p)=101.00/3.00, Cu(40kV,44mA), Saturday, December 17, 2022, 5:50 PM

☑ Zero Offset = -0.0423 (0.0124) ☐ Displacement = 0.0 ☐ Distance Slack = 0.0

☑ Kα2 Peaks Present ☐ Kα2/Kα1 Ratio = 0.5 ☐ X-Ray Polarization = 1.0

Geometry: Diffractometer Lp Fitted-Range: 2.0° - 70.0° BG-Model: Polynomial (6) λ: 1.54059Å (Cu)

PSF: pseudo-Voigt Broadening: Individual FWHM Curve Instrument: Constant FWHM = 0.1°

Phase ID (3)	Chemical Formula	PDF-#	Wt% (σ)	DD% (σ)	RIR	μ
Forsterite (PO)	$SiMg_2O_4$	98-000-1597	33.4 (3.9)	48.2 (0.5)	0.73	97.6
Augite (PO)	$FeCa_4Si_8Mg_{2.96}O_{24}$	98-000-0102	35.5 (6.5)	30.8 (0.8)	1.05	241.4
Albite - high	$Na(AlSi_3O_8)$	98-000-0040	31.1 (6.2)	21.0 (1.0)	0.63	85.4

XRF(Wt%): Fe2O3=3.2%, CaO=8.9%, SiO2=54.7%, Al2O3=6.1%, MgO=23.9%, Na2O=3.7%

Refinement Halted (R/E=1.18), ♣ Round=4, Iter=6, P=40, R=24.54% (E=20.72%, EPS=0.5)

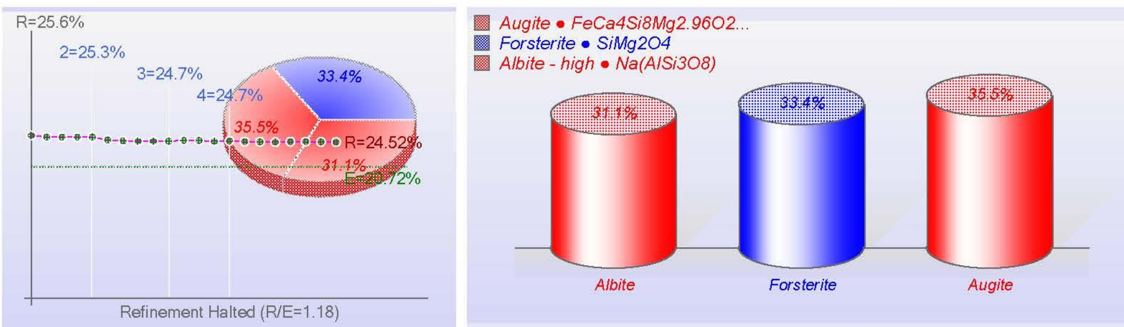

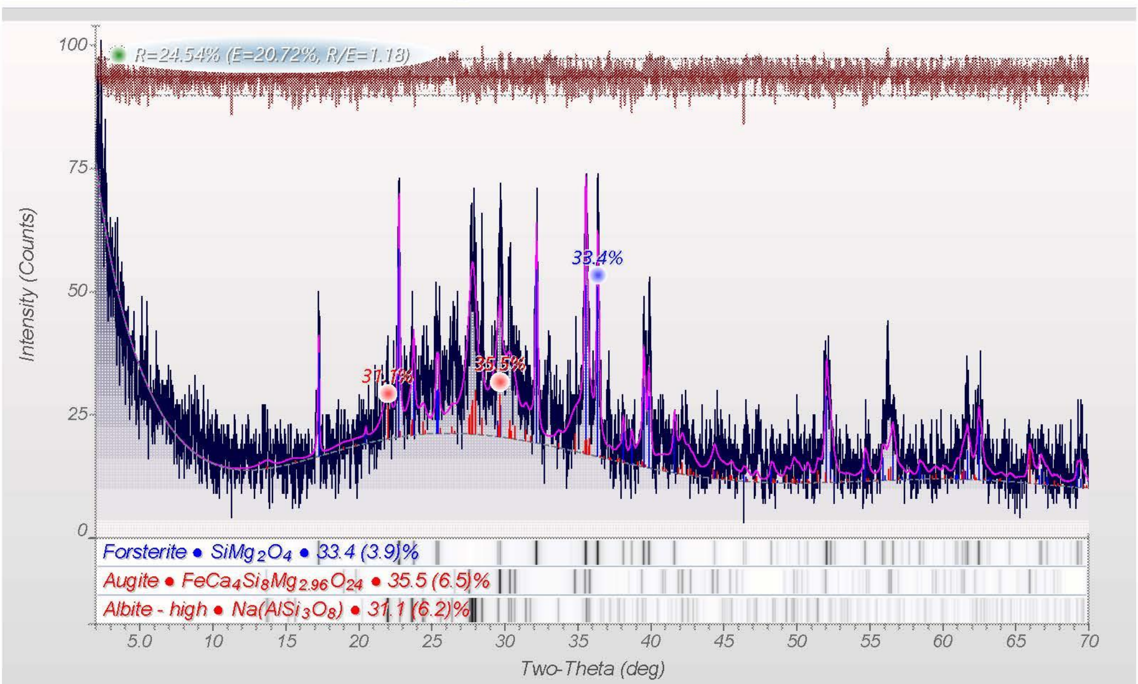

C:\Users\elwo2924\Desktop\Hi_start_SA.raw Friday, February 10, 2023, 3:09 PM ● Univ Oklahoma

HI Starting Sand XRD Results

iceland3 SA	WPF Report

Scan ID: 23-01-09-meem-iceland3.raw • iceland3 SA

Scan Parameters: 2.0°/70.0°/0.02°/2(s), I(p)=228.00/1.00, Cu(40kV,44mA), Monday, January 9, 2023, 6:18 PM

✔ Zero Offset = -0.0228 (0.0111)	☐ Displacement = 0.0	☐ Distance Slack = 0.0
✔ Kα2 Peaks Present	☐ Kα2/Kα1 Ratio = 0.5	☐ X-Ray Polarization = 1.0

Geometry: Diffractometer Lp Fitted-Range: 12.0° - 70.0° BG-Model: Polynomial (3) λ: 1.54059Å (Cu)

PSF: pseudo-Voigt Broadening: Individual FWHM Curve Instrument: Constant FWHM = 0.1°

Phase ID (4)	Chemical Formula	PDF-#	Wt% (σ)	DD% (σ)	RIR	μ
Bytownite (PO)	$(Ca,Na)(Si,Al)_4O_8$	98-000-0134	52.0 (3.4)	48.6 (0.2)	0.56	132.8
Augite	$FeCa_4Si_8Mg_{2.96}O_{24}$	98-000-0102	36.0 (2.6)	39.1 (0.1)	1.05	240.7
Forsterite	$(NiMg)SiO_4$	98-000-3707	9.8 (1.8)	8.8 (0.1)	1.19	136.5
Hematite	Fe_2O_3	04-003-2900	2.3 (0.7)	3.6 (0.0)	3.06	1139.2

XRF(Wt%): NiO=4.2%, Fe2O3=5.5%, CaO=18.5%, SiO2=46.0%, Al2O3=18.6%, MgO=7.0%, Na2O=0.6%

Refinement Halted (R/E=1.26), ♣ Round=4, Iter=6, P=42, R=28.86% (E=22.87%, EPS=0.5)

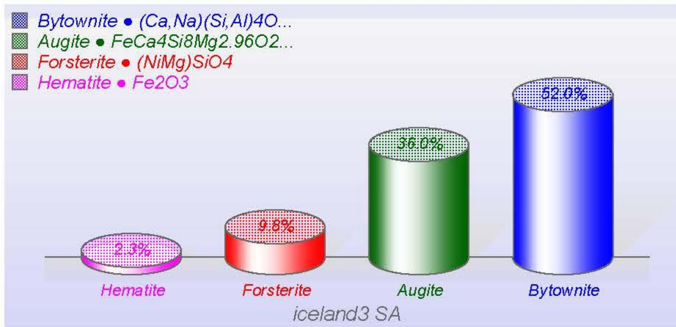

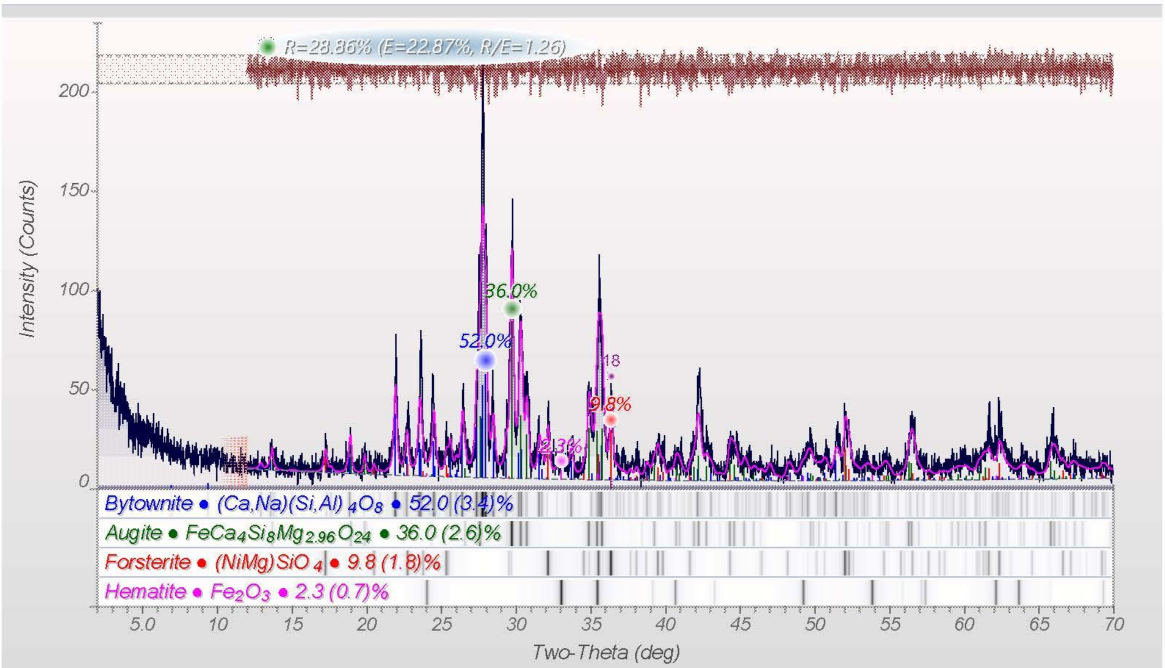

C:\Users\elwo2924\Desktop\23-01-09-meem-iceland3.raw   Friday, February 10, 2023, 2:56 PM • Univ Oklahoma

ICE Starting Sand XRD Results

ICE Dust Fraction

WPF Report

Scan Parameters: 2.0°/70.0°/0.02°/2(s), I(p)=58.000/1.000, Cu(40kV,44mA), Thursday, February 23, 2023, 11:09 AM

✔ Zero Offset = 0.04 (0.0463)	☐ Displacement = 0.0	☐ Distance Slack = 0.0
✔ Kα2 Peaks Present	☐ Kα2/Kα1 Ratio = 0.5	☐ X-Ray Polarization = 1.0

Geometry: Diffractometer Lp   Fitted-Range: 2.0° - 70.0°   BG-Model: Polynomial (6)   λ: 1.54059Å (Cu)

PSF: pseudo-Voigt   Broadening: Individual FWHM Curve   Instrument: Constant FWHM = 0.1°

Phase ID (6)	Chemical Formula	PDF-#	Wt% (σ)	DD% (σ)	RIR	μ
Bytownite	$(Ca,Na)(Si,Al)_4O_8$	98-000-0134	55.0 (23.4)	60.5 (2.0)	0.56	133.0
Indialite	$Mg_2(Al_4Si_5O_{18})$	98-000-0257	12.9 (11.0)	11.9 (1.1)	2.39	79.7
Orthoclase	$KAlSi_3O_8$	98-000-0338	3.2 (4.8)	1.2 (0.5)	0.66	125.3
Albite - low	$Na(AlSi_3O_8)$	98-000-0041	3.0 (5.5)	1.7 (0.6)	0.63	85.8
Cristobalite low	SiO_2	98-000-0178	0.6 (0.8)	1.5 (0.1)	4.97	80.1
Augite	$FeCa_4Si_8Mg_{2.96}O_{24}$	98-000-0102	25.3 (9.3)	23.2 (0.6)	1.05	240.6

XRF(Wt%): Fe2O3=2.3%, CaO=16.3%, K2O=0.5%, SiO2=49.6%, Al2O3=25.4%, MgO=5.1%, Na2O=1.0%

Refinement Halted (R/E=1.14), ♣ Round=4, Iter=7, P=80, R=29.21% (E=25.65%, EPS=0.5)

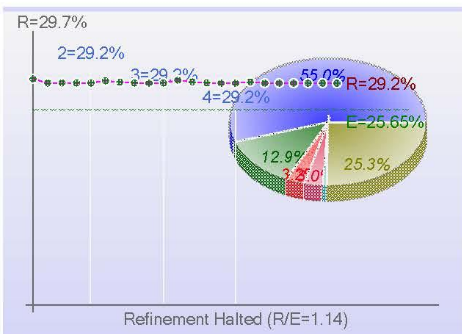

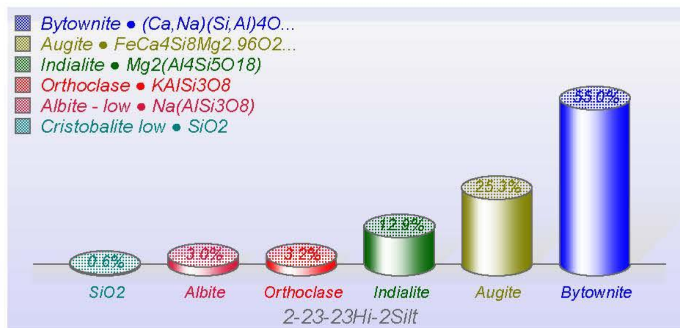

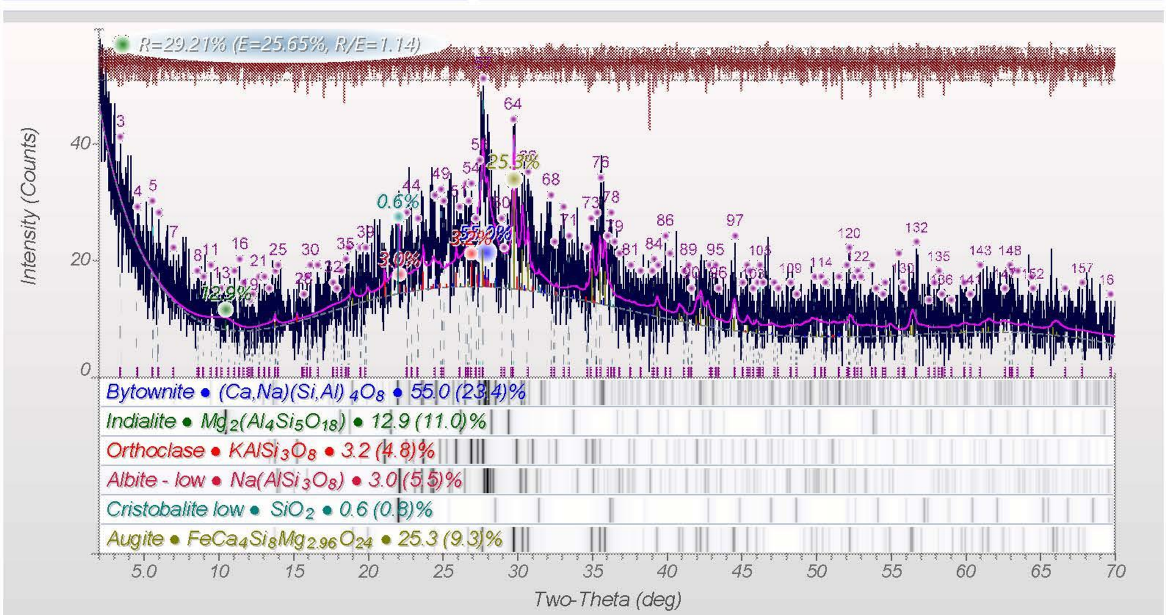

C:\Users\elwo2924\Desktop\MEEM\02-23-23-Hi-2-silt-SA.raw   Friday, March 10, 2023, 3:17 PM • Univ Oklahoma

ICE Dust Fraction XRD Results

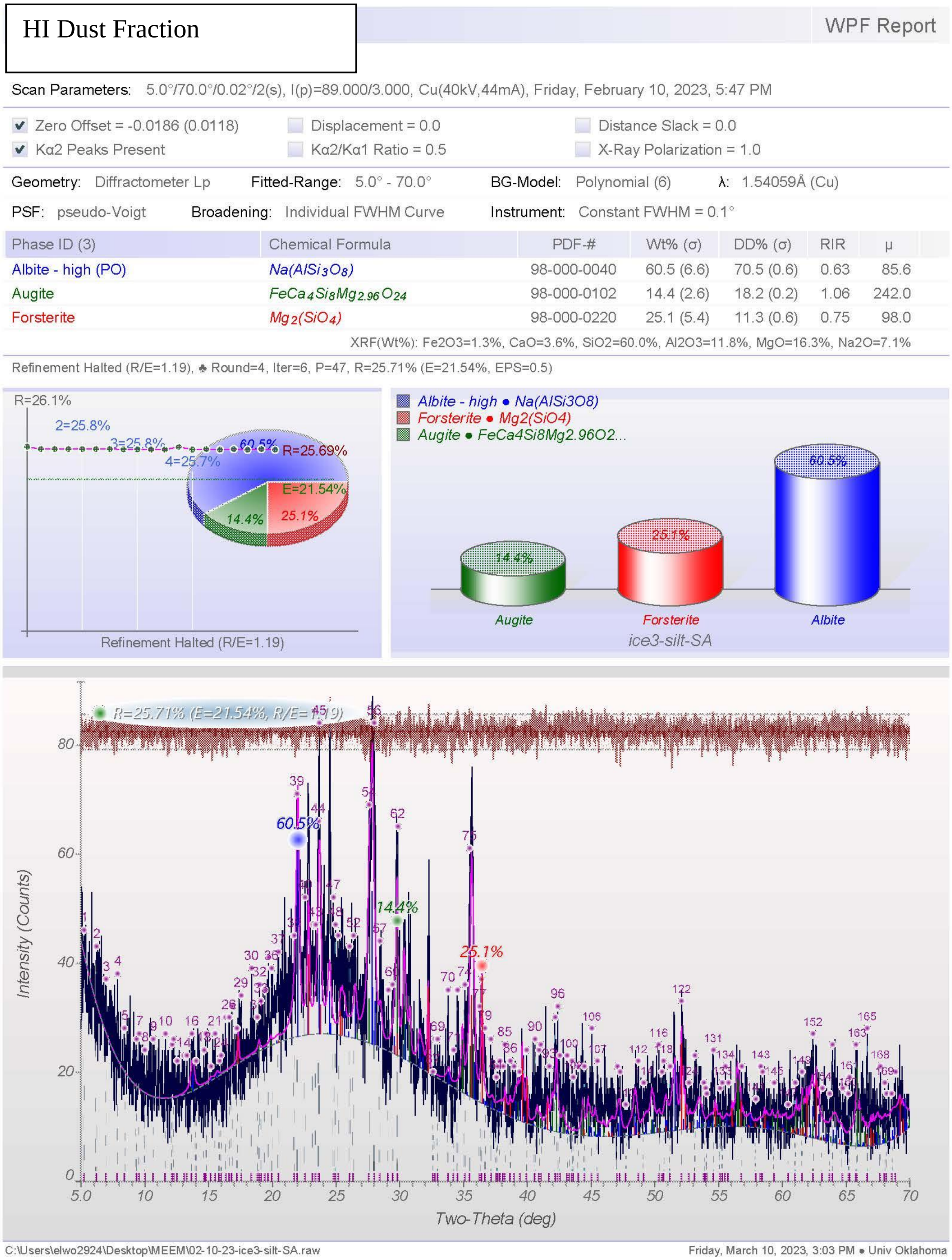

HI Dust Fraction

WPF Report

Scan Parameters: 5.0°/70.0°/0.02°/2(s), I(p)=89.000/3.000, Cu(40kV,44mA), Friday, February 10, 2023, 5:47 PM

- ✔ Zero Offset = -0.0186 (0.0118)
- ✔ Kα2 Peaks Present
- ☐ Displacement = 0.0
- ☐ Kα2/Kα1 Ratio = 0.5
- ☐ Distance Slack = 0.0
- ☐ X-Ray Polarization = 1.0

Geometry: Diffractometer Lp | Fitted-Range: 5.0° - 70.0° | BG-Model: Polynomial (6) | λ: 1.54059Å (Cu)

PSF: pseudo-Voigt | Broadening: Individual FWHM Curve | Instrument: Constant FWHM = 0.1°

Phase ID (3)	Chemical Formula	PDF-#	Wt% (σ)	DD% (σ)	RIR	μ
Albite - high (PO)	$Na(AlSi_3O_8)$	98-000-0040	60.5 (6.6)	70.5 (0.6)	0.63	85.6
Augite	$FeCa_4Si_8Mg_{2.96}O_{24}$	98-000-0102	14.4 (2.6)	18.2 (0.2)	1.06	242.0
Forsterite	$Mg_2(SiO_4)$	98-000-0220	25.1 (5.4)	11.3 (0.6)	0.75	98.0

XRF(Wt%): Fe2O3=1.3%, CaO=3.6%, SiO2=60.0%, Al2O3=11.8%, MgO=16.3%, Na2O=7.1%

Refinement Halted (R/E=1.19), ♣ Round=4, Iter=6, P=47, R=25.71% (E=21.54%, EPS=0.5)

C:\Users\elwo2924\Desktop\MEEM\02-10-23-ice3-silt-SA.raw

Friday, March 10, 2023, 3:03 PM ● Univ Oklahoma

HI Dust Fraction XRD Results

Chapter II Supplemental

Appendix 1

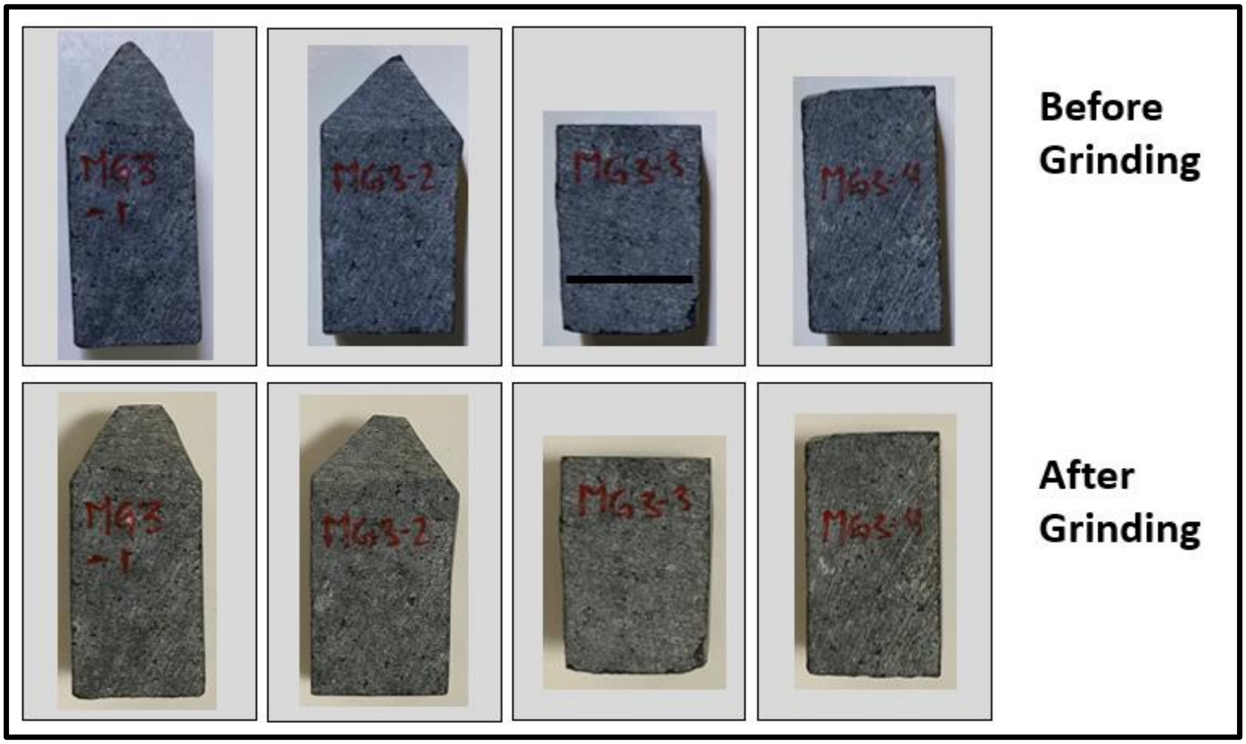
Before
Grinding
After
Grinding


Before
Grinding
After
Grinding


Before
Grinding
After
Grinding

Chapter III Supplemental

Appendix 1

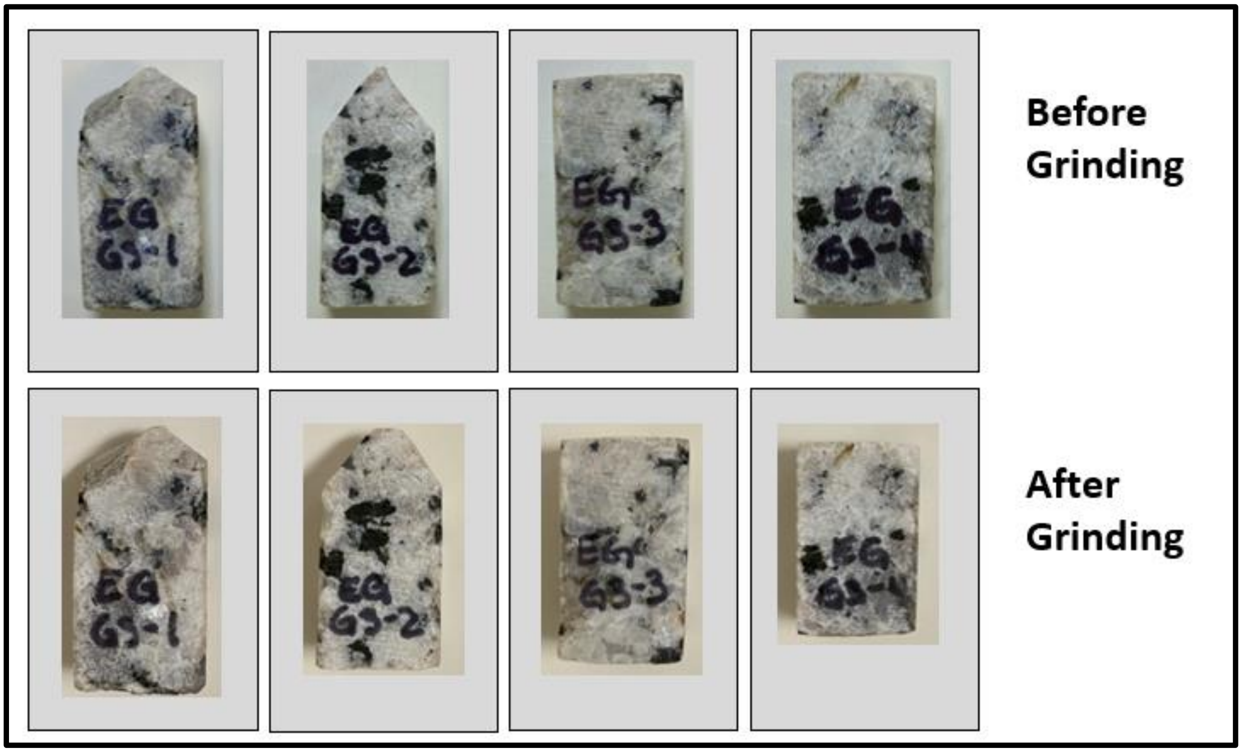
Before Grinding
After Grinding


Before Grinding
After Grinding


Before Grinding
After Grinding


Before Grinding
After Grinding

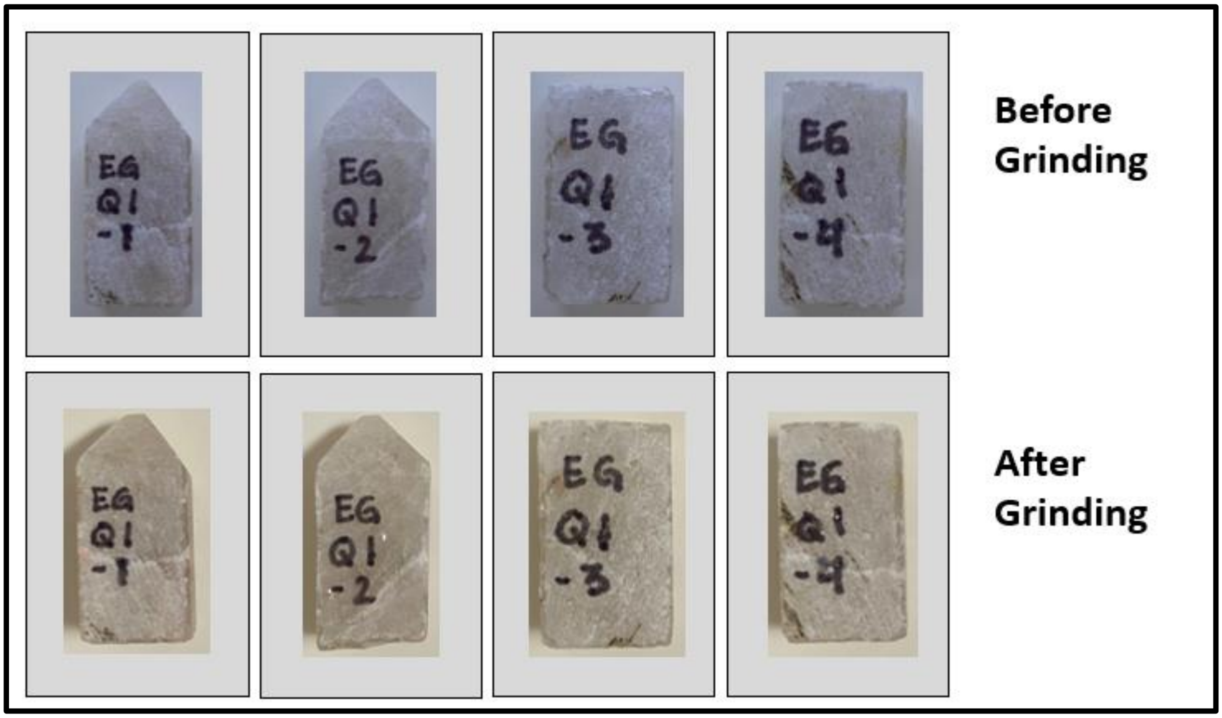
Before Grinding
After Grinding

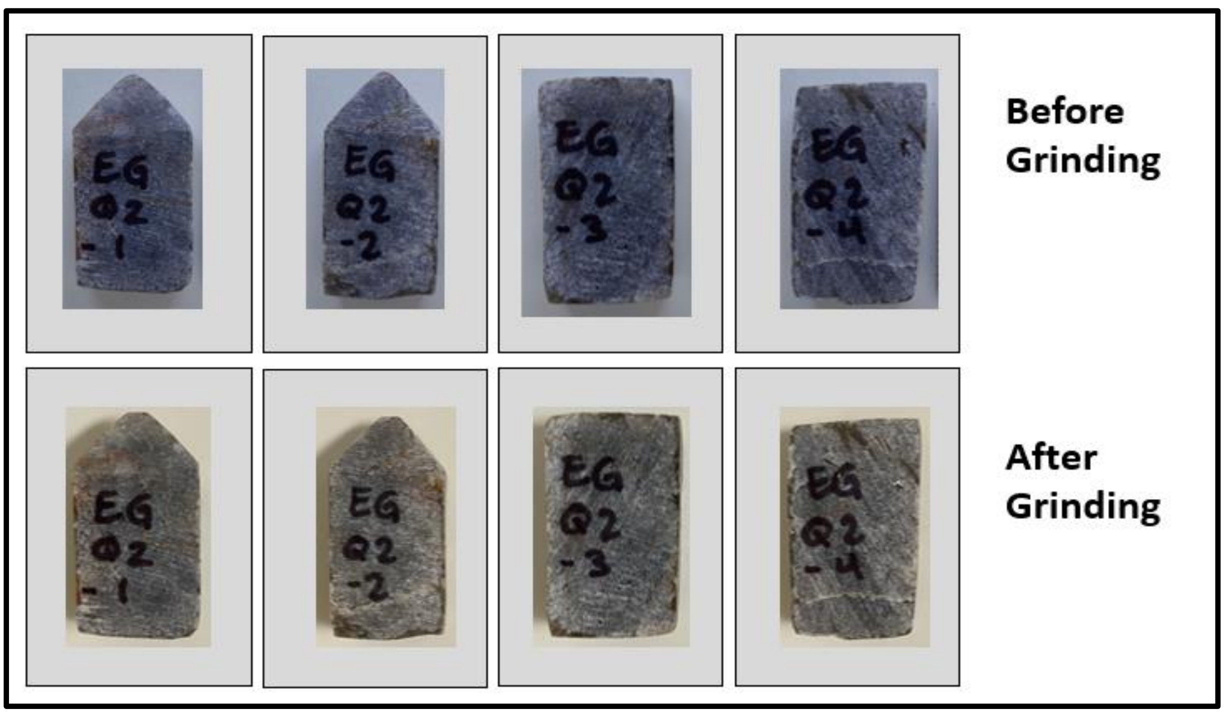
Before Grinding
After Grinding


EG SC 1
EG SC 2
EG SC 3
EG SC 4
Before Grinding
EG SC 1
EG SC 2
EG SC 3
EG SC 4
After Grinding


EG SS1 -1
EG SS1 -2
EG SS1 -3
EG SS1 -4
Before Grinding
EG SS1 -1
EG SS1 -2
EG SS1 -3
EG SS1 -4
After Grinding


EG SS2 1
EG SS2 -2
EG SS2 -3
EG SS2 -4
Before Grinding
EG SS2 1
EG SS2 -2
EG SS2 -3
EG SS2 -4
After Grinding

Appendix 2

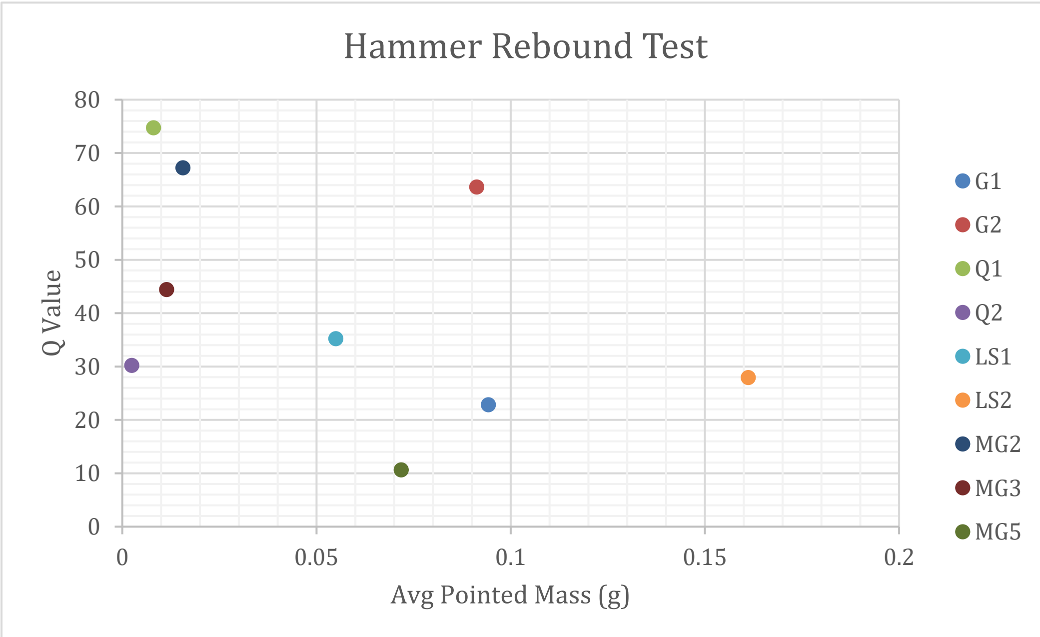

Appendix 2. Hammer rebound (Q) values plotted against the average mass produced from pointed styluses for selected samples. Note MG2 has only one mass value, the others were below the detectible range.

Appendix 3

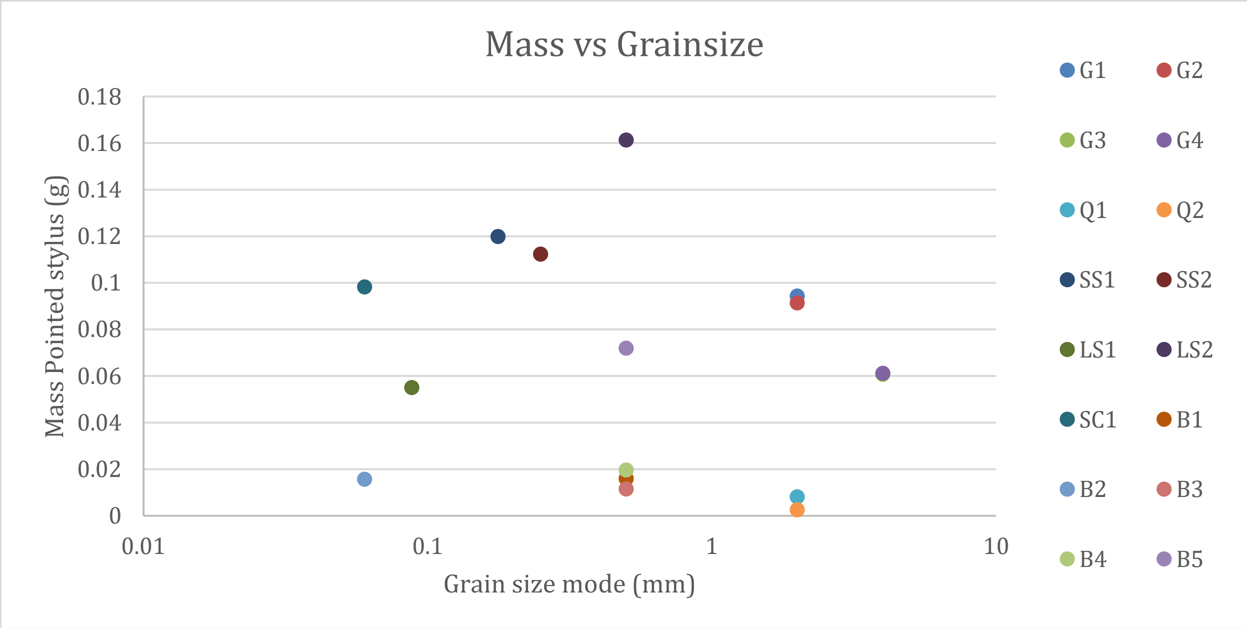

Appendix 3. Estimated grain size modes are plotted against the average mass produced from pointed styluses for each sample.